Inkjet-Assisted Printing of Encapsulated Polymer/Biopolymer Arrays

A Dissertation

Presented to

The Academic Faculty

by

Rattanon Suntivich

In Partial Fulfillment

of the Requirements for the Degree

Doctor of Philosophy in the

School of Materials Science and Engineering

Georgia Institute of Technology

August 2014

Inkjet-Assisted Printing of Encapsulated Polymer/Biopolymer Arrays

Approved by:

Dr. Vladimir V. Tsukruk, Advisor
School of Materials Science and Engineering
Georgia Institute of Technology

Dr. Johnna S. Temenoff
Department of Biochemical Engineering
Georgia Institute of Technology

Dr. Donggang Yao
School of Materials Science and Engineering
Georgia Institute of Technology

Dr. Valeria Milam
School of Materials Science and Engineering
Georgia Institute of Technology

Dr. Zhiqun Lin
School of Materials Science and Engineering
Georgia Institute of Technology

Date Approved: May 13, 2014

Dedicated to my loving family

ACKNOWLEDGEMENTS

I would like to thank Prof. Vladimir V. Tsukruk for giving me the opportunity to join his research group at the Georgia Institute of Technology. Not only for the unforgettable opportunity, but also for the thinking process, knowledge, inspiring guidance and encouragement throughout my research during these past five years. I will appreciate this learning experience for the rest of my life and implement what I have learned to generate useful products for improving the quality of living of people in our society. I would also like to thank Prof. Donggang Yao, Prof. Zhiqun Lin, Prof. Valeria Milam, and Prof. Johnna S. Temenoff for their helpful feedback, suggestions, and kind willingness to be a part of my dissertation committee.

A good support network is necessary for great outcomes, so for that I am thankful to former and current members of SEMA group. Particularly, I would like to thank Dr. Ikjun Choi, Dr. Olga Shchepelina, and Dr. Irina Drachuk for their constant support and guidance. I would also like to thank former lab members, Dr. Zachary Combs, Dr. Dhaval Deepak Kulkarni, Dr. Kyle Anderson, and Dr. Maneesh Gupta for their support, as well as current members Kesong Hu, Sidney Malak, and Weinan Xu for their help and support.

Finally, I am very grateful to my family for their unconditional love and support. Sincere thanks goes to all my family, Rinrada Luechapanichkul, Guntarika Suntivich, Sukannika Suntivich, and Boondarik Suntivich for their moral support over the years.

TABLE OF CONTENTS

LIST OF TABLES

LIST OF FIGURES

Summary

The goal of the proposed study is to understand the morphology, physical, and responsive properties of synthetic polymer and biopolymer layer-by-layer (LbL) arrays using the inkjet printing and stamping technique, in order to develop patterned encapsulated thin films for controlled release and biosensor applications. In this study, we propose facile fabrication processes of hydrogen-bonded and electrostatic LbL microscopic dot arrays with encapsulated target organic and cell compounds. We study encapsulation with the controllable release and diffusion properties of poly(vinylpyrrolidone) (PVPON), *poly*(methacrylic acid) (PMAA), silk-polylysine, silk-polyglutamic acid, pure silk films, and *E-coli* cells from the multi-printing process. Specifically, we investigate the effect of thickness, the number of bilayers, and the hydrophobicity of substrates on the properties of inkjet/stamping multilayer films such as structural stability, responsiveness, encapsulation efficiency, and biosensing properties.

In this dissertation, we find that hydrogen-bonded of PVPON/PMAA LbL films using the inkjet printing technique are grown exponentially. This indicates that the LbL films made of PVPON/PMAA are comprised of random coil component with sufficient mobility, which increases the structural stability of the LbL films in acidic solutions. The results of our study also show that because of heterogeneous evaporation of the locally deposited microliter solutions, LbL films show a coffee-ring structure. Furthermore, the dot size of LbL deposits can be controlled by changing the hydrophobicity of the substrates as a result of limited solution spreading on dewettable surfaces. The PVPON/PMAA LbL films are pH responsive and are also stable under acidic conditions because of the strong hydrogen bonding within the LbL films, whereas the films are rapidly dissolved in solution with pH above 5.5 as a result of the deprotonation of PMAA component which destroys the hydrogen bonding between PVPON and PMAA. Another type of LbL film, silk-polylysine/silk-polyglutamic acid films (i.e., ionomeric silk LbL films) can be utilized to immobilize and protect *E-coli* cells on both rigid and flexible substrates. Ionomeric silk LbL films are stable in SMM media, but several silk molecules are removed in the solution because of weak bonding between the ionomeric silk polyelectrolytes from the absence of intermediate washing steps. This result indicates

that LbL assembly using electrostatic interactions is more sensitive to the excessive polyelectrolytes in the LbL films than using hydrogen bonding because stronger ion repulsion from the excessive polyelectrolytes diminishes the strength of the electrostatic interaction in the ionomeric silk LbL films.

The results also show that stamping free-standing silk films can be used to encapsulate materials, both dye and *E-coli* cells, with high structural stability. The aqueous ink and *E-coli* cells are patterned without physical damage by inkjet printing, and the stamping technique completes the encapsulation process afterward. This outcome indicates that the pressure from inkjet printing and manually pressing during the encapsulation process is not strong enough to damage the *E-coli* cells. Free-standing silk films are fused uniformly by using moisture as a result of decreasing the glass transition temperature of silk molecules.

We suggest that a more thorough understanding of the LbL assembly using inkjet printing and stamping techniques can lead to the development of encapsulation technology with no limitations on either the concentration of loading, or the chemical and physical properties of the encapsulated materials. In addition, this study offers new encapsulation concepts with simple, cost effective, highly scalable, living cell-friendly, and controllable patterning properties.

CHAPTER 1

INTRODUCTION

1.1 Background

Ultrathin functional polymer films and microcapsules are important for diverse applications in sensing, catalysis, cell culture, tissue engineering and drug delivery.[1,2] Layer-by-Layer (LbL) assembly is one of the prominent techniques used to create nanostructure materials and structures with controlled thicknesses, morphology, diverse functionalities and unique structures with component selection that includes polyelectrolytes, dendrimers, proteins, nanoparticles, colloids, and biomaterials.[3,4,5,6,7,8,9,10,11,12,13,14,15,16] For demanding applications, further tailoring of LbL multilayer structures, beyond uniform films and spherical microcapsules should focus on the adaptation of advancements in the known nanotechnologies such as inkjet printing, micro-contact printing, micro-molding and dip-pen nanolithography.[17,18,19,20,21,22,23,24,25] Generally, these approaches allow for the facile fabrication of patterned LbL structures with controlled spatial configurations that have multicompartment periodic patterned structures at different length scales.

In particular, the formation of discrete LbL structures with controlled shapes and a periodic spatial arrangement of components remains a challenge for conventional dipping, spinning, and spraying methods.[26,27] The inkjet printing technique on the other hand, which utilizes microdroplet deposition via a microscopic nozzle, is a facile and powerful top-down route for creating complex arrays when combined with bottom-up LbL assembly. Accordingly, inkjet printing-assisted LbL multilayer assembly is

expected to yield well-defined miropatterned structures with nanometer thickness and microscopic lateral dimensions. The use of inkjet printing enables manipulation of the drop size, location, and speed. It also allows fabrication of the complex dot arrays according to a pre-programmed automatic process.[17,28,29] Therefore, inkjet-assisted encapsulation is an interesting concept for improving responsive encapsulation technology.

LbL encapsulation

Smart responsive materials are increasingly utilized for applications in optoelectronic, surface modification, photonic, biomedicine, and drug delivery. Their properties, including mechanical stability, permeability, elasticity, biocompatibility, and surface characteristics can be altered by using LbL techniques. LbL assembly can be fabricated by using electrostatic interaction, hydrogen bonding, hydrophobic interactions, and Van der Waals force.[30] There are three main categories for stimulation as shown in Figure 1.1. First, the properties of polymers such as pH-protonation, temperature responsiveness, ionic strength sensitivity, solubility, change of melting and glass transition temperature of polymers can be utilized to create responsive materials. Second, through external stimuli such as temperature, electric and magnetic field, light, sound waves, or mechanical interaction. Finally, polymers can be stimulated by chemical reactions with a functional surface such as one with enzymes or receptor-recognition of molecules.

Loading therapeutic molecules processes in LbL capsules

Inserting target chemical molecules inside the LBL capsule with high loading efficiency is a critical challenge for LBL encapsulation. There are several known techniques that are normally used to encapsulate therapeutic molecules in LbL capsules, such as drug loading in preformed LbL capsules,[31,32] encapsulating crystallized therapeutic materials with a LbL shell, [33,34] and LbL encapsulation incorporated with porous cores as shown in Figure 1.1.[35,36]

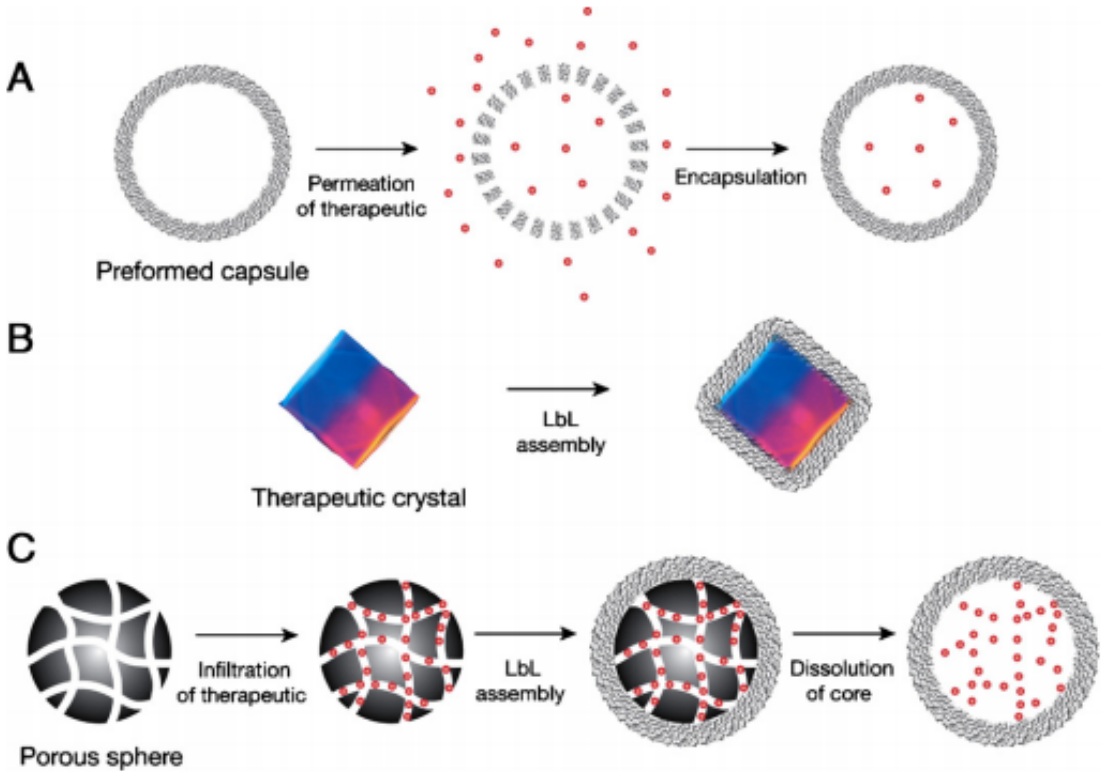

Figure 1.1 Different techniques for encapsulating therapeutic molecules: (A) loading assembled LbL capsules, (B) Encapsulating crystallized therapeutic materials with LbL shells and (C) LbL encapsulation with porous cores.[53]

1. Loading in assembled LbL capsules

Responsive LbL capsules can be assembled by using conventional processes. The loading of preferred molecules from the surrounding solution into the LbL capsule occurs via a diffusion mechanism. The responsive capsule will be opened after being stimulated by changing environment such as pH or salt concentrations. The open state allows the therapeutics molecules to diffuse into the target capsule as shown in Figure 1.1 A. Although it is a simple process to transfer molecules into the capsule, loading efficiency into the target capsules depends on the molecular weight of the therapeutic molecules and the concentration of the molecules in solution. Figure 1.2 shows the effect of the molecular weight of therapeutic molecules on the loading efficiency of PEI-(TA/PVPON-55)$_4$ capsules[37]. The loading efficiency decreases with an increase in the molecular weight of the therapeutic molecules. The maximum loading concentration is regulated by the concentration of the therapeutic molecules in the medium because of diffusion limitations. In addition, controlling the permeability using extreme salt concentrations, pH, or temperature may not suitable for biomolecules.

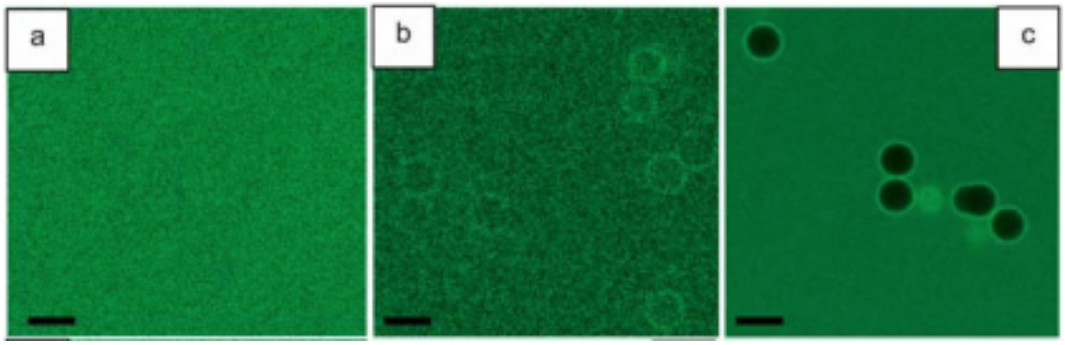

Figure 1.2 PEI-(TA/PVPON-55)$_4$ capsules in FITC-dextran solution at different FITC-dextran molecular weight. A) MW = 4000, B) MW = 70000, and C) MW = 500000.[37]

2. Encapsulating crystallized therapeutic materials with LbL shells

The low loading efficiency from the diffusion mechanism can be improved by encapsulating therapeutic crystals with electrostatic LbL assembly. This technique increases loading concentration due to the solid form of the encapsulated materials**.** The therapeutic crystals can be encapsulated by depositing polyelectrolytes directly on the therapeutic crystal. The responsive coating layer can be utilized for controlling release rate of the encapsulated crystal in desired solution. The example in Figure 1.3 shows the

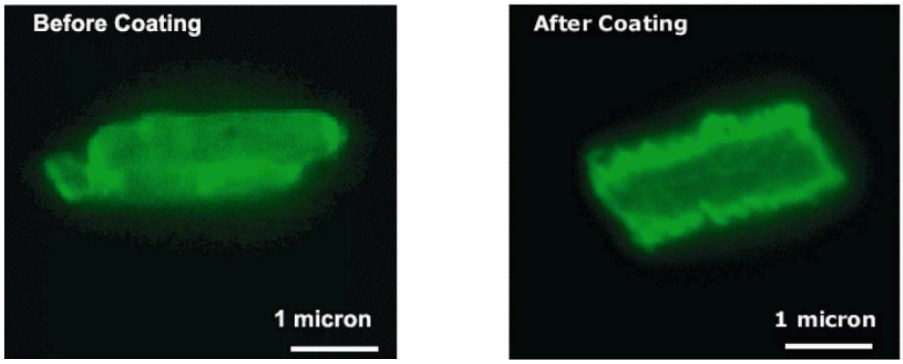

Figure 1.3 Fluorescent image of uncoated and coated furosemide microcrystals with $(PSS/PDDA)_2$ + $(PSS/\ gelatin)_6$ multilayers.[38]

encapsulation of furosemide microcrystals with the $(PSS/PDDA)_2$ + $(PSS/\ gelatin)_6$ LbL assembly. The coated LbL layer can prolong release rate of furosemide microcrystals in aqueous solution up to 300 times compared to uncoated crystals.[38] Even though the LbL encapsulation of the solid therapeutic materials enhances loading efficiency, there are limitations to this technique. Most notably, the encapsulation is required to take place in aqueous phases because of the deposition of water-based electrostatic LbL assembly on the solid templates. Therefore, this technique may not work well for poorly water-soluble therapeutic crystal, polymeric microsphere, hydrophobic materials, and some biological materials. This limitation can be improved by using a reverse-phase layer-by-

layer (RP-LbL) technique. However, it requires non-ionized polyelectrolytes in an organic phase to encapsulate the water-soluble crystals. [39]

3. LbL encapsulation with porous cores

The encapsulation of therapeutic molecules by absorbing them within porous particles is another technique that can be used to achieve high loading efficiency. Mesoporous silica spheres and calcium carbonate particles are normally used as templates for encapsulation.

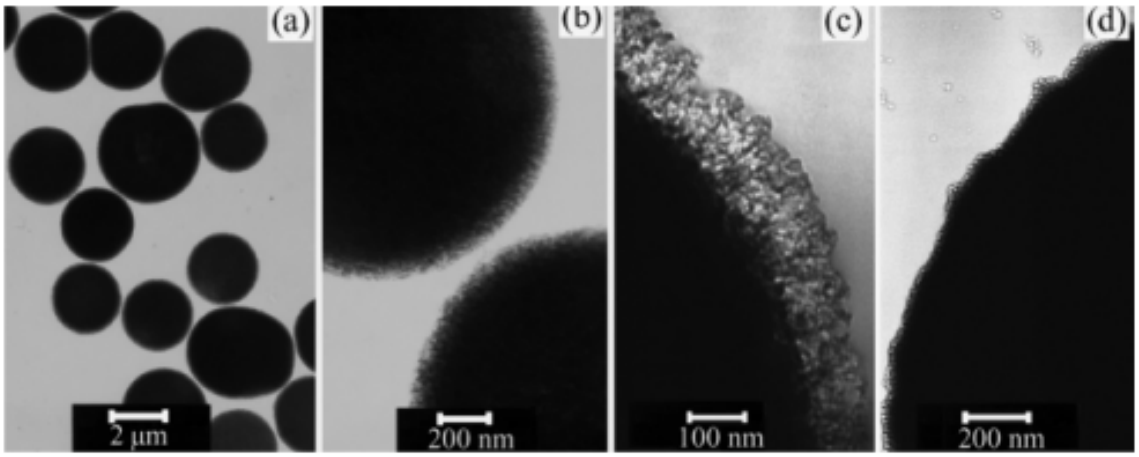

Figure 1.4. TEM images with different magnification of mesoporous silica (a-c) and three LbL layer of PDDA/Si_{NP} on the silica template (d).[40]

In this case it is the high surface area of the template particles that causes the increase in loading of the therapeutic molecules. LbL assembly on the template is the process used for the encapsulation of the target molecules, as shown in Figure 1.4.[40] The porous template can be removed using acid or specific conditions that do not significantly affect the loaded molecules. The pore size of the porous particle core has a significant influence on the loading rate of the therapeutic molecules. Large pore size can increase loading rate up to few hours while smaller pore particles extend loading time to several days. Figure 1.5 shows the effect of particle size of the mesoporous silica on loading

efficiency. This porous-assisted encapsulation can significantly increase loading amount of encapsulated therapeutic molecules in the responsive capsules.[41] For example loading lysozymes increase from 40 mg/ml to 185 mg/ml, while maximum loading amount for enzyme encapsulation was around 450 mg/ml for lysozyme. [42,43] Even though this porous core-assisted process can improve loading efficiency, the technique has still limited applications in the bio field because of the strong acids requirement in the core removal process.

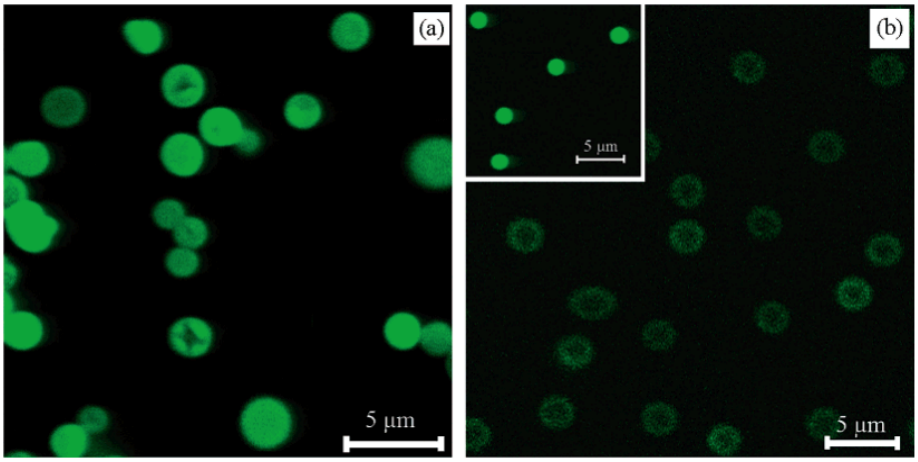

Figure 1.5. CLSM images of FITC-POD-loaded in different porous silica template. (a) large pore size 2.5 μm and (b) small pore size 1.8 μm.[41]

1.2 Inkjet printing

In contrast to conventional LbL encapsulation, inkjet printing can load therapeutic molecules inside responsive polymer structures in a fast manner without requiring a core template and core removal procedure. This technique facilitates loading target molecules directly to the proper position with controllable loading concentrations. Therefore, there is no limitation on loading from the molecular weight of the therapeutic molecules.

Figure 1.6. Formation of ink droplet using thermal DOD inkjet printing.[44]

Inkjet printing can be operated in continuous mode or drop-on-demand mode (DOD). In continuous inkjet printing, the fluid ink is pumped through inkjet nozzles. This printing mode is widely used in the industrial for coding and labeling materials due to high speed printing advantages. However, DOD printing mode is also a major printing process because of its small drop size, higher accuracy, and low limitation of ink properties. The small ink droplets are generated by periodically impulses from a reservoir through a

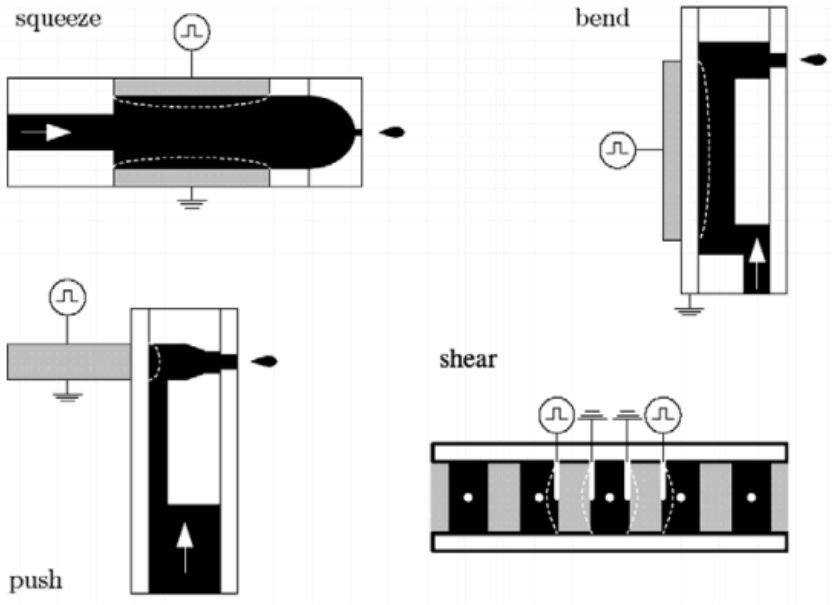

Figure 1.7. Deformation modes of piezoelectric inkjet printing for ink droplet

nozzle using electronic acoustic pulses. The pulse can be controlled by either piezoelectricity or temperature. In thermal DOD mode, ink is heated locally to produce rapid vapor bubbles that eject ink droplets as shown in Figure 1.6.[44] The thermal DOD inkjet is limited for water-based ink and some heat resistant polymer solution because of rapid heating requirement. On the other hand, piezoelectric DOD inkjet using pressure instead of heating ink solutions. The pressure is produced from various deformation modes of piezo-electric membrane that causes local pressure and droplet formation (Figure 1.7).[45] The piezoelectric DOD inkjet printing technique is in principle suited for a variety of solvents because of the non-heating requirement. Therefore, piezoelectric DOD inkjet printing is commonly used for conventional purposes.

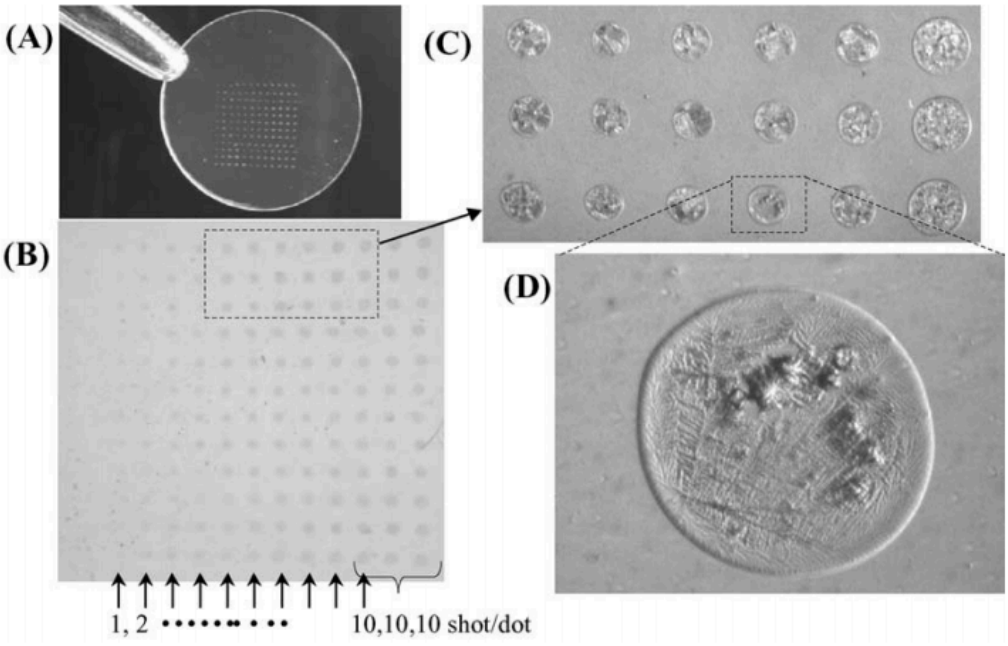

Figure 1.8. Phase-contrast microscopic images of the printed endothelial cells on PET culture disk using inkjet printing.[49]

The several advantages of inkjet printing over other deposition techniques makes it useful for various fields such as diagnostics, cellular mechanobiology, therapeutics and biosensing applications.[46,47] It is important to develop artificial cells that demonstrate the complexity of native tissue in order to understand cues of cell phenotype.[48] Inkjet printing is an outstanding candidate for the study of biomaterial systems for this assignment. For example, inkjet printing can be used to pattern individual living cells. Figure 1.8 displays a uniform pattern of endothelial cells after suspended in media and printed on a PET culture disk. The printed cells are adhered on the culture disk for proliferation during incubation period.[49] Figure 1.9 confirms that inkjet printing does not damage living cells and that the cells are alive after being patterned, using the inkjet printing technique.[50] Patterned microfilms with controllable permeability can also be

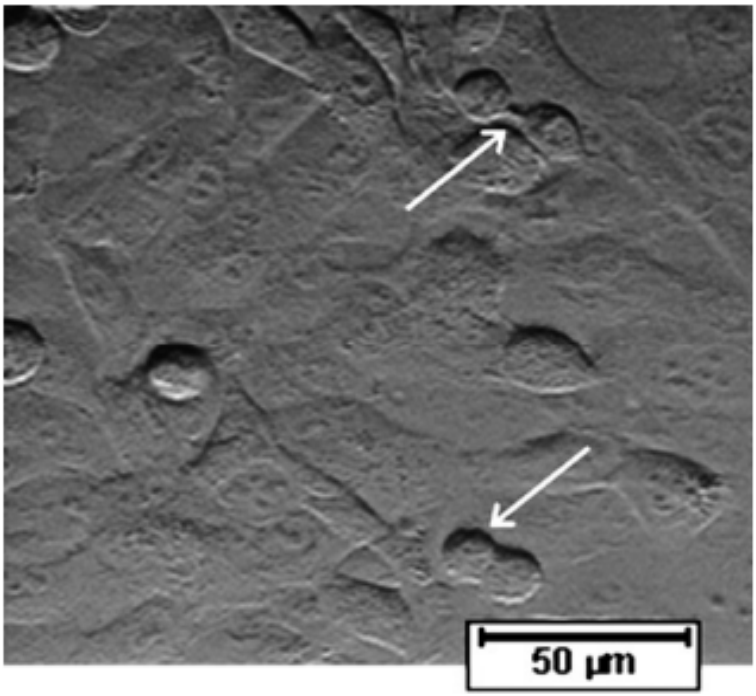

Figure 1.9. Cell diversion of Human fibrosarcoma cells after printed using inkjet printing and incubation for 48 hrs.[50]

fabricated using inkjet printing and used to protect targeted cells. In addition, these protective layers can be used to study individual cell proliferation, gene expression, shape, migration, and cell behavior regulation through independently controlled physiochemical cues.[51,52]

Inkjet printing is considered one of the outstanding candidates for patterning materials. Several examples of utilizing inkjet printing to fabricate uniform and patterned LbL film formations using different pairs of polyelectrolytes with hydrogen and ionic interactions have recently been published.[53,54] Inkjet printing can be utilized for pattering LbL films by printing crosslinking solution on target areas for subsequent partial polymer removal and patterning. In addition, inkjet technique can be applied to fabricate LbL films without intermediate rinsing steps by controlling the component concentration. This non-rinsing reduces the materials lost during LbL fabrication and shortens the required assembly time.

1.3 Motivation

Limitations of conventional loading processes

The formation of LbL capsules normally requires sacrificial colloidal particles to serve as a core template to adsorb polymer chains. This process augments each layer via electrostatic interaction or hydrogen bonding to form LbL multilayers on the selected cores. Subsequently, the sacrificial cores are removed to generate hollow LbL capsules. Finally, drug molecules can be loaded inside the empty capsule by using slow diffusion

to transfer the therapeutic molecules from solution to the volume inside the hollow LbL capsules. This traditional LbL procedure has many limitations for implementation at large scale. First, it requires a long absorption time in order for the polymer to completely spread on the solid core template. Second, LbL requires intermediate washing steps to eliminate the excess or non-absorbed molecules that disturb the assemble process.

This washing process causes massive amounts of material to be wasted and slows down the encapsulation progression. In addition, LbL shells can be affected by the strong acids that required during the core removal process. Drug loading to the LbL capsules also requires diffusion and permeability; that loading efficiency is limited to the drug concentration in the solution.[55] Furthermore, the unloaded drug in the media will be washed and will cause a decrease in effective drug loading. In addition, conditions for good permeability such as high salt concentration and temperature may not be suitable for biomolecules. Finally, patterning materials at desired positions cannot achieve by using the traditional LbL procedure.

Challenges in inkjet-assisted LbL encapsulation

One of the critical issues in inkjet printing is the uncontrolled spreading of liquid droplets on solid substrates following impact and dewetting process (e.g. coffee ring formation during the drying process) due to a mismatch in surface energy that might compromise the printing resolution. Large spreading of the droplet is another issue that complicate this technique and has been mitigated by controlling the distance between the substrate

and nozzle, the viscosity of the ink solution, the evaporation rate, and the primer coating on the substrate. It has been suggested but not demonstrated that even higher resolution can be achieved by the diminution of the nozzle dimensions, changing the viscosity of solution, the impact of liquid droplets to a substrate, and liquid spreading.[56] The size of the polymer droplets can be further reduced down to a few hundred nanometers in diameter with the assistance of an electric field.[57]

To increase the speed of the deposition process, one can rapidly dry layers of minute thicknesses to prevent a deviation from the initial shape through the use of multiple deposition cycles. Well-aligned microprinting processes have been implemented to minimize deviations from the targeted center position during the multiple repetition of LbL deposition and have demonstrated the ability to build LbL structures with microscopic precision. However, very little has been published on high-resolution micropatterned composite LbL films and arrayed LbL encapsulation via ink-jet assisted LbL assembly. In these studies, we demonstrate that inkjet-assisted LbL assembly and stamping techniques can be utilized to fabricate large scale uniform ultrathin films and patterns with a typical resolution in the range of 70-100 μm. These parameters can be used to build patterns with complex compositions for encapsulation and biosensing applications.

CHAPTER 2

RESEARCH GOALS, OBJECTIVES, AND DISSERTATION OVERVIEW

2.1. Goals

The goal of this dissertation is to understand the morphology, physical properties, and responsive properties of inkjet/stamping-assisted LbL composite systems with the aim to develop micro patterned, encapsulated, and ultra-thin dot arrays for controlled release and biosensing applications. The key approach for the inkjet/stamping-assisted LbL encapsulation to be explored in this study is the utilization of the inkjet printing technique and stamping technique to create microscopic droplets of polymer solution using various types of responsive polymers and deposit them as dots at selected positions. The objective is to fabricate responsive LbL dots with controlled size, composition, and selected encapsulated organic and biological materials as shown in Figure 2.1.

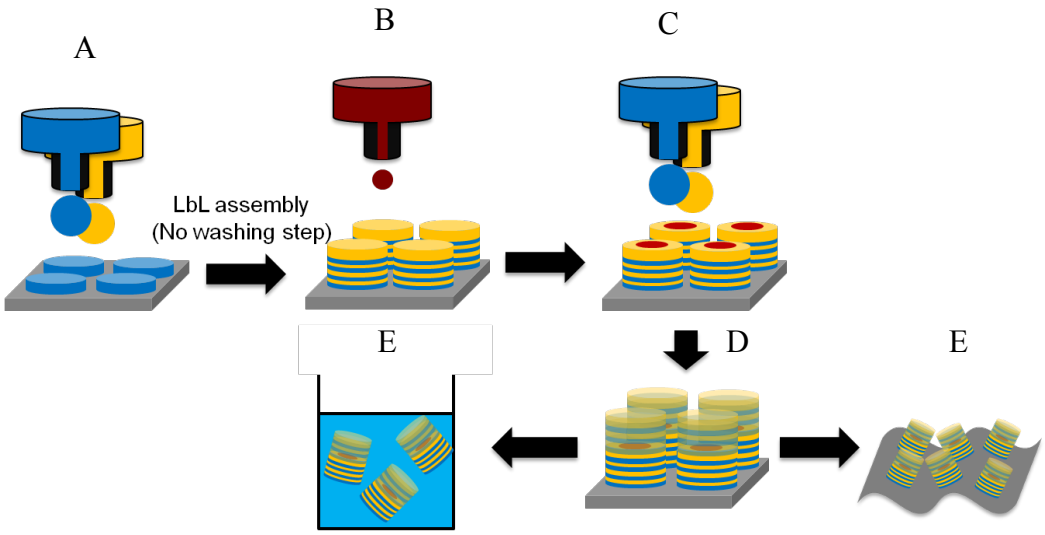

Figure 2.1. Experimental concept of inkjet-assisted LbL formation of encapsulated polymer arrays: A) Multilayer LbL assembly by inkjet printing, B) Target loading, C) Creation of additional protective layers, D) Completed sandwiched dot array, and E) Completed dots on different substrates and released structures.

2.2 Technical objectives of this study are summarized as follows:

1. Optimize printing parameters, droplet velocity, patterning procedure, limits of resolution, encapsulation performance, and size control of the inkjet-assisted LbL assembly by varying deposition parameters and the number of polymeric bilayers on various substrates with different wettability properties.
2. Conduct a thorough investigation of the structural stability, film thickness control, surface morphology, optical properties, and biosensing properties of the hydrogen bonded and electrostatic inkjet-assisted LbL encapsulated dot arrays at variable pH conditions using comprehensive surface sensitive characterization techniques.
3. Study the release rate and disentanglement of the inkjet-assisted LbL encapsulated dot arrays that have varying numbers of LbL bilayers, lateral dimensions, and crosslinking conditions under variable pH conditions by monitoring the change of film thickness and fluorescence intensity of an encapsulated fluorescent dye as a model compound.
4. Fabricate inkjet-assisted dot arrays in cooperation with a stamping process in order to develop a fast silk-based encapsulation technique that works on large scales and has possibilities for biosensing applications.
5. Understand and optimize the stamping and inkjet printing conditions for the fabrication of encapsulated dot arrays made of natural silk-based materials and study physical properties of these silk-based encapsulated films.
6. Study the encapsulation of *E-coli* cells using inkjet printing and stamping technique using silk-based materials for the development of cell-based-array biosensors that can detect different bioanalytes.

The various general approaches and routes in design and fabrication aspects of the proposed study are summarized in Figure 2.2.

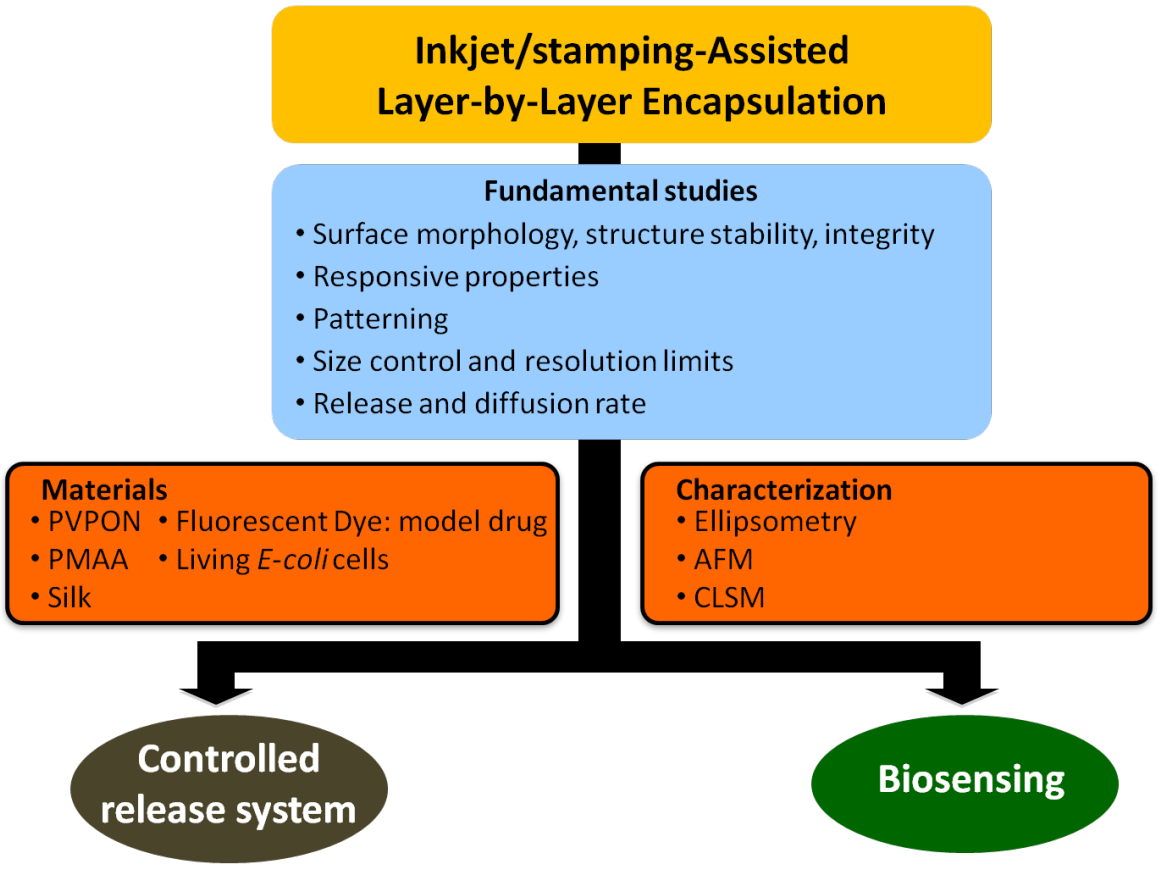

Figure. 2.2. Summary of proposed approaches of inkjet-assisted LbL encapsulation procedure.

Firstly, PVPON, PMAA, and natural silk-based polymers will be used to fabricate inkjet-assisted layer-by-layer dot arrays and protective layers. Second, target model compounds such as Rhodamine dye or *E-coli* cells will be encapsulated in the dot arrays as model for therapeutic molecules and biosensing. The inkjet/stamping-assisted LbL encapsulated dot arrays will be characterized by various techniques to understand their fundamental properties such as surface morphology, responsiveness, and release behavior. Finally, the

inkjet-assisted LbL printing will be tested for various applications in controlled release systems, and biosensing (Figure 2.2).

2.3 Organization and composition of dissertation

Chapter 1 is a critical review of issue and state of art research related to encapsulation techniques along with its limitation. The conventional encapsulation techniques include encapsulation with assembled capsule, LbL encapsulation for crystal loading molecules, and increasing loading efficiency with porous core. In addition, this chapter includes overview of inkjet printing technology and it's application in bio patterning research and unresolved challenge, which need further investigation. Detail of materials using in this research is also included in this chapter.

Chapter 2 is a description of the goal and technical objective of this dissertation. Moreover, this chapter provides a brief organization of the dissertation with short description in each chapter.

Chapter 3 includes the experimental techniques that are important in the studies presented in this dissertation. It includes sample preparation using inkjet printing, stamping technique, and characterization techniques. Sample preparation include multiple deposition of LbL films by inkjet printing, patterning with inkjet printing, cell encapsulation in free standing silk films using contact printing, and preparing *E-coli* cells. Characterization techniques include atomic force microscopy for measuring topography,

optical microscopy for printing performance and structural stability measurement, and confocal microscopy for biosensing measurement.

Chapter 4 demonstrates patterned encapsulation of Rhodamine dye as a model compound within poly(vinylpyrrolidone)/poly(methacrylic acid) (PVPON/PMAA) LbL dots constructed without an intermediate washing step. The inkjet printing technique improves encapsulation efficiency, reduces processing time, facilitates complex patterning, and controls lateral and vertical dimensions with diameters ranging from 130 to 35 μm (mostly controlled by the droplet size and the substrate hydrophobicity) and thickness of several hundred nanometers. The microscopic dots composed of hydrogen-bonded PVPON/PMAA components are also found to be stable in acidic solution after fabrication. This facile, fast, and sophisticated inkjet encapsulation method can be applied to other systems for fast fabrication of large-scale, high-resolution complex arrays of dye-encapsulated LbL dots.

Chapter 5 shows inkjet printing for the facile fabrication of microscopic arrays of biocompatible silk "nests" capable of hosting live cells for prospective biosensors. The patterning of silk fibroin nests were constructed by LbL assembly of silk polyelectrolytes chemically modified with poly-(L-lysine) and poly-(L-glutamic acid) side chains. The inkjet-printed silk circular regions with a characteristic "nest" shape had diameters of 70–100 μm and a thickness several hundred nanometers were stabilized by ionic pairing and by the formation of the silk II crystalline secondary structure. These "locked-in" silk nests remained anchored to the substrate during incubation in cell growth media to

provide a biotemplated platform for printing-in, immobilization, encapsulation and growth of cells. The process of inkjet-assisted printing is versatile and can be applied on any type of substrate, including rigid and flexible, with scalability and facile formation.

Chapter 6 demonstrates development of inkjet-assisted biosensor by cooperating with stamping technique. The patterned *E-coli* cell arrays are printed on a free standing silk film and are encapsulated by stamping another free silk standing silk film on top of the *E-coli* array. The adhesion property of the silk films is increased by exposing the silk films in humidifier. The moisture from humidifier decrease glass transition temperature of the free standing silk, and enhance inter molecular diffusion of the two silk films from stamping process. Optical images show stable pattern of water-based ink in stamping process. It indicates encapsulation stability of this concept. In addition, SEM images show no interface at the two silk films, indicating complete merging of the silk films from stamping techniques. The samples are preserved in refrigerator for 2 months. However, the *E-coli* cells in stamping silk films still active and show green fluorescent expression after expose in analyte solution. This result confirms bioactivity preservation using inkjet printing and stamping on silk freestanding films. The combination of inkjet printing and stamping technique can reduce operating cost, shorten sample fabrication time and enhance scalable possibility for biosensing applications.

Chapter 7: provides general conclusions for the overall work in the dissertation with a specific focus on impact and future directions.

CHAPTER 3

EXPERIMENTAL DETAILS

3.1. Materials

3.1.1. Silk fibroin

Silk serves as an excellent biocompatible material for many applications. Silk fibroin has been used commercially as medical sutures for decades due to its mechanical and biocompatible properties. The biological properties of silk fibroin are a result of the unique repetitive primary amino acid sequence in silk protein.[58,59] Moreover, silk fibroin is also utilized in textile and consumer products like cosmetic cream, make up, and pharmaceuticals. Silk-based materials are used to maintain the activities of enzymes and biomolecules in harsh environments and drug delivery applications due to its capability to support the adhesion and growth of mammalian cell types.[60] In addition, silk shows remarkable optical properties such as near-perfect transparency in the visible range.[61]

In its natural form, known as silk II, silk fibroin contains high concentration of β-sheet crystallites because of high number of hydrophobic repeat sequences of the amino acids glycine and alanine domains in the silk molecules. The silk crystallite regions act as native crosslinks that stabilize the protein and increase the mechanical properties of the silk fibers. The key molecular interactions in β-sheet nanocrystals are hydrogen bonds, one of the weakest chemical bonds known. This hydrogen bonding increases the mechanical properties of the silk materials because it leads to formation of nanoconfinement in the silk structure. The nanoconfinement causes uniformity of shear deformation in nano scale with molecular stick-slip deformation, which significantly

enhances mechanical properties of silk materials. [62] Silk has excellent mechanical properties such as high elastic modulus, elongation-to-break, and toughness.[63] Silk fiber can achieve strengths on the order of 3 GPa along with high extensibility (30%) and good compressibility. The strength and toughness of silk materials exceeds that of steel and other materials through the reduction of the size of the β-sheet nanocrystals via moderating the reeling speed. Spin coating also enhances the mechanical strength of the silk film by increasing the β-sheet content and inter-molecular interactions. The elastic modulus of ultrathin silk films is around 6–8 GPa while the ultimate tensile strength can reach 100 MPa after treatment with methanol.[64]

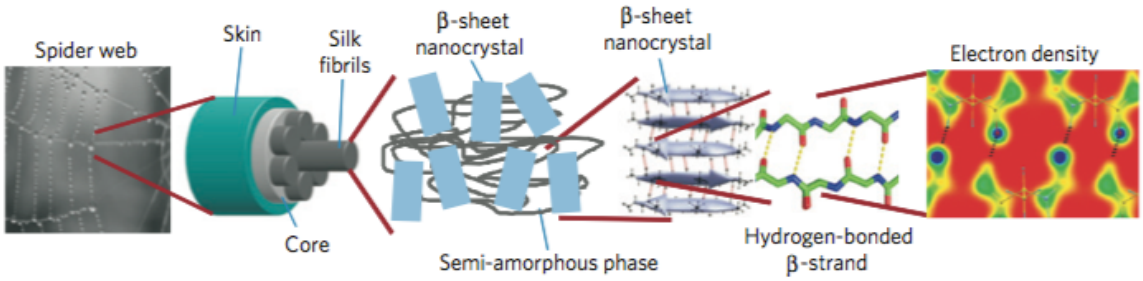

Figure 3.1.1: Schematic demonstrates hierarchical spider silk structures.

In addition to forming a crystalline structure as Silk II, silk molecules can also form a random coil conformation known as Silk I. Random coil silk is soluble or swellable in water and shows a lower elastic modulus than the silk II formation. However, silk I is more applicable in bio-related fields and tissue engineering because it biodegrades much faster than crystalline silk II.[65] The random coil silk conformation can be shifted to a crystalline form using methanol, strain, or heat. Figure 3.1.1 demonstrates the hierarchical spider silk structure both silk I (random coli) and silk II (crystalline) in the range of nano to macro-scale.

The ability to transform silk I to silk II using external stimuli enhances its applications in various encapsulation and enzyme immobilization system. [66,67,68] For example, silk fibroin can be utilized to encapsulate glucose oxidase for glucose sensing applications. The glucose oxidase is dissolved in aqueous silk I solution, encapsulated in a silk matrix by casting the mixture into a film, and finally followed by mechanical stretching to convert the random coil silk I to crystalline silk II. The immobilized glucose oxidase shows a greater stability to pH and temperature compared to its free enzyme form.[69] These outperform encapsulation results with biocompatible properties attract interest in silk fibroin for biosensing and diagnostic applications.

In this study, silk is obtained from *Bombyx mori* silkworm cocoons as outlined in the following steps.[70,71] Cocoons are first boiled for 20 min in an aqueous solution of 0.02 M Na_2CO_3 and then rinsed carefully with distilled water to extract the glue-like sericin proteins. The extracted silk fibroin is then dissolved in 9.3 M LiBr solution at 60 ° C for 4 hrs, 20% (w/v) concentration. The solution is dialyzed with distilled water by using Slide-a-Lyzer dialysis cassettes (molecular weight cutoff (MWCO) 3500, Pierce) overnight at room temperature to remove the LiBr. The silk solution is centrifuged three times at 20 °C for 20 min to remove impurities and aggregates, which may occur during dialysis. The 8% (w/v) silk solution is filtered just prior to use using 0.4 μm glass-fiber syringe filters.

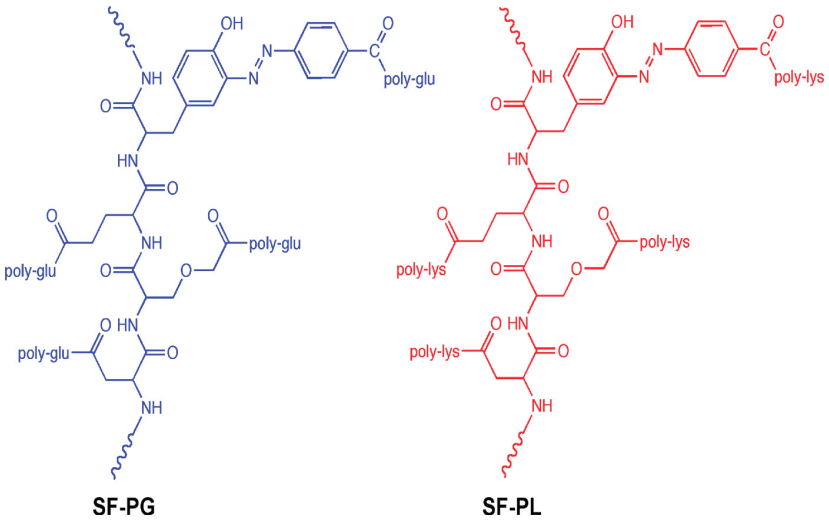

Figure 3.1.2. Chemical structure of anionic silk and cationic silk; silk-poly(glutamic) acid and silk-poly(lysine).

Silk fibroin (supported by Prof. David L. Kaplan, Tufts University, Massachusetts) can be modified to increase its responsive behavior by directly grafting polyelectrolytes onto the silk fibroin molecules. The incorporation of polyelectrolytes leads to cationic or anionic charges on the silk fibroin molecules which is utilized to obtain electrostatic interactions and can also be used for crosslinking purposes. In this study, silk fibroin molecules are linked with polylysine or polyglutamic acid by grafting with activation of the abundant tyrosine side chains in the silk molecules using diazonium followed by poly(amino acid) grafting as shown in Figure 3.1.2.[72]

3.1.2. Synthetic polymers

Poly(vinylpyrrolidone) (*PVPON*; molecular weight 40 kDa), Poly(4-vinylphenol) (PHS, molecular weight 25 kDa), Polyethylene glycol (*PEG;* molecular weight *1 kDa*) Rhodamine 6G (Dye content ~95%), galactose, hydrochloric acid, sodium hydroxide,

dibasic, monobasic sodium phosphate, Rhodamine, and fluorescein isothiocyanate (FITC) were purchased from Sigma-Aldrich. Polystyrene (PS, molecular weight 250 kDa) and toluene were purchased from Janssen Chimica and J.T. Baker. *Poly*(methacrylic acid) (*PMAA;* molecular weight *100 kDa*) was purchased from PolyScience. All chemicals were used without any further purification. Nanopure water (Barnstead) with an 18.2 MΩ·cm resistivity was used for all experiments.

3.1.3. Substrates

Silicon substrates were cut freshly in 1x2 cm^2 pieces. Piranha solution (3:1 concentrated sulfuric acid and hydrogen peroxide mixture) was used to clean the substrate according to the normal procedure (*warning: hazardous solution*).[73,74,75] Consequently, the silicon substrates were rinsed with Nanopure water and dried with a dry nitrogen stream. Covered glass slides were purchased from VWR and cleaned with Nanopure water using spin coating. For specific coated films, 2%wt PS was dissolved in toluene and spun coated at 3000 rpm onto a covered glass substrate for 30 s to change surface property of the glass slide. 2% wt PHS solution in dioxane was also used to alter surface property of the glass substrate by placing on the glass slide substrate and rotated for 30 s at 3000 rpm.

3.2 Fabrication of inkjet-assisted LbL arrays

3.2.1. Multiple deposition of LbL films by inkjet printing

The inkjet-assisted LbL encapsulation process was presented in Figure3.2.1. First, 1mg/ml of *PVPON* solution was prepared by dissolving PVPON in distilled water. The solution was adjusted to a pH of 3.5 with diluted HCl and was stored in an inkjet

cartridge. 1 mg/ml PMAA and Rhodamine dye were also prepared with the same conditions. To assemble thin films by inkjet printing, the printer nozzles were cleaned with isopropyl and distilled water to remove possible contaminates. The cartridges were placed in holders and were ready to operate.

Printing parameters such as pressure, droplet speed, and digital printing signals were adjusted for consistent performance. After cleaning and calibration, 1 mg/ml PVPON droplets were printed from the nozzle onto a clean substrate in a desired pattern, with only a single droplet of PVPON printed at each position. Next, a single 1 mg/ml PMAA droplet was printed with the same pattern on top of each PVPON film to achieve the first bilayer (PVPON layer and PMAA layer).

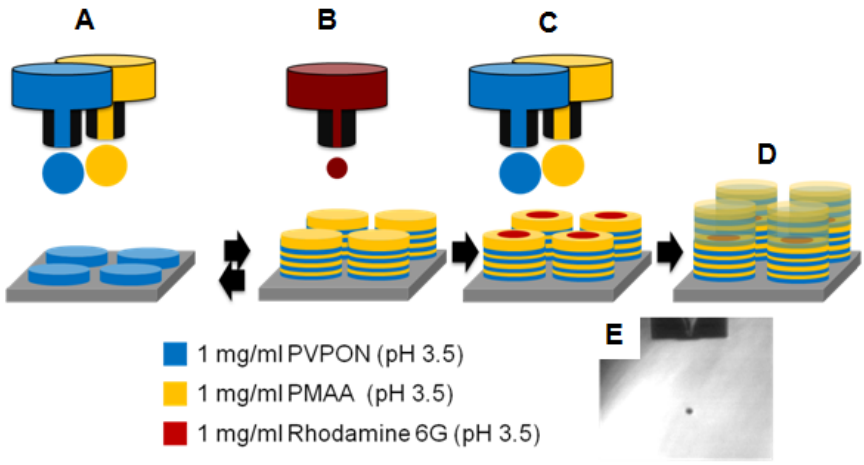

Figure 3.2.1. Inkjet-assisted LbL printing and encapsulation of LBL arrays: A) Formation of LbL dots, B) Rhodamine dye loading, C) Formation of capping film, D) dye-encapsulated array, and E) An optical image of a PVPON droplet injected from a 50 µm nozzle.

This printing process was repeated to obtain the desired number of bilayers. Rhodamine dye was used as a representative of therapeutic molecules and was printed at the center of the multi deposition films with a smaller nozzle and droplet size. The Rhodamine dye was covered and protected by the deposition of additional PVPON and PMAA layers using the same deposition procedure and number of bilayers which concluded the inkjet-assisted LbL encapsulation process. Arrays of LbL dots with encapsulated fluorescent dye sandwiched between a different of number of bilayers were formed: 2 bilayers (1+1 bilayer), 6 bilayers (3+3 bilayer), and 10 bilayers (5+5 bilayers).

3.2.2. Patterning with inkjet printing

A variety of complicated patterns can be fabricated using the JetLab II Ink-jet Printer, which was applicable for all Bitmap files. A desired pattern was selected and saved as a monochrome bitmap file (black and white format) and uploaded to the JetLab II program prior to use. The white pixels were denoted as "print" areas whereas the black areas were "do not print" areas. The size of the pattern and lateral dimensions of the dot were controlled by the number of pixels and distance between the pixels in both the x-axis and the y-axis. The maximum operation speed was 900 Hz, which was controlled by printing speed and distance between pixels in the x-axis.

3.2.3. Encapsulation using inkjet printing and stamping technique

Silk fibroin solution was extracted from *Bombyx mori* silkworm using conventional preparation mentioned in chapter 2. The silk films were prepared by drop casting silk fibroin solution onto a PET petri dish. The silk fibroin solution was air-dried at room

temperature and formed transparent silk films. The silk films were cut to the desired size and kept in a petri dish for the next sample preparation. The GT pattern of water-based ink were fabricated on the silk film using Microsoft word and an HP conventional inkjet printer, whereas the *E-coli* cells are printed on silk films using a Jetlab II printer. After the target materials were printed onto the silk films, the GT patterns or *E-coli* cell arrays were encapsulated by placing the printed silk films and another neat silk film in a humidifier for 15 seconds. The moisture in the humidifier increases the adhesion properties of the wetting silk films. After exposing to the humid environment in the humidifier, the GT pattern or *E-coli* cell arrays were encapsulated using another silk film by manually stamping the wetting silk film on top of the printed silk films for 30 seconds. After manual pressing, the stamped silk films were mechanically pressed overnight to complete the encapsulation.

3.2.4 Preparing *E-coli* cells

E.coli cells (supported by Nancy Kelley-Loughnane, Air Force Research Laboratory, Ohio) in this study were transformed to encode the theophylline synthetic riboswitch RS21.1[76], which was placed upstream of the GFPa1 gene within pSAL vector (pSAL:RS12.1GFPa1). Cells were grown in incubator (Brunswick) at 37 °C with shaking at 225 rpm in Luria-Bertani (LB) broth containing 100 mg/L of ampicillin and harvested at early stage of exponential growth (0.3-0.4 a.u. based on 0-2 scale). In order to control cell viability and activation of riboswitch (RS), synthetic cell medium containing reduced concentration of amino acids was used along with theophylline stock solution (100 mM) in DMSO, which was diluted into assay to the final concentration of 2.5 mM and 5 mM.

For printing, cells were collected in 15 mL centrifuge tubes by centrifugation at 3,000 rpm for 2 min, washing three times with phosphate buffer (Na^+ 0.05 M and K^+ 0.1M, pH5.5) and kept in a medium containing M9 mineral salts supplemented with 0.1% casamino acids and 0.008% glycerol. Confocal imaging was performed at defined times on a confocal system. Live-dead staining was performed according to the manufacturer's protocol and visualized on a confocal microscope with excitation at 488 nm (live) and 544 nm (dead).

3.3. Characterization of encapsulated arrays

3.3.1. Ellipsometry

Film thickness of inkjet-assisted LbL films is characterized by ellipsometry. This technique is non-destructive and calculated the film thickness by modeling changes in the polarization of light undergoing reflection from a sample surface.[77] The polarization angle (Ψ) and the phase difference (Δ) was measured and evaluated using a Cauchy model to determine the optical constants *n* and *k*. These data were used to calculate the thickness of the thin films with the mean squared error (MSE) for data fitting limited to 5 or below.

3.3.2. Atomic Force Microscopy (AFM)

Atomic force microscopy (AFM) is a high-resolution scanning probe microscopy that can measure the surface morphology of sample on the nanoscale level. Various scanning can be performed in various modes including contact, tapping, and non-contact in order to

obtain topographical images. In this study, AFM images were obtained using a DI Multimode microscope and Nanoscope IIIa controller to investigate surface morphology of the inkjet-assisted LbL encapsulated arrays. The AFM images were obtained using a Dimension 3000 AFM microscope (Digital Instruments) under a "light" tapping mode regime according to standard procedures.[78,79] The samples were scanned at 100 μm x 100 μm, 20 μm x20 μm, and 5 μm x 5 μm scan sizes using triangle cantilevers with resonance frequencies near 330 kHz and spring constants of 40 N/m (MikroMasch). By scanning the sample area and substrate area in the same scan, the AFM images can be used to explore the film thickness of the inkjet-assisted LbL encapsulated arrays. The difference in height between the film and substrate from AFM images was calculated using AFM software and was used to determine the thickness of the inkjet-assisted LbL encapsulated arrays.

3.3.3. Confocal Laser Scanning Microscopy (CLSM)

CLSM can record the change of the fluorescent intensity at particular position at different times to study release and diffusion mechanisms for drug release and biosensing applications. Therefore, CLSM was used to study encapsulation efficiency, release properties and biosensing capabilities of the inkjet-assisted LbL encapsulated arrays. The confocal images of the inkjet-assisted LbL encapsulated arrays were obtained with a LSM 510 NLO META inverted confocal laser scanning microscope equipped with a 63 × 1.4 oil immersion objective lens (Zeiss, Germany). The excitation/emission wavelengths were 488/515 nm.[70]

3.3.4 Optical microscopy

Optical microscopy is a standard technique used to observe structural properties and printing quality of samples. Optical microscopy obtains optical images from the light absorption and reflection of the samples. An optical fluorescent microscope (DM 4000M, Leica) was used to investigate the overall stability and patterning performance of the LbL arrays before and after encapsulation of Rhodamine dye. The inkjet-assisted LbL encapsulation arrays were placed on an optical microscope frame, which was then used to observe the uniformity of the multi deposition process and the stability of the thin film with different resolution.

3.3.5.Attenuated Total Reflection Fourier Transform Infrared Spectroscopy (ATR-FTIR)

Crystalline β-sheets of silk molecules can be explored using ATR-FTIR techniques. For the ATR-FTIR measurement, the samples were tested with a Bruker FTIR spectrometer Vertex 70 equipped with a narrow-band mercury cadmium telluride detector and the internal components of FTIR were purged with dry nitrogen. Spectra were collected at 4 cm^{-1} resolution with a 120 averaged scanning cycle. The bare ATR crystal was used as a background and D_2O buffer solution was used to eliminate overlap of the IR spectra of silk and other polymers in the 1700-1500 cm^{-1} region.[80] The light absorption peak at 1623 cm^{-1} demonstrated the formation of silk β-sheets in inkjet-assisted LbL encapsulation films.[81] In addition, a C=O bond in the silk backbone coupled to N-H bending and C=N stretching at 1660-1700 cm^{-1} can be confirmed as the characteristic of amide I band.[82]

3.3.6. Scanning Electron Microscope (SEM)

SEM (Hitachi-3400, LEO 1530, and Zeiss Ultra 60) was used to investigate the morphology of the inkjet-assisted arrays. In SEM analysis, samples were mounted on conductive carbon tape, sputtered with Au to make a film of approximately 10 nm, and imaged with an operating voltage of 5-10 keV. The samples were observed under different resolutions to investigate surface morphology, structural stability, and LbL assembly.

3.4. Experimental studying of inkjet-assisted LbL encapsulated arrays property

3.4.1. Printing and patterning performance

The patterned films were investigated in order to determine the accuracy of multi-film deposition from inkjet printing. An optical fluorescent microscope was used to study the uniformity of film structures and the drop size in both overall pattern and within individual films in order to investigate printing quality, misprinting and patterning results. Fluorescent images were also used to confirm the deposition of Rhodamine dyes in the inkjet-assisted LbL encapsulated arrays.

3.4.2. Surface morphology and film thickness

After finishing the sample preparation, the surface morphology of the inkjet-assisted LbL encapsulated arrays was characterized using AFM. The samples were scanned with 100 μm x 100 μm, 20 μm x 20 μm, and 5 μm x 5 μm scan sizes to investigate surface morphology of the inkjet-assisted LbL encapsulated arrays. Film thickness can be

characterized by scanning both an inkjet-assisted LbL encapsulated dot and a surface of the substrate. AFM program (NanoScope) was used to obtain the average film thickness from the AFM images.

3.4.3. Film stability

The inkjet-assisted LbL encapsulated arrays were deposited in phosphate buffer at pH 3.5 with different exposure times to investigate their structural stability in solution. After being exposed to an acidic buffer, the thin films were washed with distilled water at pH 3.5 to remove any salt remaining on the arrays. The samples were dried with air and inspected using an optical microscope and AFM to determine the change of film structure, surface morphology, and thickness. The stability of the encapsulated Rhodamine dye in the arrays was investigated by measuring the change of fluorescence intensity using optical fluorescent microscopy.

3.4.4. Cell viability

Cell viability was assessed with live-dead and rezasurin assay kits according to manufacturer's protocols (BioVision). For the live-dead test, representative images were collected with a Zeiss 510 Vis LSM using a band-pass filter (Ex/Em=488/515 and 543/560 nm for detection of FITC and Rhodamine). Confocal micrographs were analyzed with the Zen2009 software to quantify the number of pixels corresponding to fluorescent emission from live (green) and dead (red) cells. According to the protocol for the live-dead cell staining kit, only healthy cells were strained by the cell-permeable live-dye and emit green fluorescence. Dead cells were stained by both the cell-permeable

live-dye (green) and the cell non-permeable PI (red), and therefore exhibit a yellow-red fluorescence. In short, to total number of green cells corresponded to the total number of living cells.

3.4.5. pH responsive properties of inkjet-assisted LbL dot array

The samples were deposited in buffers with different pH to investigate the pH responsive properties of the inkjet-assisted LbL encapsulated arrays. First, the samples were submerged in a pH 3.5 buffer and inspected to determine the change of fluorescence intensity of the Rhodamine dye in the inkjet-assisted LbL encapsulated arrays by a Zeiss LSM 510 NLO w/ META MPE confocal microscope. The fluorescent intensity was measured with different deposition times in the buffer and is shown in the graph of fluorescence intensity versus deposition time in the confocal software. The samples were also deposited in buffer with different pH and investigated to determine the change of fluorescence intensity of rhodamine dye in the inkjet-assisted LbL encapsulated arrays with a variety of deposition times. All data was plotted in one graph to demonstrate the relationship between the changes of fluorescence intensity and buffer pH with different deposition time.

3.4.6. Biosensing properties of inkjet/stamping-assisted LbL encapsulated *E-coli* array

Inkjet-assisted LbL encapsulated cells are incubated using 5 mM theophylline in SMM media at 30 ^{o}C to induce riboswitch expression. Theophylline molecules diffuse from the media through protective layers and the cell wall to interact with sensing organs in *E-coli*

cells. The cells emit light after interaction with theophylline molecules. The emission can be visualized by consecutive scanning mode using two filters with excitation/emission wavelengths 488/515 and 543/560 nm. The fluorescent intensity is measured while exposing the samples to an analyzed solution with different exposure times for understanding biosensing property of the inkjet/stamping-assisted LbL encapsulated cells.

CHAPTER 4

INKJET-ASSISTED LAYER-BY-LAYER PRINTING OF ENCAPSULATED ARRAYS

4.1 Introduction

Ultrathin functional polymer films, micropatterned arrays, and microcapsules are important for diverse applications in sensing, catalysis, cell culture, and drug delivery.[83,84] LbL is one of the prominent techniques which can be used to create such materials and structures with controlled thicknesses, morphology, diverse functionalities and unique structures.[85,86] LbL component selection might include regular polyelectrolytes, dendrimers, proteins, nanoparticles, colloids, and biomaterials.[87,88,89,90,91,92,93,94,95,96,97,98] Further tailoring of LbL multilayer structures, beyond uniform films and spherical microcapsules, for demanding applications is focused on the adaptation of such advancements in the known nanotechnologies such as inkjet printing, micro-contact printing, micro-molding and dip-pen nanolithography.[99,100,101,102,103,104,105,106107] These approaches allow for the facile fabrication of patterned LbL structures with controlled spatial configurations which have multicompartment periodic patterned structures at different length scales.

However, despite significant progress, the formation of discrete LbL structures with controlled shapes and a periodic spatial arrangement of components in large arrays remains a challenge while using conventional dip-, spin-, and spraying methods.[108,109] On the other hand, the inkjet printing technique, which utilizes microdroplet deposition

via a microscopic nozzle, can be considered a facile and powerful top-down route for creating complex arrays when combined with bottom-up LbL assembly. Accordingly, inkjet printing-assisted LbL multilayer assembly is expected to yield well-defined micropatterned structures with nanometer thickness and microscopic lateral dimensions. Using inkjet printing enabled manipulation of the drop size, location and speed to fabricate the complex dot arrays according to a pre-programmed automatic process.[17,110,111] The uncontrolled spreading of liquid droplets on solid substrates following impact and dewetting processes due to a mismatch in surface energy might compromise the printing resolution due to e.g. coffee ring formation during the drying process. Droplet spreading is a common issue complicating this technique and its effect can be mitigated by controlling the distance between substrate and nozzle, viscosity of the ink solution, evaporation rate, and the use of a suitable primer coating on the substrate. To increase the speed of the deposition process, rapidly drying layers of minute thicknesses are used which helps preventing a deviation from the initial shape during multiple deposition cycles. Well-aligned microprinting processes lead to minimized deviation from a targeted center during the multiple repetition of LbL deposition and thereby builds LbL structures with microscopic precision. The size of the polymer droplets can be further reduced with the assistance of an electric field, down to a few hundred nanometers in diameter.[112]

Several examples of applying inkjet printing for LbL film formation from different pairs of polyelectrolytes with hydrogen and ionic interactions have recently been demonstrated.[113,114] In these studies, the authors demonstrated that inkjet-assisted LbL

assembly can be indeed utilized to fabricate large scale uniform ultrathin films and micropatterns with a typical resolution in the range of 100-300 μm. It has been suggested that even higher spatial resolution can be achieved by reducing the nozzle dimensions, viscosity of solution, impact of the liquid droplets to a substrate, and liquid spreading.[115] These parameters can be used to build patterns with complex compositions. However, very little has been published to date on high-resolution micropatterned composite LbL arrays via inkjet-assisted LbL assembly.

Here, we report on the fabrication of higher-resolution and large scale arrays of LbL dots with encapsulated fluorescent dye via facile inkjet-assisted LbL assembly without a rinsing step. The model dye compound, Rhodamine 6G, was efficiently encapsulated within pH responsive hydrogen-bonded robust PVPON/PMAA LbL dots. Microscopic LbL dots around 100 μm in diameter were fabricated with different numbers of bilayers ranging from 2 to 15 with the thicknesses between 50 nm and 500 nm. Moreover, we achieved higher spatial resolution with LbL dot diameter decreasing to below 40 μm by applying microprinting with the narrowest nozzle and limiting droplet spreading on highly hydrophobic substrates.

4.2 Experimental details

Inkjet-assisted LbL printing was conducted by adjusting pH condition of a 1 mg/ml *PVPON* solution to pH 3.5 and printing the polymer solution on a glass substrate both with and without a polymer coating. A 1 mg/ml PMAA solution at pH 3.5 was printed at the same positions on top of the PVPON layer in order to form a single bilayer. The

printing process was repeated by following these steps to fabricate LbL dots of varying thickness. Intermediate rinsing steps, otherwise common in LbL fabrication, was not used in these inkjet-printing processes. A JetLab II ink-jet printer (MicroFab Technologies) was used for experiments with 50 and 20 μm nozzle diameters for printing PVPON/PMAA dots and 20 μm nozzle for deposition of Rhodamine dye. The printing speed was around 100 dots per 30 second without intermediate drying steps.

Encapsulation of fluorescent dye into LbL dots was achieved by first fabricating 1, 3, or 5 bilayers followed by the addition of Rhodamine 6G deposited from an independent nozzle in the middle of the existing polymer bilayer dot structure (Figure 3.2.1). The dot was then capped with 1, 3 or 5 LbL bilayers. Arrays of LbL dots with encapsulated fluorescent dye between different of number of bilayers were formed: 2 bilayers (1+1 bilayer), 6 bilayers (3+3 bilayer), and 10 bilayers (5+5 bilayers). The pattern used for printing was uploaded from a monochromatic (black and white) bitmap file. The white pixels denoted “print” areas whereas the black areas were “do not print” areas and was uploaded to the JetLab II program prior to use. The number of pixels controlled the size of the pattern and the distance between the printed dots both on the x- and y-axis. The maximum speed of operation was 900 Hz and number of LbL dots was 100.

4.3 Results and discussion

Inkjet-assisted LbL printing is conducted by adjusting pH condition of a 1 mg/ml PVPON solution to pH 3.5 and printing the polymer solution on a substrate. A 1 mg/ml PMAA solution at pH 3.5 is printed at the same positions on top of the PVPON layer in order to form a single bilayer. Encapsulation of Rhodamine 6G into LbL dots is achieved by first fabricating 1, 3, or 5 bilayers. Subsequently, the Rhodamine 6G, a model of therapeutic molecule, is deposited from an independent nozzle in the middle of the existing polymer bilayer dot structure. The dot is then capped with 1, 3 or 5 LbL bilayers.

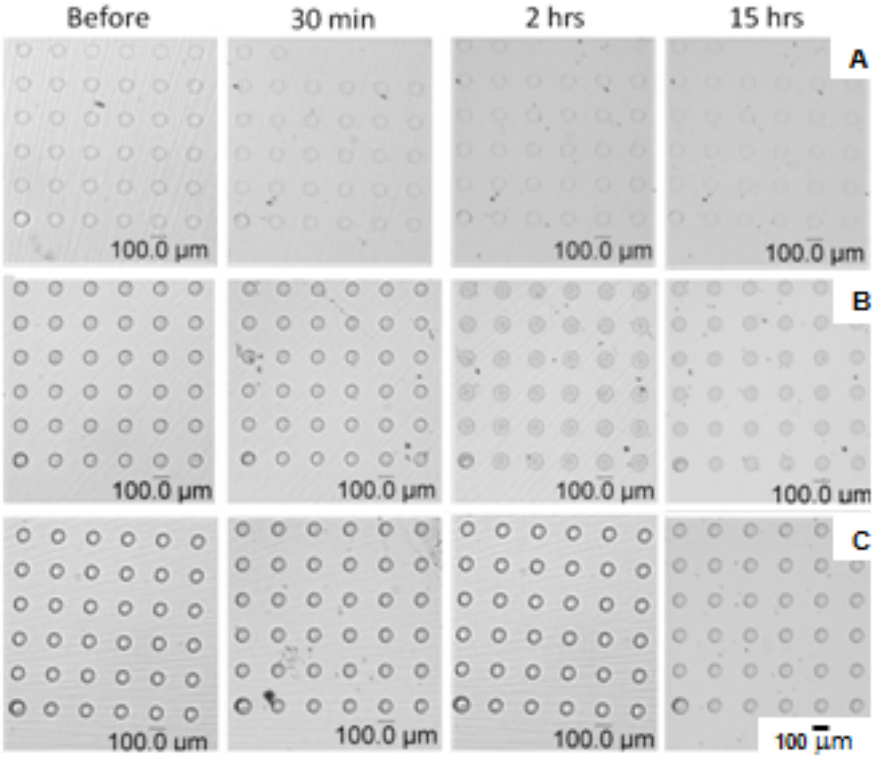

Figure 4.3.1. Optical microscopic images demonstrate the LBL dot array with different exposure times in buffer with pH 3.5: (A) 1 bilayer, (B) 3 bilayers, and (C) 5 bilayers.

Finally, arrays of LbL dots with encapsulated fluorescent dye between different of number of bilayers are formed: 2 bilayers (1+dye+1 bilayer), 6 bilayers (3+dye+3 bilayer), and 10 bilayers (5+dye+5 bilayers). Inkjet printing is conducted on different hydrophilic and hydrophobic substrates including hydrophilic (glass, silicon) and hydrophobic (PHS, PS) substrates. Optical images in Figure 4.3.1. demonstrate a 6 x 6 dot array with different numbers of LbL bilayers printed on a PHS substrate. LbL dots printed on PHS and PS surfaces are the primary focus of this work since the hydrophobic surface allowed higher resolution printing than glass or silicon substrates. The hydrophobic surfaces prevent the spreading of the liquid droplets after impact allowing it to remain confined to a single area with better resolution (Figures 4.3.2 and 4.3.3).

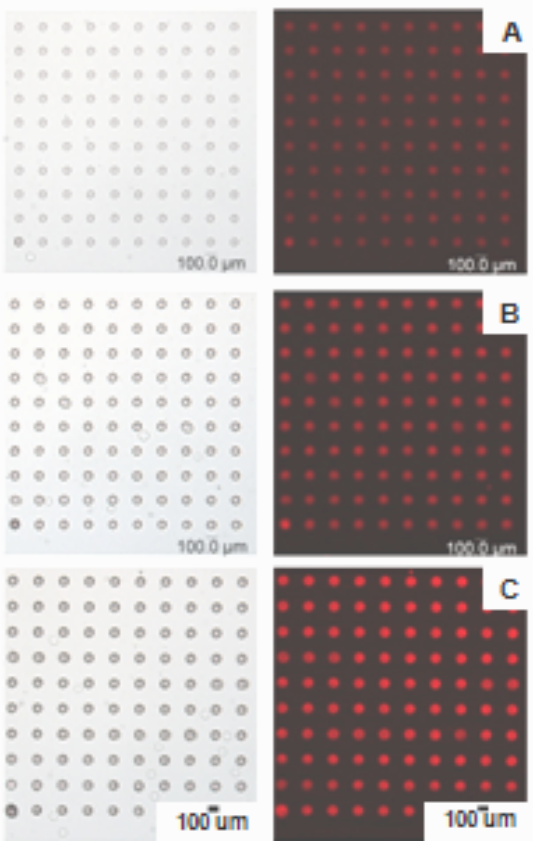

Figure 4.3.2. Optical (Left) and fluorescent (Right) images of a 10x10 array PVPON/PMAA LbL films with encapsulated Rhodamine dye on PS coated substrates: A) 2 bilayers, B) 6 Bilayers, and C) 10 bilayers.

The droplet diameter during deposition under optimized conditions with a 50 μm nozzle is around 45 μm (Figure 4.3.5). However, the average diameter of the LbL dots on PHS substrate is around 90 μm due to the spreading behavior of the polymer solutions from impact during printing (Figures 4.3.4). The diameter of the LbL microdots remains constant for different numbers of LbL bilayers and varies from 95.7 ± 1.8 μm for 1 bilayer dots to 87.9 ± 1.1 μm for 5 bilayer dots.

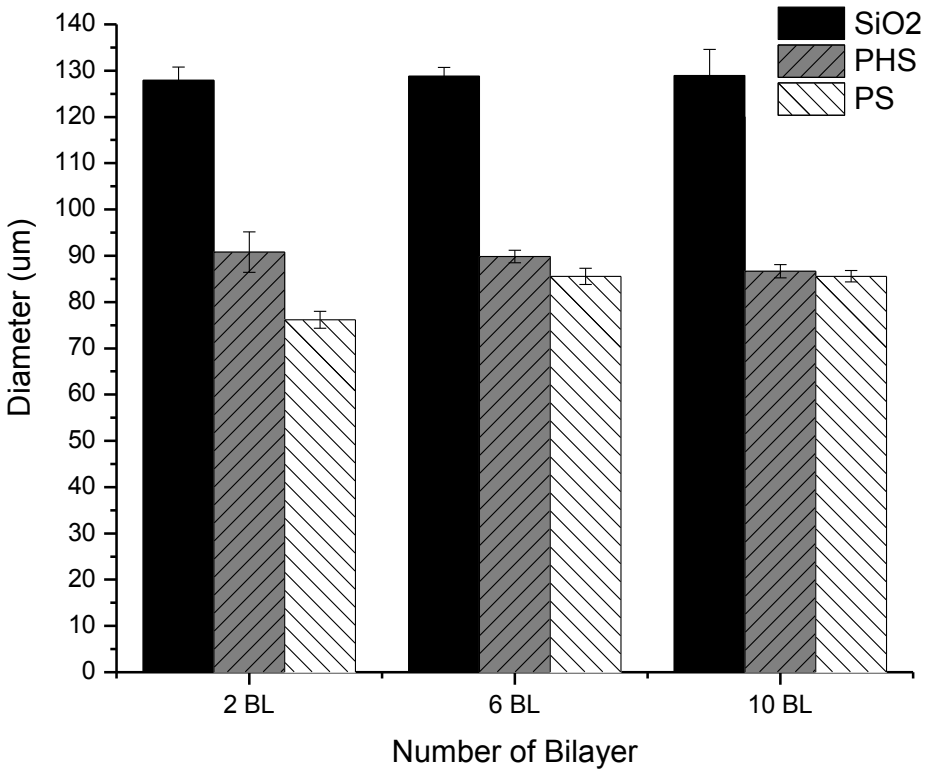

Figure 4.3.3. Variations of diameter of LbL encapsulation films as a function of number of bilayers on different substrates.

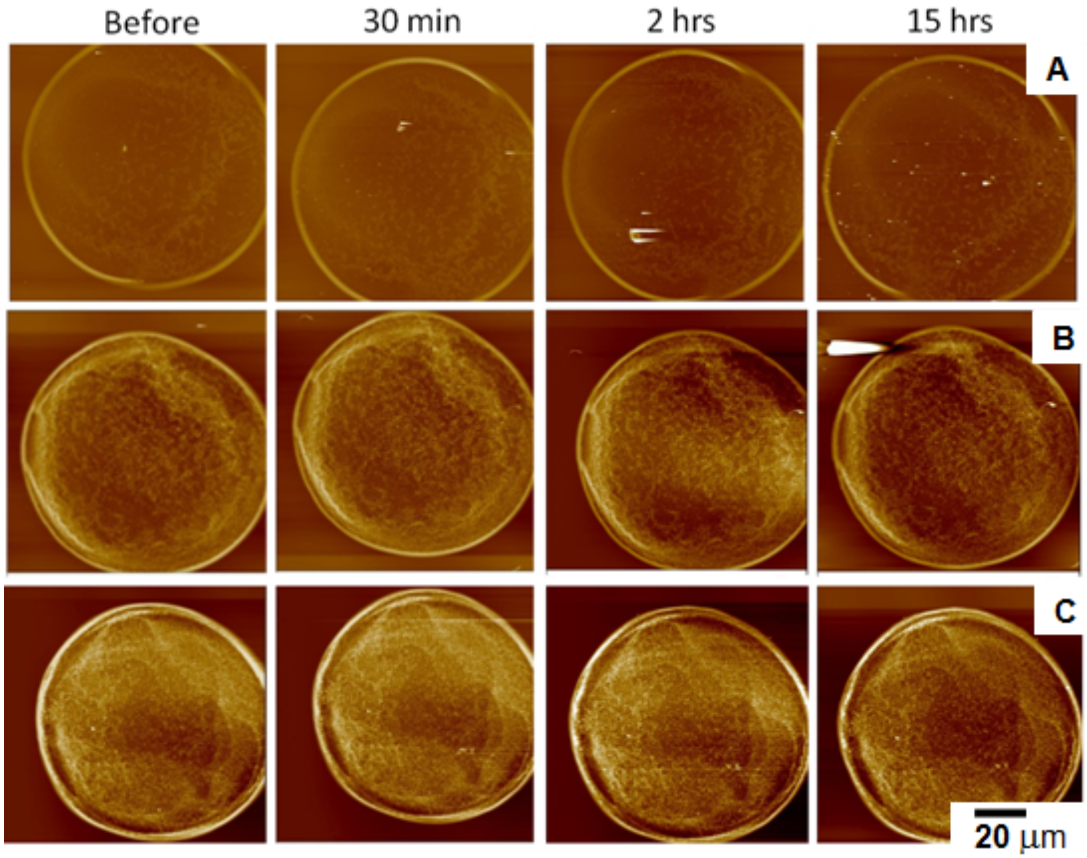

Figure 4.3.4. AFM images of LBL dot with diffrent exposure times in buffer pH 3.5: (A) 1 bilayer, (B) 3 bilayers, and (C) 5 bilayers. The bottom right image in (C) is a 3-D image of 5 bilayer LbL dot after expose to buffer for 15 hrs. The scale size is 100 µm for all images. The height is 500 nm for all AFM images and 2 µm for 3-D AFM image.

We suggest that this consistency in dimension is due to the restriction of solution spreading on the hydrophobic polymer surface, even after multiple repetitions of LbL deposits. A PVPON droplet printed on a PHS substrate formed a coffee ring structure where the height of the edge of the dot is higher than the center of the structure (Figure 4.3.4). The stability of LbL dot arrays after printing is tested by storing LbL arrays in a pH 3.5 buffer solution for different periods of time up to 15 hrs. The dots are then monitored optically for any degradation or dissolution and with AFM for any changes in surface morphology (Figures 4.3.7).

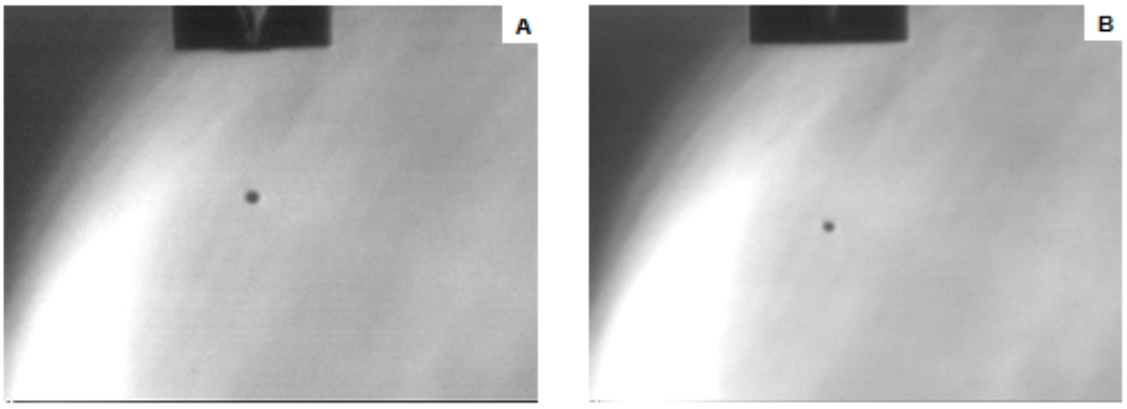

Figure 4.3.5. Optical images display the nozzle and droplet size of (A) PVPON droplet from a 50 µm nozzle in diameter and (B) Rhodamine droplet from a 20 µm nozzle in diameter.

AFM images at different scales show relatively uniform surface morphology of the LbL dots even after prolonged exposure to the buffer solution (Figures 4.3.4, 4.3.7, and 4.3.8). The AFM images demonstrate very consistent shape and dimensions of different LbL dots at different locations and after different deposition cycles. The subsequent droplets, which are placed on the same position, are limited in spreading and the overall diameter of the growing LbL dot remains confined to this initial size. The elevated height of the

LbL dot edges after the initial deposition is a direct result of the coffee-ring effect which occurs during the formation of the film and subsequent drying.[116,117,118,119] The evaporation of the polymer solution after deposition on a substrate create a capillary outward flow from the center of the film to the edge, which caused the formation of characteristic coffee-ring structure.[120,121,122]

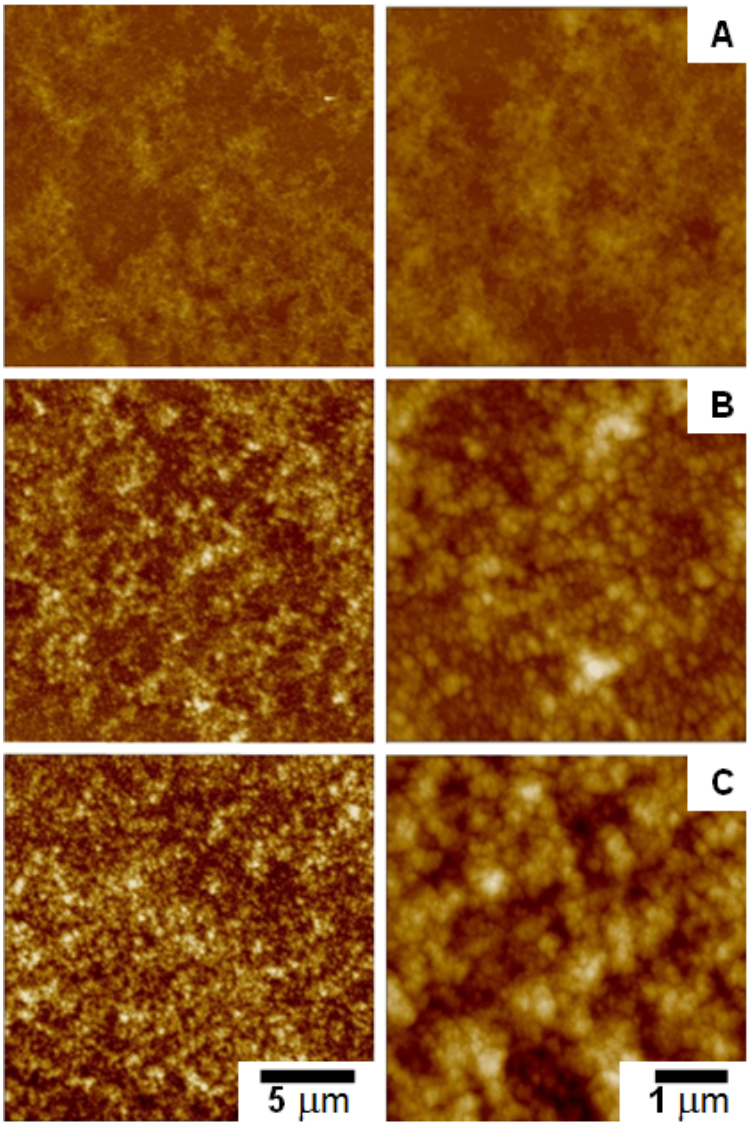

Figure 4.3.6. Higher resolution AFM images (Left; 20x20 µm and Right; 5x5 µm) displaying the surface morphology of LBL dots with (A) 1 bilayer, (B) 3 bilayers, and (C) 5 bilayers. The height is 200 nm for all images.

We suggest that this consistency in dimension is due to the restriction of solution spreading on the hydrophobic polymer surface, even after multiple repetitions of LbL deposits. A PVPON droplet printed on a PHS substrate formed a coffee ring structure where the height of the edge of the dot is higher than the center of the structure (Figure 4.3.4). The stability of LbL dot arrays after printing is tested by storing LbL arrays in a pH 3.5 buffer solution for different periods of time up to 15 hrs. The dots are then monitored optically for any degradation or dissolution and with AFM for any changes in surface morphology (Figures 4.3.7).

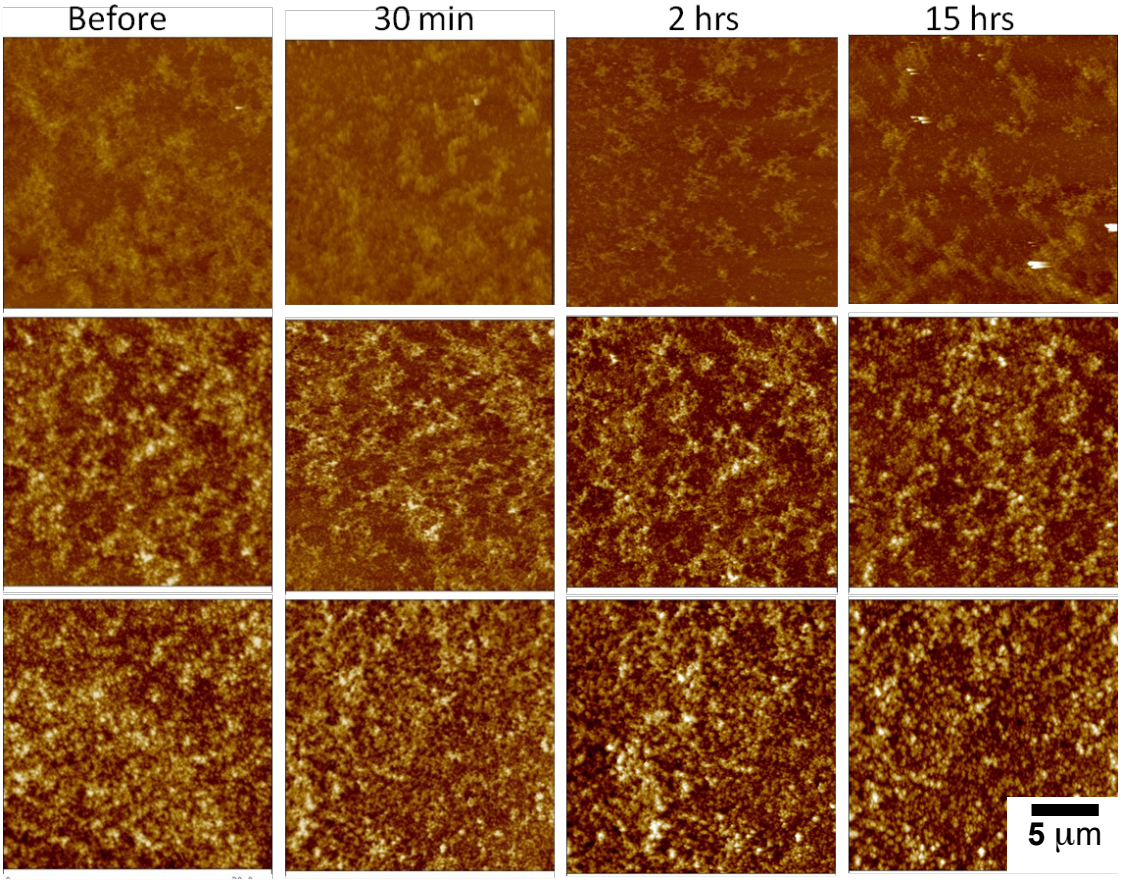

Figure 4.3.7. High resolution AFM images displaying the surface morphology of LBL films with different exposure times in buffer at pH 3.5: (A) 1 bilayer, (B) 3 bilayers, and (C) 5 bilayers. The scale size is 20 µm and the height is 200 nm for all images.

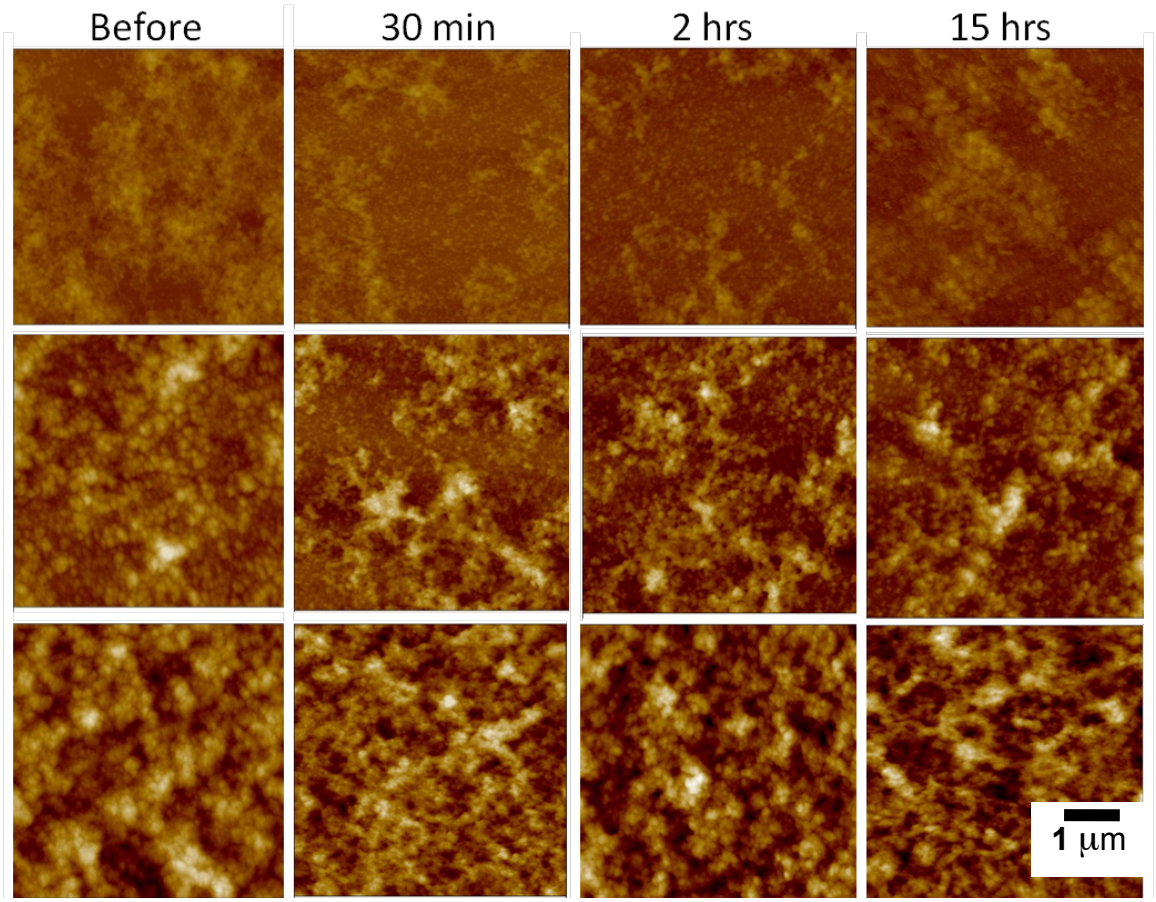

Figure 4.3.8. High resolution AFM images displaying the varied surface morphology of the LbL films with diffrent exposure times in buffer pH 3.5: (A) 1 bilayer, (B) 3 bilayers, and (C) 5 bilayers. The scan size is 5 μm and the height is 200 nm for all images.

The AFM images demonstrate uneven surfaces associated with such a redistribution of polymer components during the droplets impact followed by solution drying with large-scale roughness (20 μm x 20 μm) ranging from 12 nm to 30 nm, still well below the average dot thickness.[123,124] The relatively smooth morphology is observed at higher magnification with modest domain surface texture associated with local domain

formation caused by component aggregation as traditionally observed for hydrogen-bonded LbL films.[125,126,127,128]

The micro roughness at small scale surface areas (1 μm x 1 μm) is much lower, between 6 and 20 nm. This value corresponds to typical values previously observed for hydrogen-bonded planar LbL films[129] and LbL microcapsules. [130,131] The similarities in surface roughness indicate that LbL formation of microscopic dots with high-speed droplet delivery does not significantly alter the local morphology and microstructure from that of previously studied hydrogen-bonded LbL films and structures.

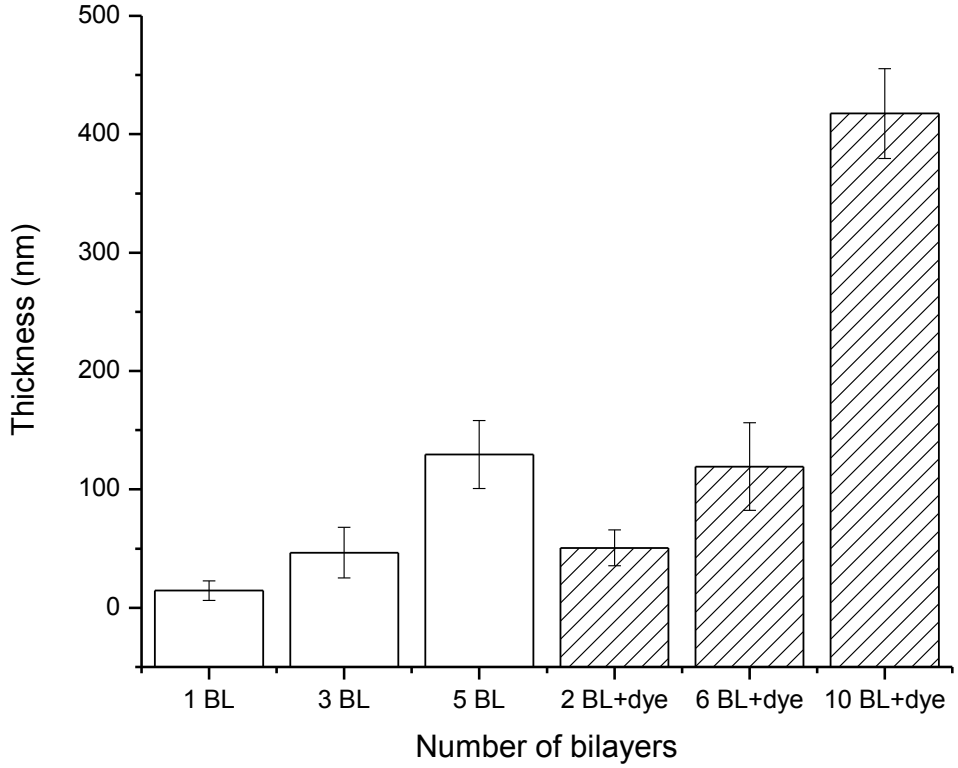

Figure 4.3.9. Thickness of LbL dots (empty) and LbL dye-encapsulated dots (dashed) vs number of bilayers. The error bars represent the average micro roughness of each sample.

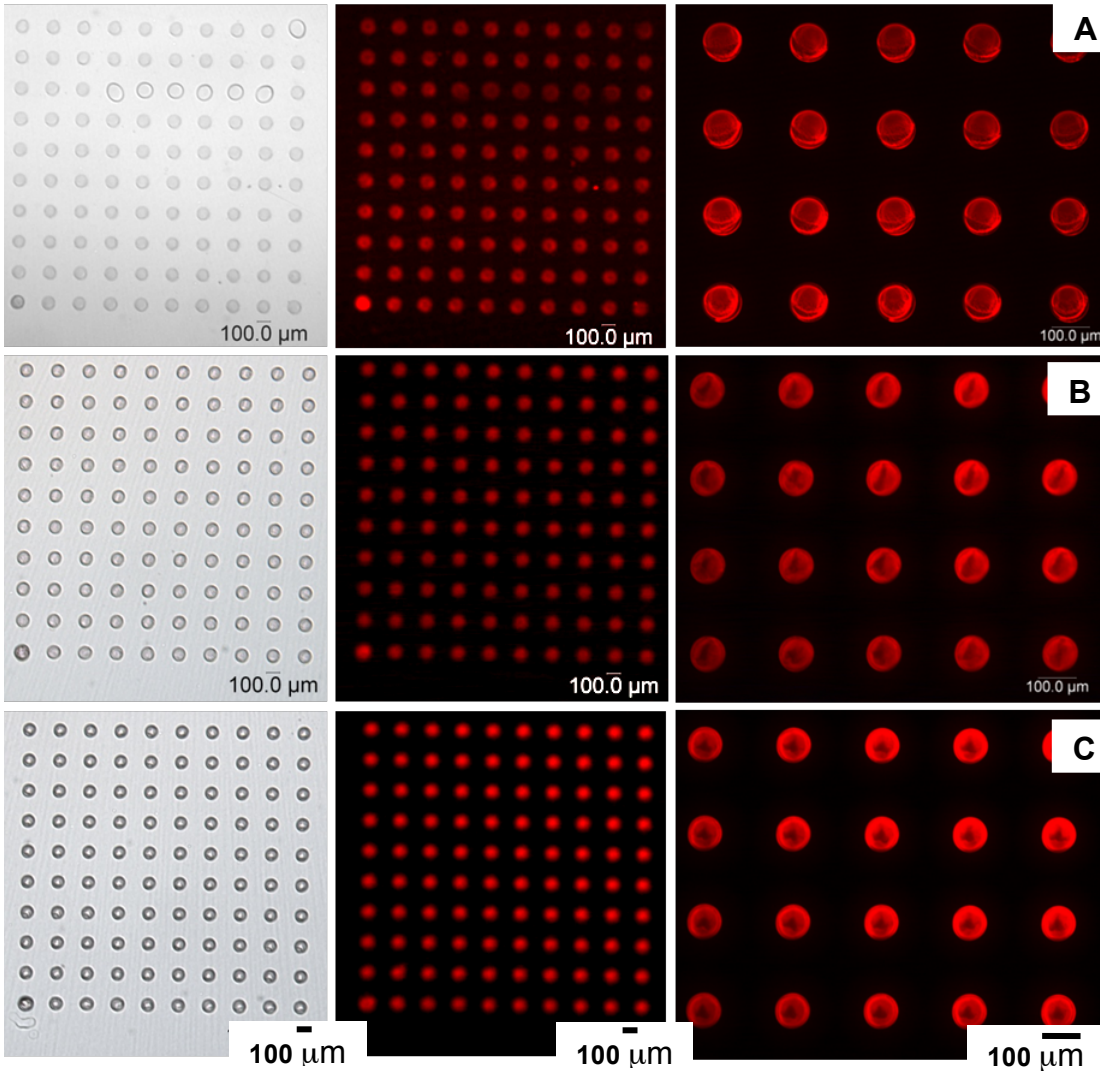

Figure 4.3.10. Optical and fluorescent images of 10x10 arrays of PVPON/PMAA LbL dots with encapsulated Rhodamine dye with different number of bilayers: A) 2 bilayers, B) 6 bilayers, and C) 10 bilayers.

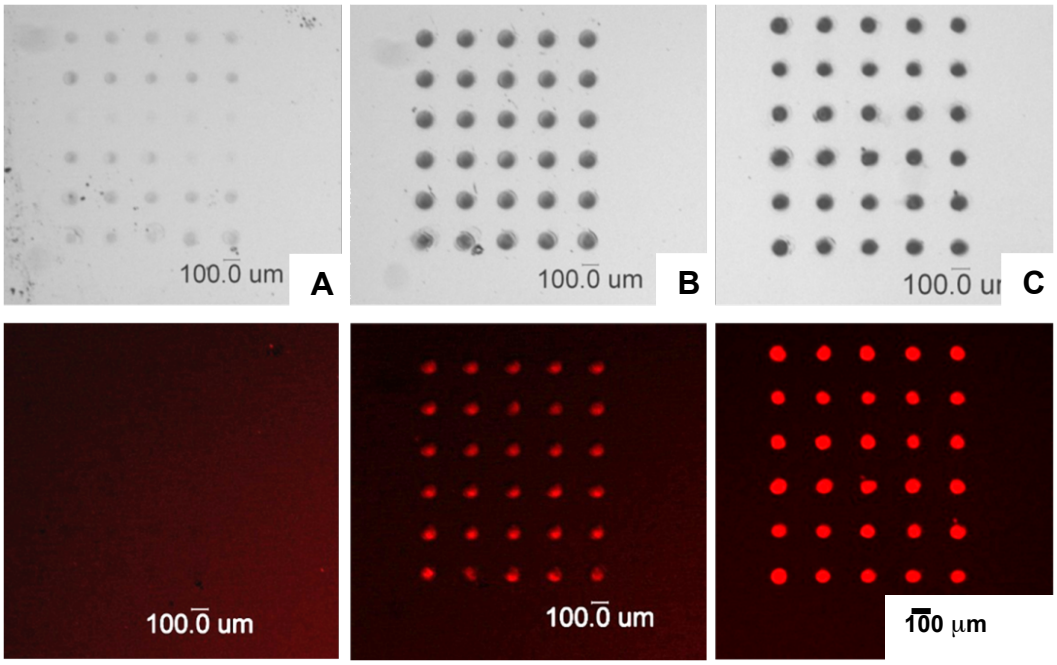

Figure 4.3.11. Optical microscopic (top) Fluorescent images (bottom) of the LBL encapsulation with Rhodamine dye inside after deposited in buffer pH 3.5 for 15 hrs: (A) 2 bilayers, (B) 6 bilayers, (C) 10 bilayers.

The thickness of the LbL dots increases dramatically with the number of depositions where the average thickness reaches 130 nm for 5 bilayers and 400 nm for 10 bilayers (with added dye deposit) (Figure 4.3.9). The average increment of the thickness growth is close to 40 nm per bilayer for the thicker dots. This thickness increment is much higher than thicknesses of other LbL films fabricated from similar components (around 4-6 nm per bilayer).[132,133,134,135] This difference in thickness growth rate might be caused by several important differences between ink-jet assisted LbL fabrication and traditional LbL assembly methods.

First, it is apparent that the forced delivery of the components to the confined surface area is limited by the initial spreading/dewetting of the aqueous solution on the hydrophobic substrate. This confinement results in the presence of an excess amount of material within the area surrounded by the elevated rim. Second, the absence of the washing step causes any excess amount of polymer solution to stay within this limited surface area thus promotes the formation of relatively uniform and thick additions of weekly bonded material. Third, we suggest that high inter-diffusion of polymer chains into pre-formed swollen films can be promoted by both strong impact as well as high mobility of weakly bonded polymer components common for this type of LbL films.[136,137,138]

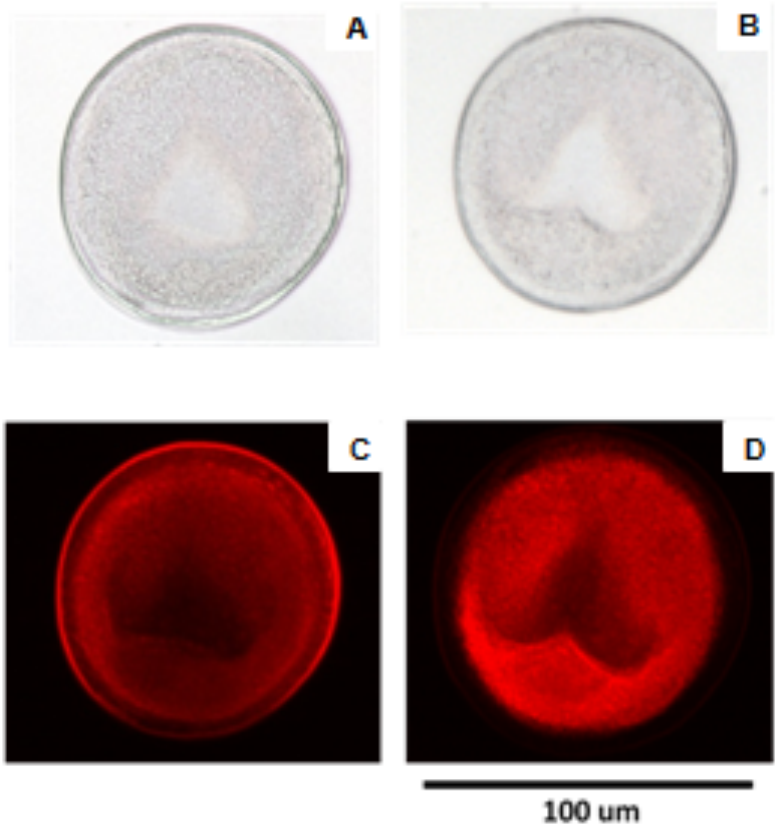

Figure 4.3.12. Optical (A, B) and fluorescent (C, D) images of 10 bilayers (5+dye+5 bilayers) of PVPON/PMAA LbL films with encapsulated Rhodamine dye: before (A, C) and after (B, D) exposure to buffer solution of pH 3.5 for 15 hrs.

Next, the deposition of fluorescent dye in the center of LbL dot followed by the capping polymer film with different number of bilayers resulted in the uniform array of highly fluorescent dots which saw the thickness increase to about 400 nm for 10 bilayer dots (Figure 4.3.9 and 4.1.10). The fluorescent images indicated the consistency of the printing process and the long-term stability of the encapsulation printing under acidic buffer condition, even as the number of deposition cycles exceeds 6 (Figures 4.3.11 and 4.3.12). The average diameter of the printed dots is 82.4 ± 5.4 μm with the 50 μm diameter inkjet nozzles and remains virtually unchanged for different printing conditions and also after exposure to the buffer solution (Figure 4.3.13).

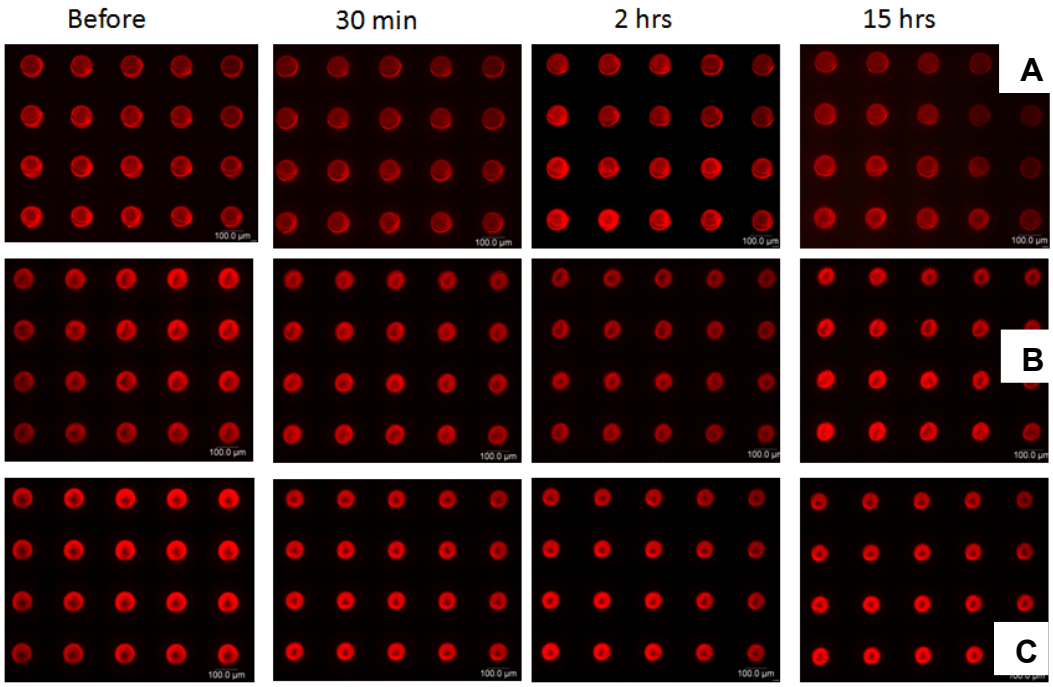

Figure 4.3.13. Fluorescence microscopic images the LBL encapsulation with (Rhodamine dye inside) with diffrent number of bilayers: (A) 2 bilayers, (B) 6 bilayers, and (C) 10 bilayers.

AFM images show that despite an overall uniform appearance, the central area of the dots seems to be depressed as indicated by reduced optical scattering, fluorescent intensity, and the overall elevation (Figure 4.3.14). We suggest that both confined spreading and impact at the central location result in such a non-uniform distribution of components after deposition. Also, the fluorescent dye might be partially re-dissolved and forced from the center of the dot after multiple depositions. Such a coffee ring-like structure still remains visible for the thickest dots fabricated here (around 400 nm) but overall dot smoothing resulted in the central depression not exceeding 30-40% of the overall thickness (Figure 4.3.14). Increasing uniformity of the dots is observed with the increasing thickness through multiple layer depositions. These results demonstrate that capillary flow, central-area impact, and elevated rims play a significant role in the final morphology of the microscopic LbL dots.

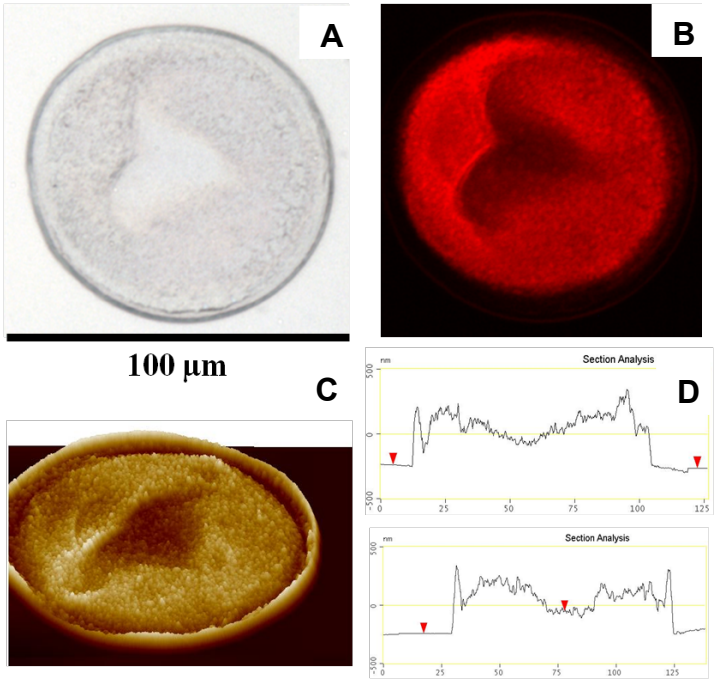

Figure 4.3.14. (A) Optical image, (B) Fluorescence image, (C) 3D AFM image with z-scale is 2 µm, and (D) cross-sections of 10 bilayer (5+dye+5) dots.

AFM images confirm the stability of the inkjet-assisted LbL dye-encapsulated dots under long term storage in acidic conditions. Only minor changes in the initial surface morphology and smoothing of the central depression are observed (Figures 4.3.15, 4.3.16, and 4.3.17). A minor reduction in the average thickness (5-15%) of the dots is observed after extended exposure to the acidic environment. The reduction in thickness is due to the dissolution of excess polymer, which remained in the structure since no rinsing step is used during fabrication to remove these unbound chains. The dots overall though showed excellent stability of the hydrogen bonded polymer layers, even after extended exposure to an acidic environment (Figure 4.3.18).

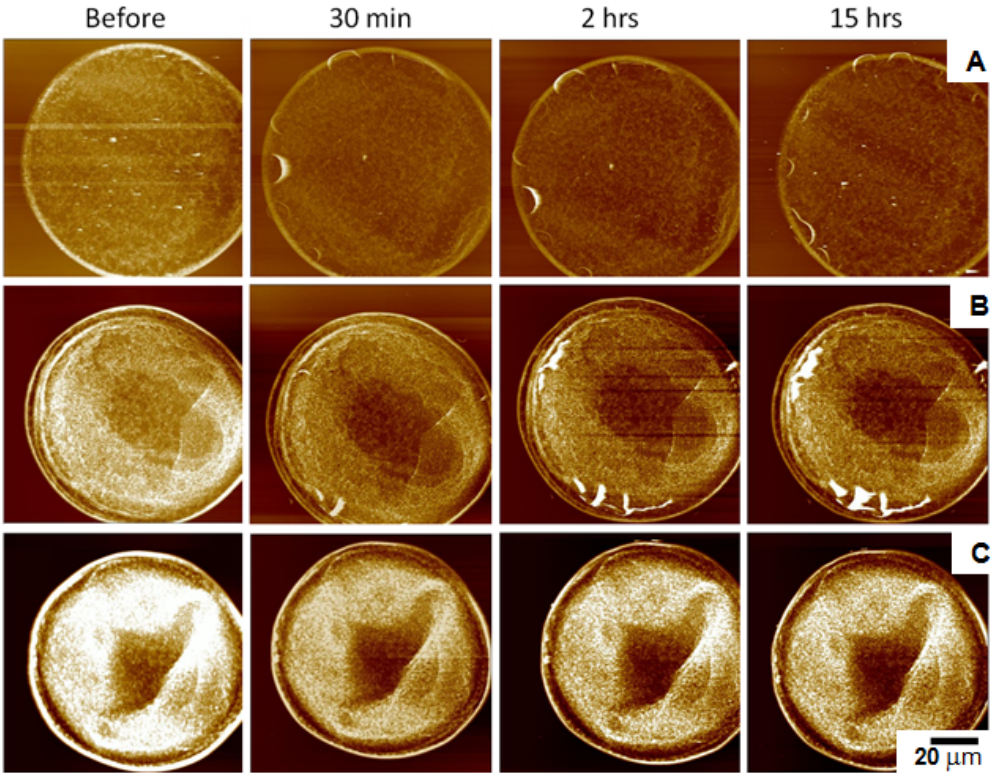

Figure 4.3.15. AFM images of inkjet-assisted LbL dye encapsulated dots with different exposure times in buffer pH 3.5: (A) 2 bilayers, (B) 6 bilayers, and (C) 10 bilayers. The scale size is 100 um and the height is 500 nm for all images.

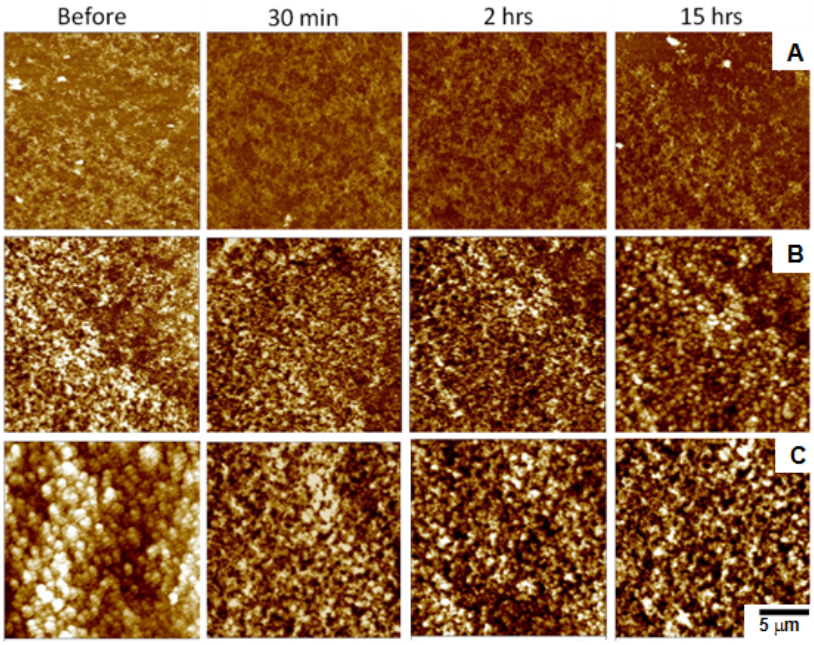

Figure 4.3.16. High resolution AFM images of LbL encapsulation with diffrent deposition time in buffer pH 3.5: (A) 2 bilayers, (B) 6 bilayers, and (C) 10 bilayers. The scale size is 20 µm the height is 200 nm for all images.

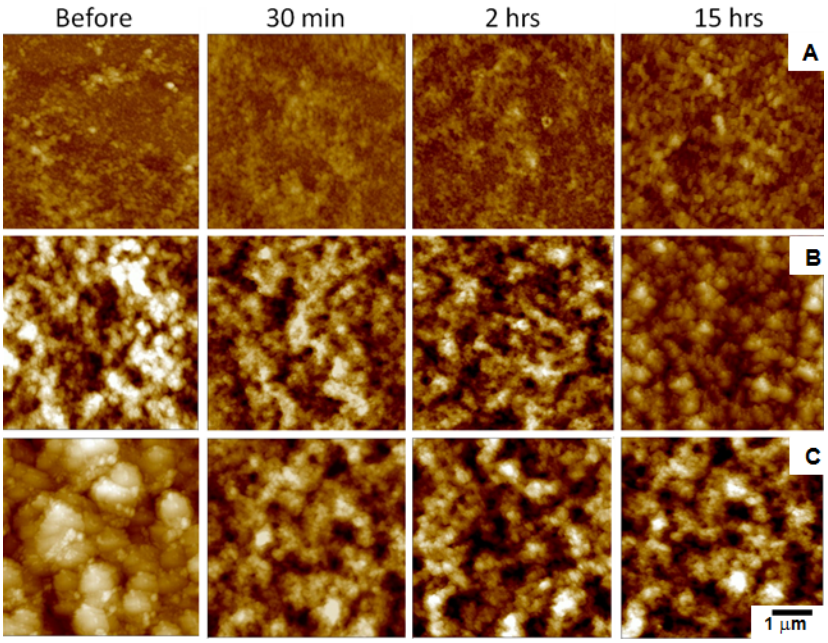

Figure 4.3.17. High resolution AFM images displaying the surface morphology of LbL encapsulation films with diffrent exposure time in buffer pH 3.5: (A) 2 bilayers, (B) 6 bilayers, and (C) 10 bilayers. The scan size is 5 µm and the height is 200 nm for all images.

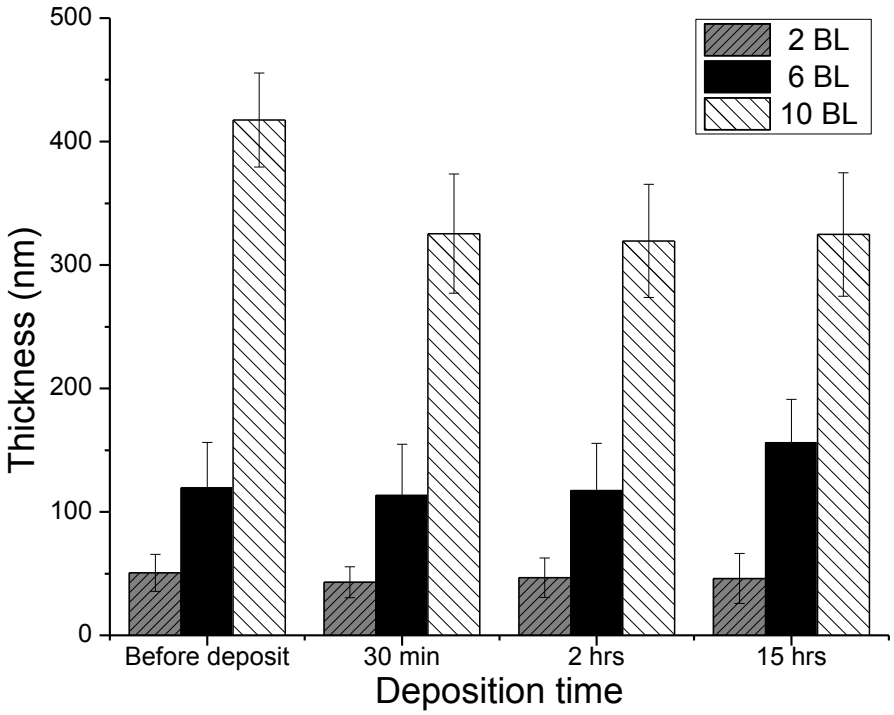

Figure 4.3.18. Thickness profile of LbL encapsulation films with diffrent deposition time in buffer pH 3.5. The error bars are the average roughness of each sample.

A direct comparison of various substrates is performed to assess the role of surface wettability and its impact on the inkjet assisted LbL printing (Figure 4.3.19). The encapsulated dot arrays are printed on substrates with the following surface wetting properties: clean SiO_2 wafers (contact angle 8^o), PHS coated glass (contact angle 71^o), and PS coated glass slides (contact angle 86^o) (Figures 4.3.20). As we observed, the smallest LbL dots formed on the hydrophilic surface with a diameter of 129 ± 3.5 μm, well exceeding the diameter of the deposited liquid droplet (50 μm). This sizable increase indicates major spreading of the polymer at the liquid-solid contact interface on the highly wettable surface. The size of the LbL dots decreased to 89 ± 2.4 μm and 82.4 ± 1.6 μm on PHS and PS substrates. Additionally, the overall brightness and uniformity

of the fluorescent array increase dramatically on the hydrophobic substrates (Figure 4.3.19).

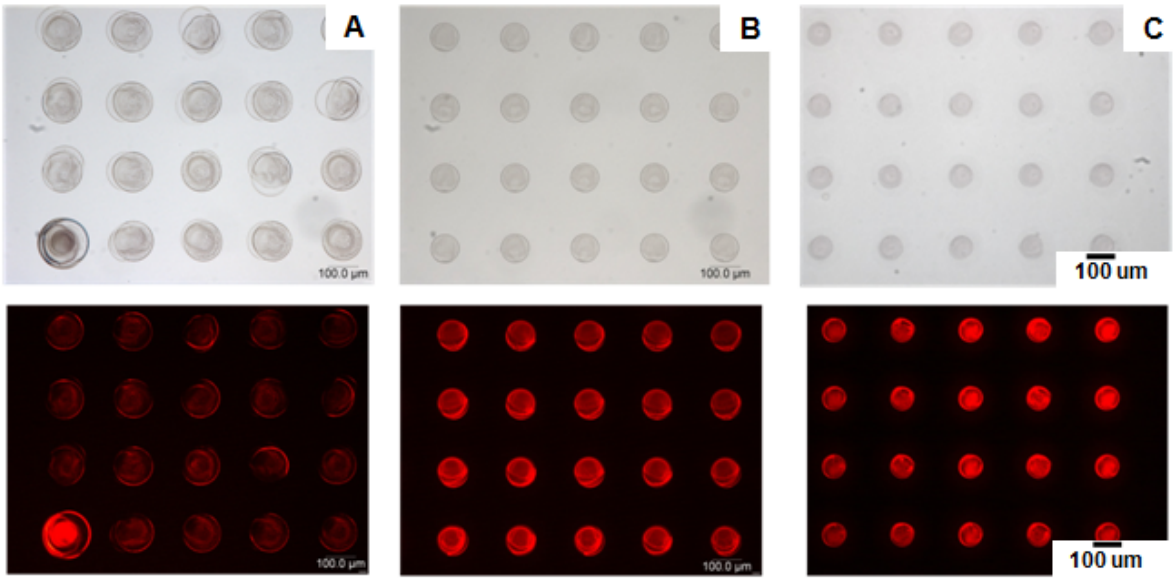

Figure 4.3.19. Optical and fluorescent images of 2 bilayer LbL dye-encapsulated dot arrays on different substrates: (A) silicon, (B) PHS substrate, and (C) PS substrate. The printing process start from the bottom left dot and ends at the top right spot.

Using the 20 µm diameter nozzle, the droplet size is reduced to 35 µm and the resulting printed LbL dot is measured at the smallest diameter of 37 µm on the PHS coated substrates. Using these substrates, we are able to fabricate features much smaller than those reported in earlier literature examples of LbL printing (around 100 µm) (Figure 4.3.21). This key observation indicates that the limiting factor in spatial resolution on a

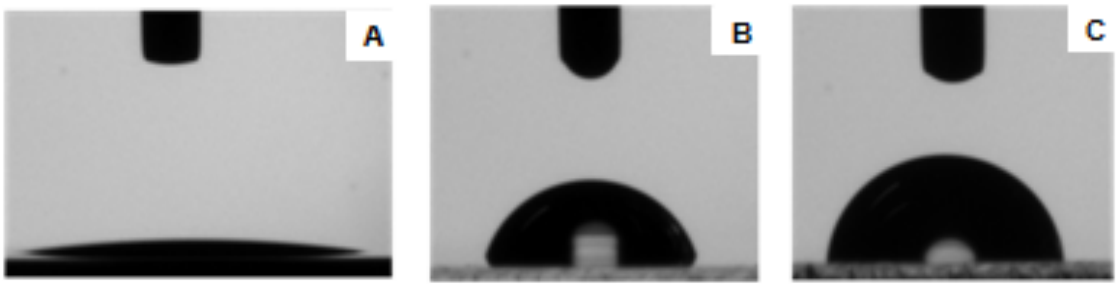

Figure 4.3.20. Contact angle measurement of substrates with different hydrophobicity: A) clean silicon, B) PHS coated substrate, and C) PS coated substrate

properly prepared substrate is the droplet size rather than the impact or spreading of the droplet on the non-wettable surface during printing. Hydrophobic surfaces designed to reduce solution spreading, are an essential component of the printing process to achieve printing of the smallest features possible. Thus, we suggest that the practical limit of inkjet-assisted LbL printing of polymer dots is about 10 μm as this is the size of the smallest commercial nozzle available.

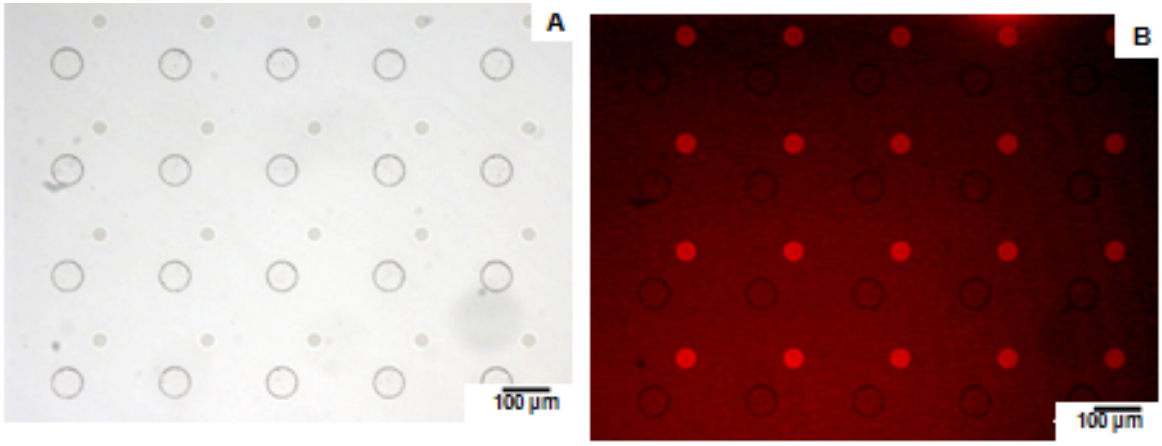

Figure 4.3.21. Optical (A) and fluorescence (B) images of an array of PVPON dots (large dots) and Rhodamine dots (small dots) printed from a 50 μm and a 20 μm nozzle, respectively.

Finally, we fabricate *GT* and inversed *GT* logos composed of fluorescent LbL dots on a PHS coated substrate using inkjet LbL printing to demonstrate the potential to create complicated patterns of dye-encapsulated dots (Figure 4.3.22). The Rhodamine solution is printed from a 20 μm in diameter nozzle and show well-resolved bright dots in the *GT* patterns (Figure 4.3.22). The dot size is around 35 μm and the printing process can be completed within 20 second, retaining high patterning accuracy.

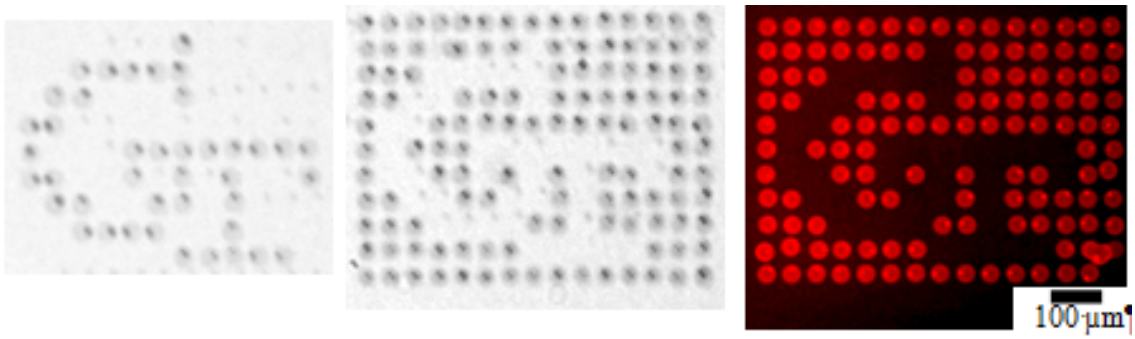

Figure 4.3.22. Optical (A, B) and fluorescent (C) image of inkjet-assisted LbL patterns: (A) GT logo, (B, C) Inversed GT logo.

pH responsive PVPON/PMAA films

The unique property of PVPON/PMAA LbL multilayer is pH responsiveness. The hydrogen bonding between PVPON and PMAA is stable below the pKa of PMAA (pH 5.5). The FTIR spectrum in Appendix confirms that hydrogen bonding is present between PVPON and PMAA around 3230 cm^{-1} (Figure A1). Therefore, the inkjet-assisted PVPON/PMAA multilayer films are stable in acidic condition as shown in Figure 4.3.23. The stability of the PVPON/PMAA multilayer films can be applied for encapsulation a variety of therapeutic molecules. In this study, Rhodamine fluorescent dye was used as an encapsulated therapeutic molecule in inkjet-assisted LbL films. The fluorescent intensity of the Rhodamine dye was consistent in buffer pH 3.5 for all number of inkj

et-assisted bilayer. These results indicated that the multilayer films from inkjet printing can be used as stable protective layer for encapsulation intention.

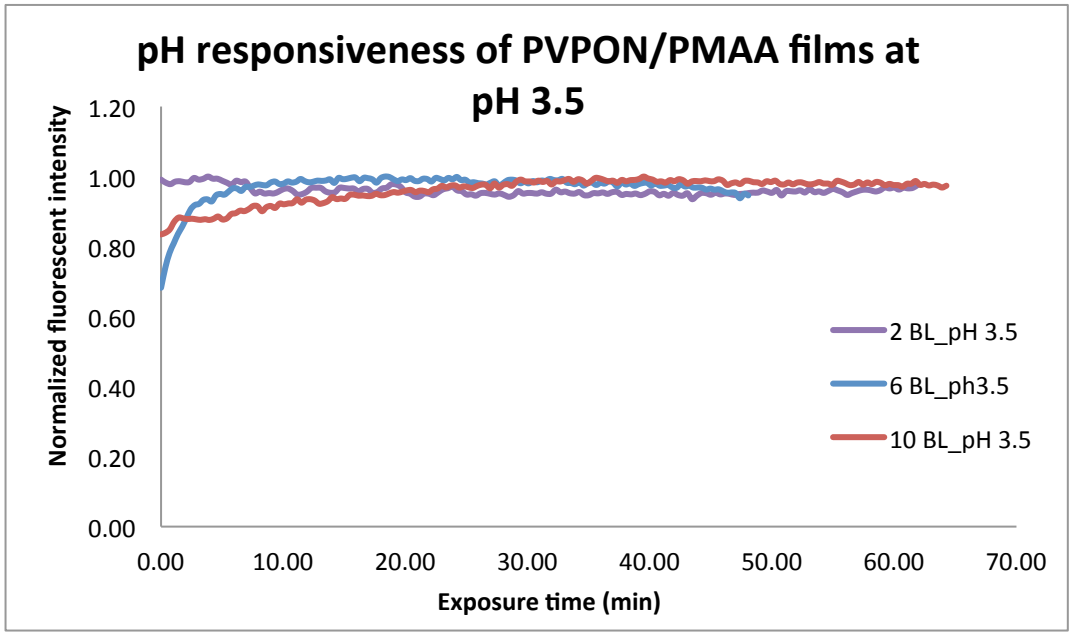

Figure 4.3.23. Fluorescent intensity of Rhodamine dye in acidic buffer using different number of bilayer of inkjet-assisted multilayer films: 2 bilayers, 6 bilayers, and 10 bilayers.

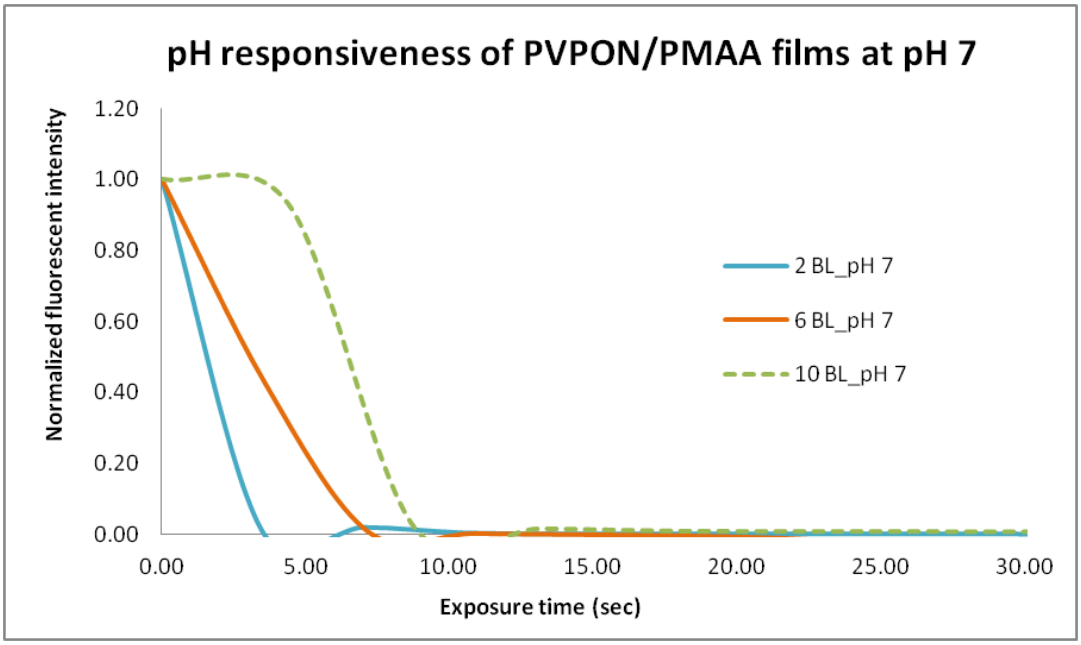

Figure 4.3.24. Fluorescent intensity of Rhodamine dye in buffer pH 7 using different number of bilayer of inkjet-assisted multilayer films: 2 bilayers, 6 bilayers, and 10 bilayers.

To activate release of the encapsulated therapeutic molecules, the inkjet-assisted multilayer films were exposed in buffer pH 7, above pKa of PMAA. The basic environment change ionic charge of carboxylic group in PMAA polymer chain from non-charge to negative charge. This change diminished hydrogen boning between PVPON and PMAA and caused disintegration of the inkjet-assisted bilayers. The Rhodamine dye was released due to the dissolution of the pH responsive film. Therefore, the fluorescent intensity of the Rhodamine dye was decreased along with the film dissolution as show in Figure 4.3.24. The dissolution rate depended on number of bilayer of the PVPON/PMAA LbL films. Thicker encapsulated film demonstrated slower release rate in basic solution. However, the dye release was completed within 10 seconds for all condition. These results indicated that PVPON/PMAA inkjet-assisted LbL films are pH responsive, which the release rate was significantly depended on the rate of dissolution, not number of bilayer of the inkjet-assisted LbL films.

To study the release mechanism of the PVPON/PMAA LbL films, the films were cross-linked and exposed to a buffer of pH 7. It was inconclusive for the release mechanism of the inkjet-assisted PVPON/PMAA LbL films because they were structurally deformed and delaminated during the experiments. The fluorescent intensity did decrease with different exposure times, which is the same as the dye release behavior. However, the deformation led to a reduction in the fluorescent intensity as a result of a loss of confocal focus, causing the experiment to be misleading (as shown in Appendix, Figure A2).

CHAPTER 5

INKJET PRINTING OF SILK NEST ARRAYS FOR CELL HOSTING

5.1 Introduction

Fabrication of large-scale functional arrays of organic, polymeric, or biological materials is a crucial challenge in the field of biosensing for the controlled placement of living cells on various substrates.[139] There are many advanced patterning techniques that can be utilized for the wet-fabrication of such arrays including inkjet printing, micro-contact printing, micro-molding and dip-pen nanolithography.[140,141,142,143,144,145,146,147,148] These techniques allow target molecules to be deposited on various substrates in controlled configurations with a variety of periodic patterns and the inclusion of components at different spatial scales. The selection of proper materials for such arrays, especially for environmentally-sensitive cell-based biosensors, is a critical issue, where biocompatibility and natural material scan offer significant benefits.

Among natural polymers considered for such applications, silk fibroin is one of the most promising materials due to its excellent physical, chemical and biological properties.[149,150,151,152,153,154,155,156,157] Silk has been used in medical sutures due to its biocompatibility. Silk can be applied as dispersant for hydrophobic materials due to its amphiphilic properties, and the protein in various material formats can be exploited as a tough matrix or as a universal binder for nanocomposite materials. The protein can be applied as flexible and optically transparent biomaterial for photonic devices, or used as a biocompatible scaffold for composite materials for biosensing

applications.[158,159,160,161,162,163,164,165,166] For biosensing, silk is a useful material because it can be genetically modified for production of specificity.[167] Moreover, silk can be used for enzyme immobilization and stabilization for biosensing and for cell protection.[168,169] The silk secondary structure can be changed from random coil (amorphous state) to beta sheet (crystalline state) structure upon controlled drying and with methanol treatment.[170,171] On the other hand, the solubility of silk can be improved by ionic polymer grafting such as with polylysine or polyglutamic acid.[172,173]

Silk and modified silks are compatible with a variety of conventional wet-chemistry fabrication processes such as drop casting, spin casting, electrospinning, Langmuir-Blodgett deposition, and LbL assembly. Among these, LbL technology is widely used to fabricate ultrathin coatings and complex materials from synthetic and natural polymers, nanoparticles, and fibers with a variety of functionalities, controlled thickness, permeability, strength, porosity, and environmentally responsive properties.[174,175,176,177,178,179,180,181,182,183,184,185,186,187,188] In recent studies, responsive silk microcapsules have been assembled by electrostatic interactions.[189] Combining biodegradable silk materials and LbL assembly was utilized for microcapsules and ultrathin coatings.[190,191,192] In addition, the release properties could be tuned by changing treatment conditions.[193] However, making patterned arrays from silk materials with conventional microfabrication remains challenging due to long-term solution stability, need to work with low solution concentrations, and easily changing secondary structure.

Inkjet printing is a promising patterning process, widely applied to fabricate complex arrays on the microscopic level.[194,195] In addition, this technique can be used to pattern target molecules on virtually any substrate, including those that are flexible, porous, and rigid, and the technique can be adapted to large scale manufacturing. Moreover, inkjet printing can be combined with LbL technology to fabricate patterns with controlled local thickness and from biological materials.[196,197,198,199] However, robust inkjet printing of cell-based biosensors has not been demonstrated due to issues related to the damaging conditions of direct cell printing on solid supports.[200]

Therefore, in this study, the facile fabrication of patterned arrayed substrates from silk materials via inkjet printing technique was the focus. Successful patterning of silk arrays constructed by the LbL assembly of ionomeric silk chemically modified with poly-(L-lysine) and poly-(L-glutamic acid) side chains was demonstrated. Inkjet-assisted LbL multilayer structures with diameters of ~70-100 μm were stabilized by ionic pairing and by the formation of silk II to generate characteristic "nest" structures on both rigid (glass) and flexible (polymer) substrates. These "locked-in" silk nests with depleted central regions and elevated rims remained anchored to the substrate during incubation in cell growth media, thereby providing a biocompatible platform for immobilization of biological cells without compromising their viability.

5.2 Experimental details

Materials. Polystyrene (PS, MW = 250,000) and toluene (J.T. Baker grade) were purchased from VWR (San Dimas, CA). Anhydrous sodium carbonate (Na_2CO_3), lithium bromide (LiBr), sodium chloride (NaCl), sodium monobasic phosphate (NaH_2PO_4) were purchased from *Sigma-Aldrich (Saint Louis, MO).* All chemicals were used without further modification. Genetic modified *E-coli* cells were supported by Nancy Kelley-Loughnane, Air Force Research Laboratory, Ohio. Nanopure water (Barnstead) with an 18.2 MΩ·cm resistivity was used for all experiments.

Silk was obtained from *Bombyx mori* silkworm cocoons as described previously.[190,201] The solution was dialyzed with deionized water by using Slide-a-Lyzer dialysis cassettes (molecular weight cutoff (MWCO) 3500, Pierce) overnight at room temperature to remove the LiBr. Silk was modified to obtain cationic or anionic ionomers for electrostatic interaction by grafting polylysine (MW=15,000 Da) or polyglutamic acid (MW=15,000Da) on silk molecules with diazonium activation of the abundant tyrosine side chains in the silk molecules followed by poly(amino acid) grafting as we have described previously.[189,202,203,] *E. coli* cells (supported by Nancy Kelley-Loughnane, Air Force Research Laboratory, Ohio) for printing were transformed to encode a theophylline synthetic riboswitch RS21.1.[204] For activation of riboswitch (RS), synthetic minimal medium (SMM) containing reduced concentration of amino acids was used along with theophylline stock solution (100 mM) in DMSO, which was diluted into assay to the final concentration of 5 mM. For printing, cells were collected in 15 mL centrifuge tubes by

centrifugation at 3,000 rpm for 2 min and washed three times with phosphate buffer (Na+ 0.05 M and K+ 0.1M, pH5.5) and kept in SMM medium.

Fabrication and Characterization. Inkjet patterns were fabricated by adjusting the pH of the silk-polylysine (1 mg/ml in 0.05M NaH_2PO_4) to pH 5.5 and printing the silk solution on a PS coated glass substrate to avoid silk film dewetting (Figure 5.2). A solution of silk-polyglutamic acid (1 mg/ml in 0.05M NaH_2PO_4, pH5.5) was printed on top of silk-polylysine dots at the same positions to generate the first silk bilayer stabilized by ionic interactions. The printing process was repeating to produce the desired number of silk bilayers (number of bilayers from 1 to 6) without using washing during the intermediate steps. For preliminary evaluation of the feasibility of silk arrays for cell encapsulation, the solution with *E. coli* cells was printed at the center of the silk nests followed by capping the silk. A JetLab II inkjet printer (MicroFab Technologies) was used for experiments with a 50 μm nozzle diameter for all experiments in this study. Surface morphology and thickness of inkjet-assisted ionomeric silk bilayers was characterized with AFM. The silk arrays were scanned at selected surface areas of 100 μm x 100 μm, 20 μm x 20 μm, and 5 μm x 5 μm.

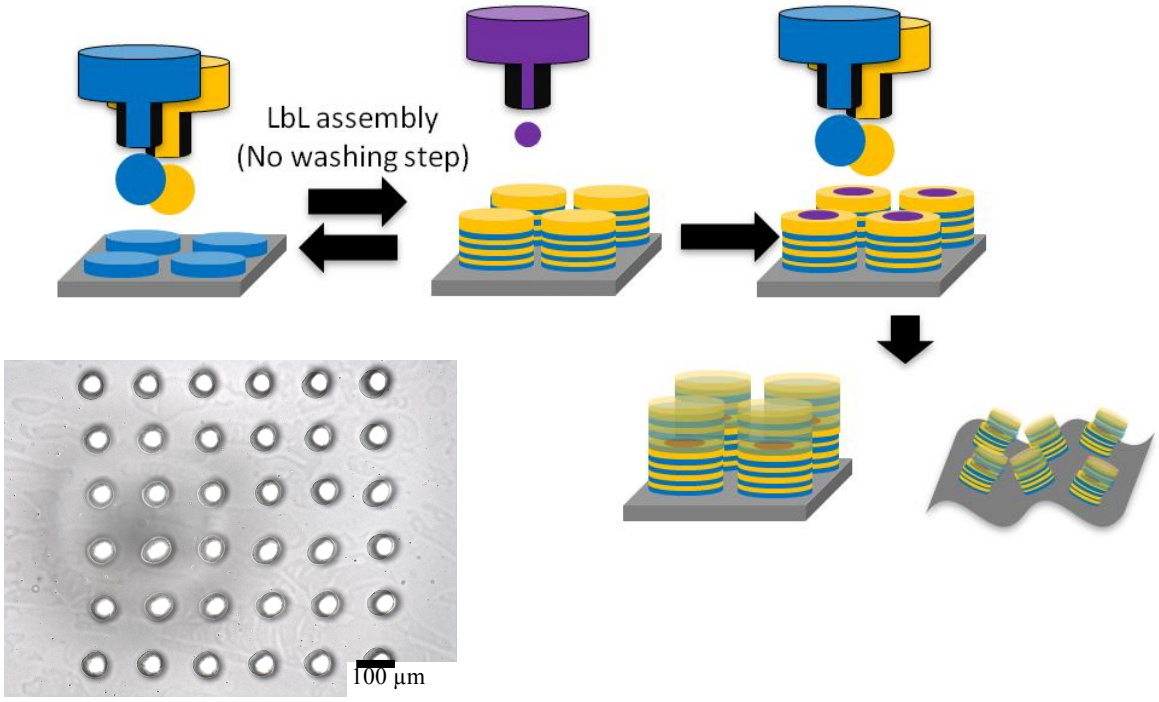

Figure 5.2: (Top) Fabrication process of inkjet-assisted silk array for cell encapsulation. (Bottom) Optical image of silk array with encapsulated cells.

5.3 Results and discussion

Morphology of silk nest arrays.

The thickness of the deposited silk regions with diameters varying from 70 µm to 100 µm was controlled by varying the silk concentration and the number of printed silk bilayers. The shape and dot size of the array depended on the hydrophobicity and smoothness of the substrate as well as deposition conditions (jet velocity, solution concentration) and overall alignment of the deposition steps.[205]

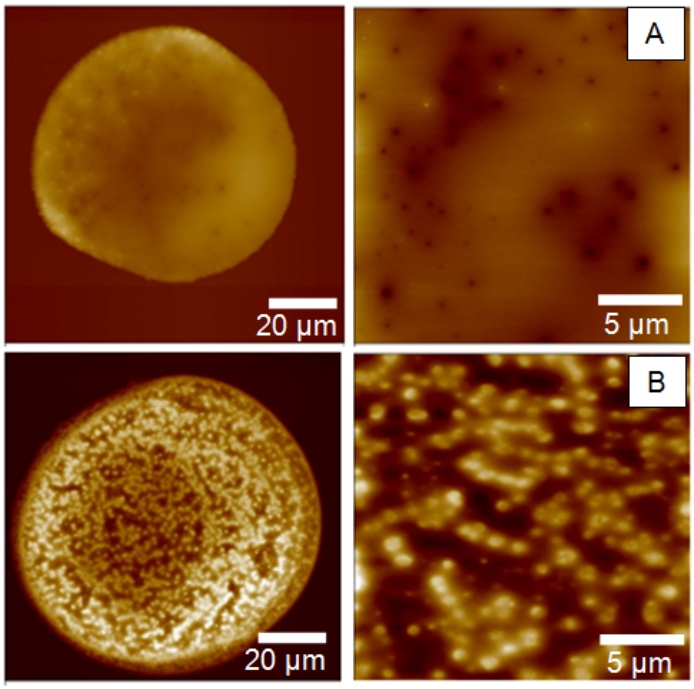

Figure 5.3.1: AFM surface morphology of 0.5 mg/ml inkjet-assisted silk nests with different numbers of silk bilayers at different magnifications: A) 1 bilayer; B) 5 bilayers. Z-scale is 1000 nm for all AFM images.

The silk dot arrays were printed on hydrophobic substrates (glass coated with a thin PS film) to obtain uniform surface covering, to avoid severe dewetting during deposition and drying of aqueous solution, and to assure a smaller dot size (below 100 µm). The freshly-cleaned hydrophilic glass substrates resulted in fine dispersion of the solution and

dewettable dot morphologies with larger sizes due to the spreading of the initial solution. The processing steps were similar to those described for the aqueous-based polymer arrays in our previous study. [206] The typical dot size for silk multilayered films was around 100 μm with minimal sizes reaching about 70 μm.

Surface morphology of a typical silk structure prepared from 0.5 mg/ml silk solutions with 1 and 5 bilayers is illustrated in Figure 5.3.1 (for 3 bilayers see Supporting Information). The initial silk regions were uniform with thicker regions showing significant aggregation, a common behavior of silk materials on solid substrates at low solution concentrations due to strong tendency of silk molecules to form nanofibrillar bundles and globular aggregates with strong intermolecular interactions.[207,208,209,210] Increasing silk solution concentration and the number of deposition cycles (number of

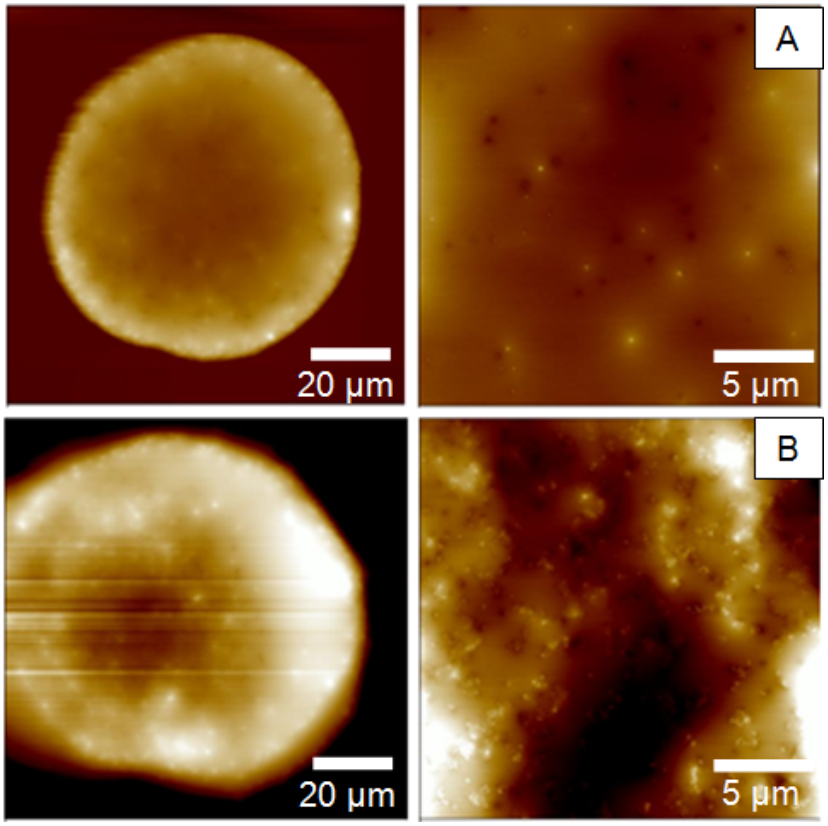

Figure 5.3.2: AFM surface morphology of 1 mg/ml inkjet-assisted silk nests at different number of silk bilayers at different magnifications: A) 1 bilayer; B) 5 bilayers. Z-scale is 1,000 nm for all AFM images.

bilayers) resulted in more uniform, round silk regions (Figure 5.3.2). The microroughness of silk regions (measured within 10 μm x 10 μm surface areas) decreased significantly with increasing solution concentration and higher thickness of the silk regions: from 6.1 nm to 4.6 nm for the thinnest deposits and from 58.7 nm to 9.1 nm to the thicker (5 bilayers) silk dots (Figures 5.3.1, 5.3.2, and 5.3.3).

All dot-like deposited silk regions with different numbers of silk bilayers possessed characteristic "nest" shapes (Figure 5.3.3,). The cross-section of these regions showed elevated rims (430 nm height for 1 bilayer regions) and depleted central regions (150 nm) (Figure 5.3.3C). Such a characteristic shape is caused by a complex balance of solution impact, outward microflow distribution, and different evaporation rates between the center and the periphery of the deposited material during formation of so-called coffee-ring structures.[211,212,213] Overall, a capillary-driven outward flow from the center of the silk dots to the edge resulted in the excessive accumulation of material and much higher silk thickness at the edge of round regions.[214,] Such characteristic "nest" shapes have been observed in our previous studies of inkjet printing of LbL arrays from synthetic polyelectrolytes but are more pronounced here, probably due to the higher viscosity of the silk solution used in the present experiments.[206] The overall morphology of the silk dots can be controlled by adjusting the evaporation rate, solution concentration, and drying temperature.[215,216,217]

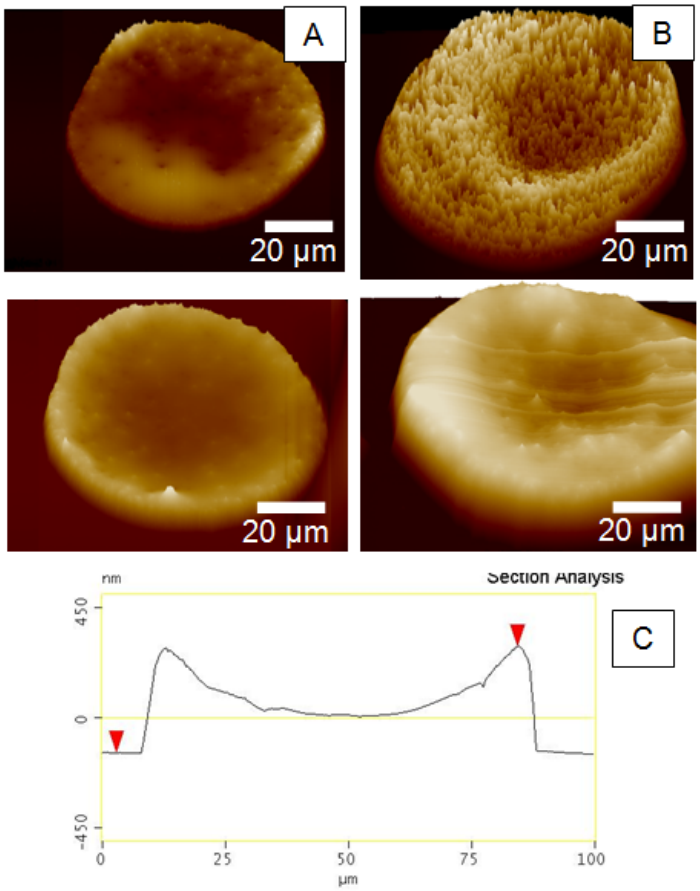

Figure 5.3.3: 3D surface morphology of silk nests inkjet-fabricated from 0.5 mg/ml (top) and 1 mg/ml (bottom) silk solutions at different number of silk bilayers: A) 1 bilayer; B) 5 bilayers. Figure 3C is a cross section of AFM image of 1 bilayer dot showing silk nest shape. The scan size is 100 µm and z-scale is 1,000 nm for all AFM images.

The thickness of these silk nests, as measured from cross-section profiles in the central region, increased from 100 nm to 600 nm with an increasing number of bilayers from 1 to 6 and with increasing solution concentration (Figure 5.3.4). The growth characteristics of the silk regions during ink-jet deposition of ionomeric silks were similar to conventional LbL films with a linear regime controlled by ion pair interactions.[218] However, the average thickness of 115 nm per bilayer was much higher than the average thickness of

other LbL films prepared from synthetic and natural polyelectrolytes fabricated by traditional dip- and spin-assisted LbL methods (around 4-6 nm per bilayer).[219,220] This high average thickness per bilayer may be attributed to the partial transition of silk molecules from silk I (water soluble) to silk II (water insoluble) form during shear stress, which locks in the silk materials in water insoluble forms.

It is important to note that the elimination of washing steps between depositions due to the continuous ink-jet deposition process is, in part, responsible for excessive accumulation of silk material, in contrast to traditional LbL technology with intermediate washing steps. This excessive material does not decrease the global stability of the nest morphologies due to the subsequent conversion to stable silk II format. In contrast, it is important to note that very small microdroplet volumes (60-90 pl) of silk solution used to fabricate the silk nests in a single deposition step limits the overall amount of silk material delivered in a single spot and allows for consistent growth of the silk dots without clogging the silk dot arrays. Finally, some excessive silk material could be partially removed by exposing the silk nests to aggressive cell medium as discussed below.

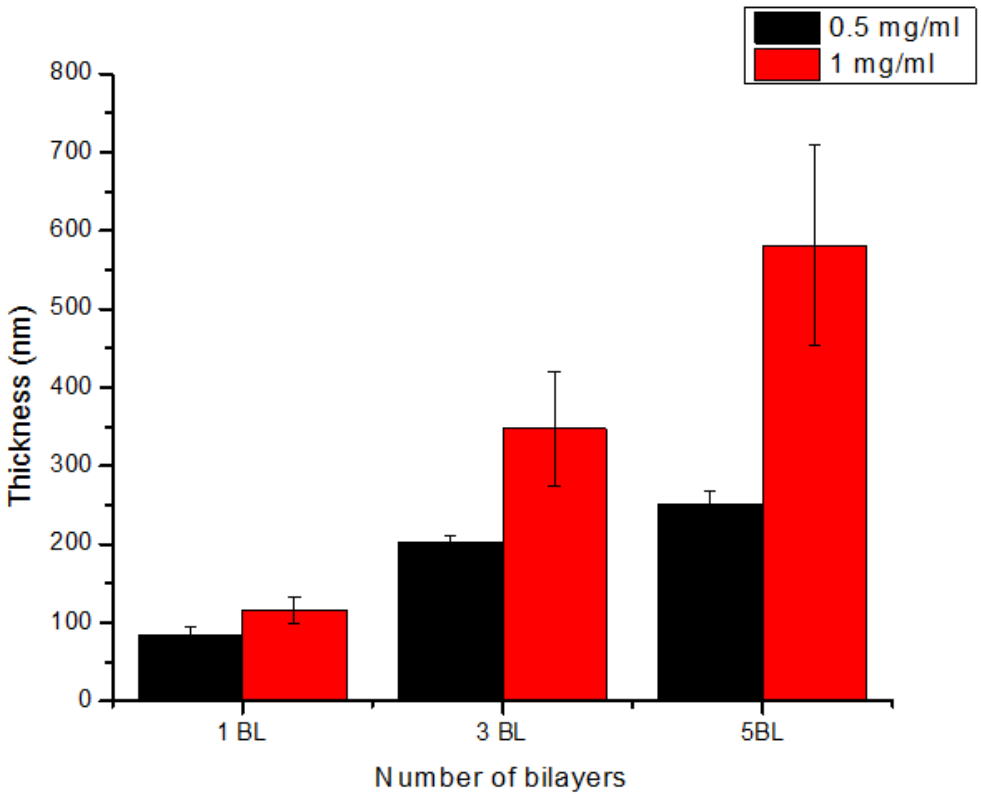

Figure 5.3.4: Thickness at the center of silk nests fabricated from 0.5 mg/ml and 1 mg/ml silk solutions with different numbers of bilayers.

Stability of inkjet array of silk nests.

In order to test the stability of silk nest arrays in liquid media for further encapsulation of cells, the arrays were exposed in a SMM medium for different periods of times (Figure 5.3.5). The general shape of the silk nest arrays remained intact after exposure to the cell media for 12 hours. However, the excessive silk material was partially removed during the immersion in SMM media based on the AFM images of silk dots collected at different magnifications (Figure 5.3.6). Such removal resulted in a significant reduction of silk dot thickness (from approximately 400 nm to 150 nm) immediately after exposure to cell media. This removal of silk material stabilizes at longer exposure times (2 to 12

hours) with some possible re-arrangement of silk protein molecules of material or more likely swelling of the silk.

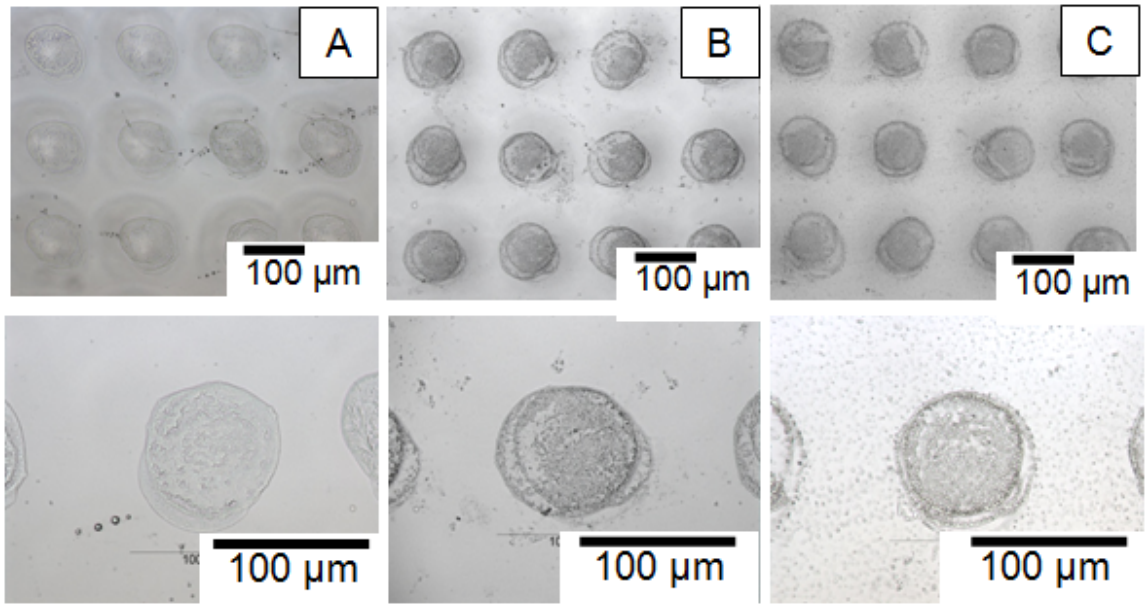

Figure 5.3.5: Optical images at different magnifications of inkjet-assisted silk nests (3 bilayers) at different exposure times in SMM media A) before exposure, B) after exposure for 30 min, and C) after exposure overnight.

The ink-jet printing process can be applied to various targeted substrates with proper wetting properties with respect to the aqueous silk solution. A substrate should not be completely wettable by aqueous solution and can be instantly dried without significant swelling. The fabrication process can be applicable modestly hydrophobic substrates, both rigid and flexible. One of those arrays is demonstrated for commercial PET plastic film in Figure 5.3.7.

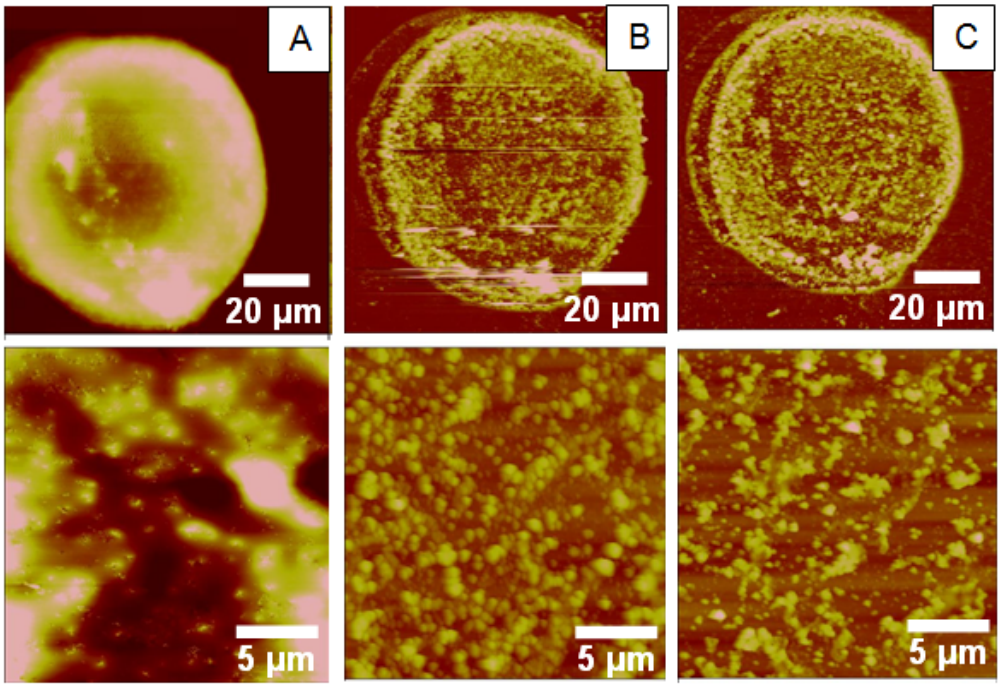

Figure 5.3.6: AFM images at different magnifications of inkjet-assisted silk nests (3 bilayers) at different exposure times in SMM media A) before exposure, B) after exposure for 30 min, and C) after exposure overnight. Z-scale is 1,000 nm for all images.

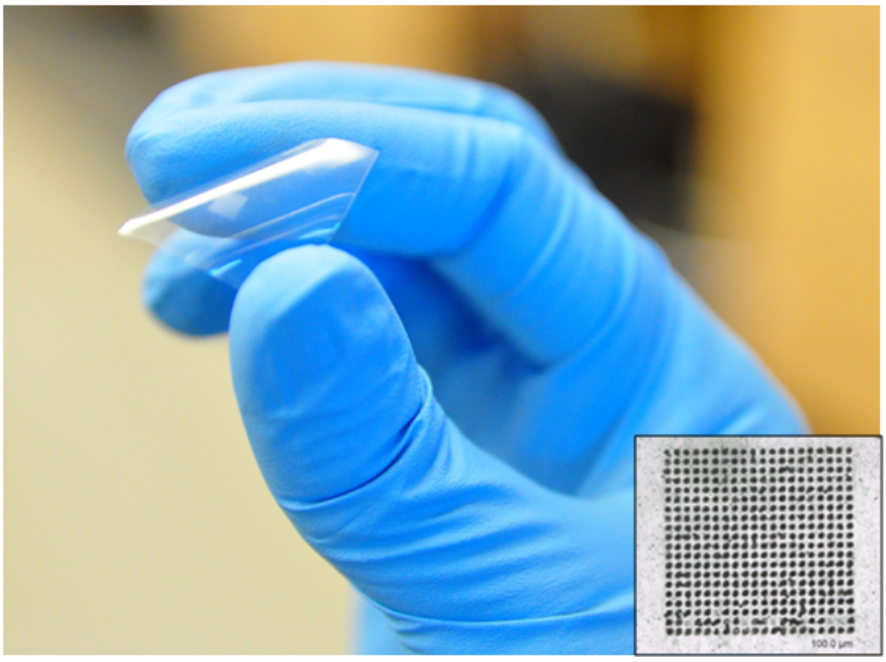

Figure 5.3.7: 20 x 20 inkjet array of silk nests on a flexible PET substrate. Inset image is a high resolution optical image of this array.

Applicability of inkjet silk nest arrays for cell encapsulation.

For preliminary studies of the applicability of these silk nest arrays for cell encapsulation, *E. coli* cells were ink-jet printed in 6x6 arrays directly on pre-printed silk arrays according to the fabrication process (Figure 5.2). *E. coli* dispersions in cell media were injected in the center of the dried silk nest regions and additional silk bilayers were deposited on top of the *E. coli* cells to complete the encapsulation process.

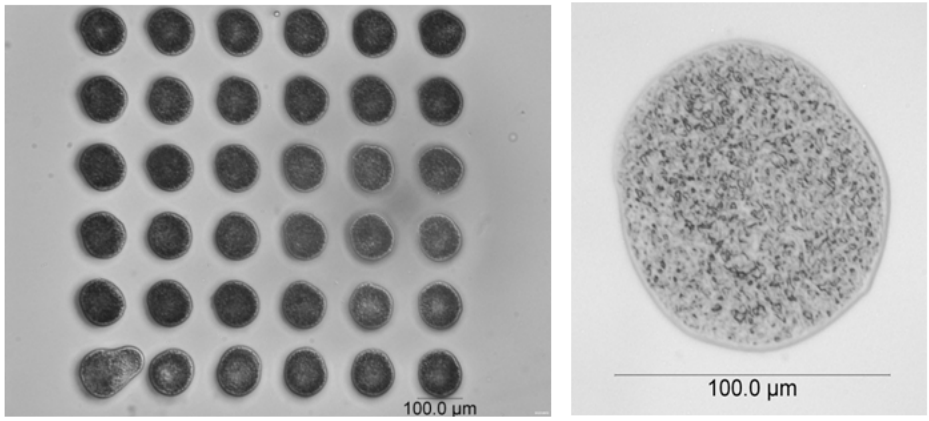

Figure 5.3.8: Optical images of silk nests with encapsulated *E. coli* cells (darker dots within silk region).

The optical microscopy demonstrated that the ink-jet printed *E. coli* cells could be consistently encapsulated within the silk dots (Figure 5.3.8). Encapsulated cell spreading was limited to the circular silk nest regions and the injected cells were confined within the rim of silk regions, which serve as a natural barrier to cell spreading across the whole substrate (see high resolution optical image in Figure 5.3.8). Furthermore, the AFM images confirmed the high density of cell encapsulation within the individual circular silk regions and the preservation of their characteristic cylindrical shapes after the impact and forced jet-assisted deposition on the silk-pretreated nest-shape regions of arrays (Figure 5.3.9).

Moreover, the silk encapsulated cells retain their ability to function after encapsulation and exposure to the cell-activating buffer within silk dots, as was preliminary verified with the dead-alive test (Figure 5.3.9d). In addition, they show a high intensity of GFP expression (Appendix, Figure A3), which indicates that they could be used for biosensing applications.

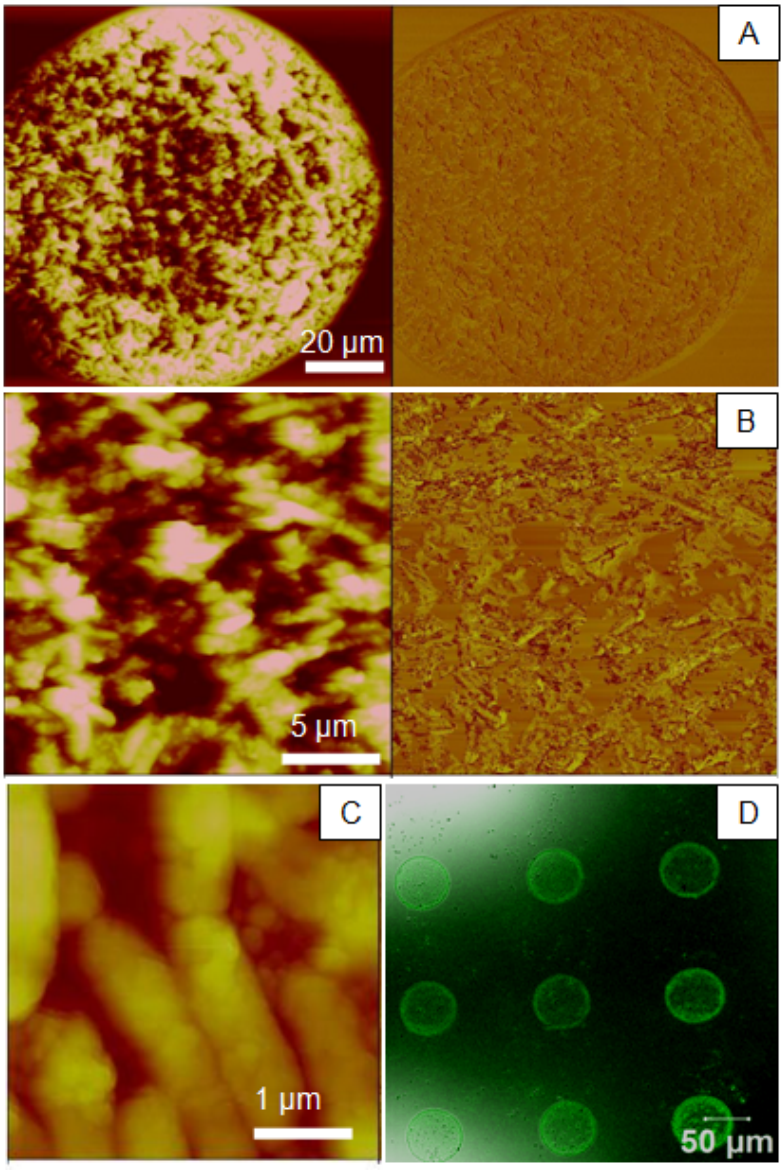

Figure 5.3.9. A-C: Surface morphology (left) and phase (right) of silk nests with encapsulated *E. coli* cells (3 silk bilayers (1 bilayer for C) beneath and on top of cells). Z-scale is 1,500 nm, 1,000 nm, and 500 nm for A, B, and C images. D – Fluorescent image of live *E. coli* cells expressing GFP after 5 hours of incubation in SMM medium.

CHAPTER 6

FREE STANDING SILK-BASED ENCAPSULATION WITH INKJET PRINTING AND STAMPING TECHNIQUE

6.1 Introduction

The protective shells with responsive properties and controllable permeability have a variety application in the field of drug delivery, food industry, biomedicine, electronic, and biosensing.[221] The shell can be utilized to protect the encapsulated materials from environmental factors such as moisture, heat, hazardous chemicals or other unfavorable conditions.[222] Conventional strategies for encapsulating materials with polymers are primarily focused on liquid-based protocols. There are several approaches for fabricating capsule and protective shells, such as emulsion polymerization, polymer layer-by-layer assembly using hydrogen bonding or electrostatic interactions, and self assembly of block copolymers.[223,224,225] However, the challenges of liquid-based encapsulation fabrication remain, including high polydispersity, uneven coverage, aggregation, and solidification during the fabrication process.[226] In addition, encapsulation for bio-related applications should provide high encapsulation efficiency, biocompatibility, non-toxicity and high physical stability with wide range of functioning environments.

The limitations encountered in wet encapsulation can be eliminated using these dry encapsulating approaches. There are several dry encapsulation techniques such as plasma-enhanced chemical vapor deposition (PECVD), initiated CVD, and atomic layer deposition.[227,228] However, these dry encapsulation techniques are complicated, costly and have limitations with regard to living cell encapsulation. The combination of

stamping and inkjet printing techniques is one of the promising candidates for overcoming these conventional encapsulation limitations. The desired materials can be loaded to particular positions using inkjet printing and encapsulated by stamping processes in dry conditions. This dry encapsulation process is applicable for a variety of loading materials, including living cells. Stamping is an inexpensive processing technique used to pattern and print materials on substrates for many applications, such as electronic devices, chemical sensing, tissue engineering, vehicle manufacturing, and printing media.[229,230,231] A variety of materials including nanoparticles, polymers, protein, DNA, ink can be transferred to target positions by directly stamping the chosen materials onto the desired areas.[232] The transferred objects are kinetically controlled by switching between adhesion and release of solid objects to and from an elastomeric stamp.[233] The pattering resolution from stamping depends on size of the elastomeric stamp, which can be changed from the micrometer to the nanometer range.

For a variety encapsulation uses, the protective shell should be stable for securing the entrapped molecules from particular external environments, biocompatible or biodegradable, which are important for biosensing applications. Therefore, silk fibroin is an outstanding material for use as protective shell for encapsulation. It has been used for decades in biomedical sutures, drug delivery, tissue engineering and biotechnology applications.[234,235] The advantages of silk fibroin include its biodegradability, various silk modification protocols, and excellent mechanical properties. Silk is a natural protein made by silkworms and spiders. Most commercial silk is made by silkworms because of their higher production yield from larvae.[236] Silk fibroin has been used as smart

protective shell for many areas of research.[237,238,239] However, there is no study demonstrating the encapsulation of therapeutic molecules using free standing silk films fabricated by stamping and inkjet printing techniques. Herein we demonstrate novel encapsulation technique using stamping and inkjet printing. Free standing silk films are utilized as protective shells that are stable in water and preserve the activity of *E-coli* cells for biosensing applications.

6.2 Experimental details

Materials. Silk fibroin aqueous solution was obtained from *Bombyx mori* silkworm cocoons using splitting, degumming, dissolving, and dialysis procedures.[240] Briefly, silk was dissolved in ionic liquids. The silk fibroin solution was collected after dialysis using Slide-a-Lyzer dialysis cassettes (molecular weight cutoff (MWCO) 3500, Pierce) overnight at room temperature to remove the LiBr. Subsequently, the silk fibroin solution was purified by centrifugation (9000 rpm, 20 min, 5^{o}C), diluted to 2% wt% concentration and stored in a refrigerator at 2^{o}C.

E.coli cells (supported by Nancy Kelley-Loughnane, Air Force Research Laboratory, Ohio) were genetically modified to encode the theophylline synthetic riboswitch RS21.1[241], which was placed upstream of the GFPa1 gene within pSAL vector (pSAL:RS12.1GFPa1). The *E-coli* cells were grown in an incubator (Brunswick) at 37 °C with shaking at 225 rpm in Luria-Bertani (LB) broth containing 100 mg/L

ampicillin and harvested at early stage of exponential growth (0.3-0.4 a.u. based on 0-2 scale).

Inkjet inks (Artisan Epson 50) were purchased from Seiko Epson Corporation. Anhydrous sodium carbonate (Na_2CO_3), lithium bromide (LiBr), sodium chloride (NaCl), and sodium monobasic phosphate (NaH_2PO_4) were purchased from *Sigma-Aldrich.* All chemicals were used without further modification. Nanopure water (Barnstead) with an 18.2 MΩ·cm resistivity was used for all experiments.

Fabrication and Characterization.

Silk freestanding films were fabricated by drop casting the silk fibroin solutions on a PET petridish and air-drying at room temperature. The free-standing silk films were shaped using normal cutting techniques for further use. Water-based ink was patterned on the silk free-standing films by depositing the films on paper and then printing of the GT pattern using Microsoft word and an HP printer. *E-coli* cells were patterned on the free-standing silk films by using a JetLab II inkjet printer (MicroFab Technologies) with a 50 μm nozzle diameter. After printing the water-based ink or E-coli cells on the free – standing silk films, the ink and E-coli cells were encapsulated by placing the printed and neat silk films in humidifier for 20 seconds. The exposed silk films were manually stamped on top of the printed silk film for 30 seconds and continuously pressed until dry to complete the encapsulation procedure as shown in Figure 6.2.1.

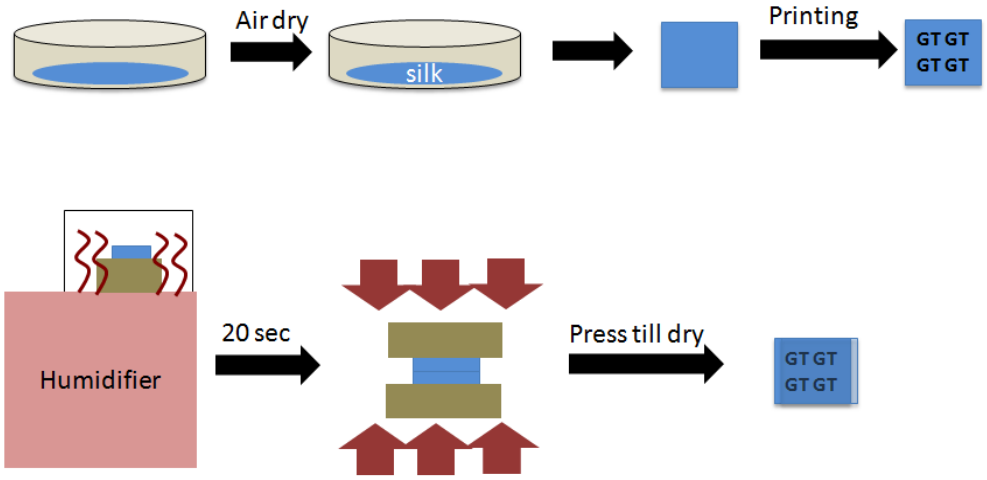

Figure 6.2.1. Free-standing encapsulation processes using stamping and inkjet techniques.

The performance of printing and stamping was characterized using optical microscopy and photography. The stability of stamped silk films was measured by exposing the stamped silks to water and probing the changes of water-based patterns. Biosensing properties of *E-coli* cells in stamped silk were studied by exposing the samples to SMM media with 5mM theophylline and examining expression of the green fluorescent protein (GFP).

6.3 Results and discussion

Morphology of stamping silk and stamping performance

Free-standing silk films were fabricated by dropping 2% wt silk fibroin solution on a PET petridish and air-drying. The silk solution was evaporated and condensed to form a free-standing silk film. Figure 6.3.1 demonstrated that the average thickness of the silk film was around 10.5 μm, which is much thicker than those obtained from conventional spin-coated deposition (around 450 nm).[242] Molecules of silk fibroin are highly repetitive regular block copolymers consisting of ten highly hydrophobic blocks and nine less hydrophobic blocks.[243,244] The secondary structure of silk fibroin can be transformed to a β-sheet structure after treatment with methanol.[245] However, the smooth nature and transparency of the free-standing silk film indicated that the film structure consisted primarily of a random coil formation with the β-sheet formation comprising a portion.[246]

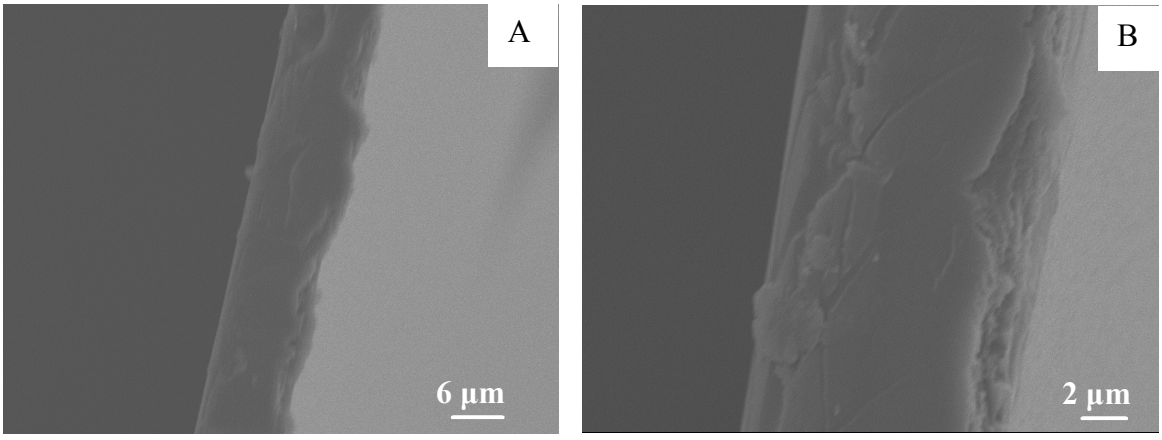

Figure 6.3.1. 2% wt free-standing silk film (A) Low resolution SEM image and (B) High resolution SEM image.

Adhesion property of the free-standing silk film was increased by decreasing the glass temperature using moisture from a humidifier.[247] The glue-like silk films were stamped together to complete encapsulation process. The thickness of the stamped silk was doubled to 21 μm (10.5 μm per layer) after stamping. Figure 6.3.2 indicates that the two free-standing silk films were merged completely with the absence of a film interface. These results denoted that the moisture induced reduction in the glass transition of the silk fibroin molecules occurs only at the film interface. Short exposure time in the humidifier prevented the diffusion of water molecules through the entire silk structure while longer exposure in the humidifier induced the gelation of the free-standing silk films. The aqueous solution caused silk fibroin gelation by producing hydrophobic regions in silk fibroin through hydrophobic interaction of the silk fibroin molecules.[248] Gelation of silk fibroin can be controlled by temperature, Ca2+, pH, and poly(ethylene oxide) (PEO).[249] This gelation led to a deformation of the planar structure of the free-standing silk films, which decreased encapsulation performance of the stamping technique. Therefore, a short exposure time (20 seconds) was suitable for homogenously fusing two free-standing silk films for producing a biodegradable protective shell.

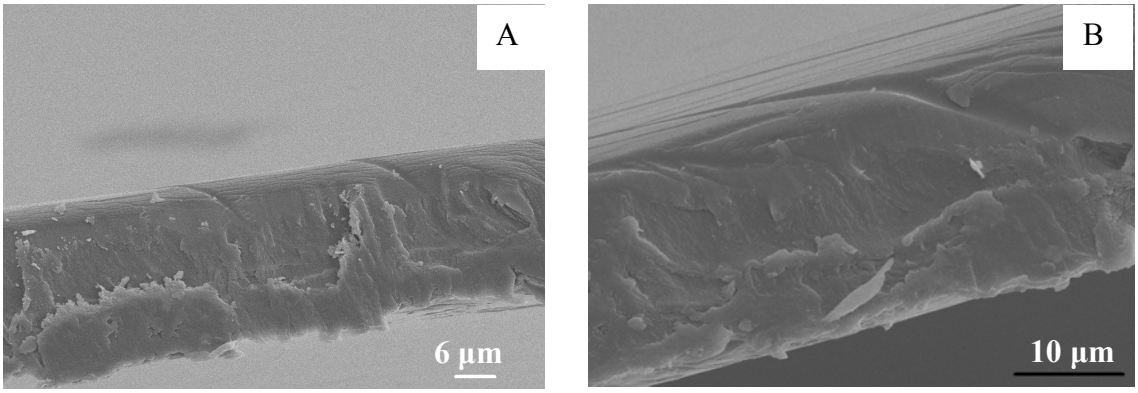

Figure 6.3.2. SEM images of two free-standing silk films after stamping. A) Low resolution, and B) High resolution.

Patterning performance and encapsulation efficiency

Water-based ink was used as an example of therapeutic molecules and was printed on a free-standing silk film using a piezoelectric inkjet printer, with an array of the GT logo patterned to serve as an example of the patterning capabilities of this technique (Figure 6.3.3). It shows that the pattern was uniformly immobilized on the film due to the

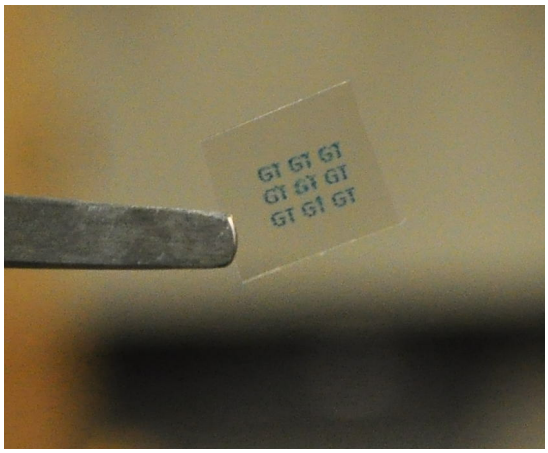

Figure 6.3.3. GT pattern on a free-standing silk film using inkjet printing technique.

flatness of the free-standing silk. Loading dye molecules using inkjet printing is fast, simple, and applicable for high loading concentrations. This inkjet-assisted loading technology avoids the limitations of conventional loading process that which depends on the diffusion mechanism which can lead to low loading efficiency.[250] Therefore, the maximum concentration of therapeutic molecules inside conventional capsules is limited to the concentration of these molecules in the solution. The loading concentration of water-based therapeutic molecules from conventional LbL capsules was around 7- 20% w/w for low molecular weight molecules.[251] In contrast to the conventional LbL loading techniques, inkjet printing is capable of depositing various concentrations of dye

molecules by printed repeatedly on the substrate. This repeatable inkjet-assisted loading process allow for an unlimited loading concentration for encapsulation.

The GT pattern was fabricated on the free-standing silk films within 30 seconds. This loading procedure is much faster than loading of molecules into conventional capsules using diffusion or polymerization, which require hours for the loading process to finish. In addition, the aqueous ink was printed directly on the free-standing silk without further washing. This direct loading process could avoids the wasting of large amounts of the material during the chemical loading process, a common problem encountered when using conventional LbL encapsulation based on diffusion.[252]

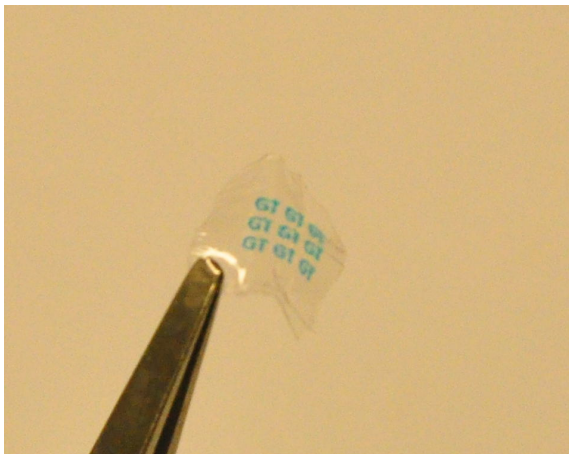

Figure 6.3.4. GT pattern in free-standing silk films using stamping technique.

The GT pattern was protected from external environment by stamping another free-standing silk film on top of the based free-standing silk and allowing air dry overnight under constant pressure. The encapsulated ink still maintained a nice GT pattern after stamping as shown in Figure 6.3.4. This result mentioned that the stamping process did

not damage dye molecules or the pattern on the silk film. The stamping technique required approximately 30 seconds to complete encapsulation whereas the conventional LbL encapsulation required several hours to prepare the capsules and load therapeutic molecules.

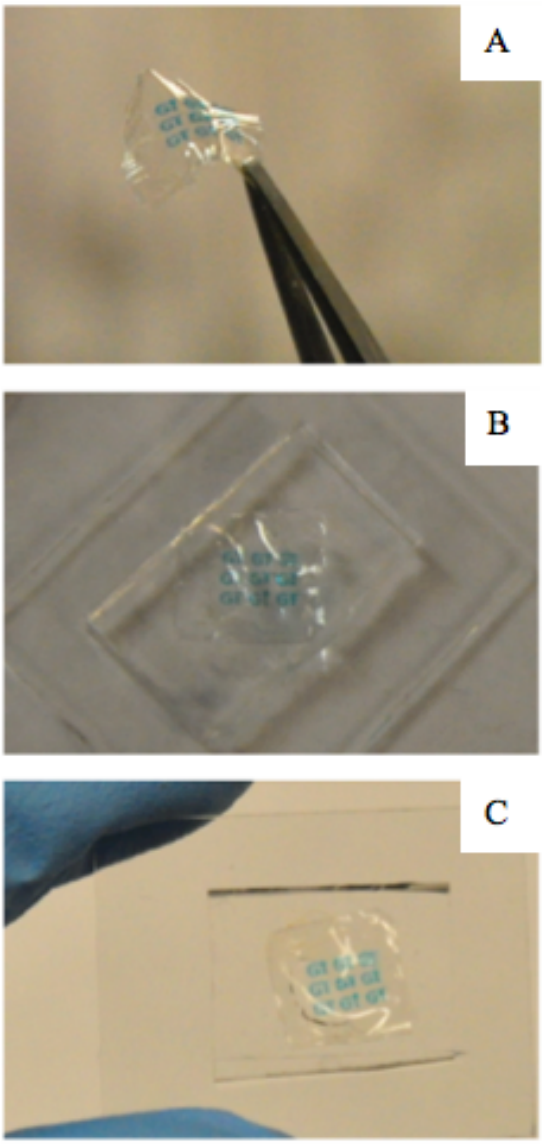

Figure 6.3.5. GT pattern in free-standing silk films after exposed in water. A) before exposure, B) expose 2 hrs, and C) exposed overnight

The stamped silk films still maintained high transparency, indicating that the majority of the silk structure, random coil molecules, was not affected by from stamping or constant pressure. However, Figure 6.3.4. denoted small wrinkles in the stamped silk films due to errors caused by manually stamping. In this study, the free-standing silk films were placed on small pieces of PDMS. The good stamping results required bending of PDMS master during the stamping process to avoid hollowness and wrinkles in the stamped silks from heterogeneous pressure. The manual pressing may cause non-uniform pressing and slipping, which is likely reason wrinkles formed. However, this problem could be eliminated by using automatic roll-to-roll stamping machines. In order to test the stability of the stamped silks, the sample were exposed in water at different period of time (Figure 6.3.5). The transparency of stamped silks was decreased due to gelation and absorption of water molecules in the silk films. The wrinkles were diminished during gelation and did not regenerate after air dry. This decreasing of the wrinkles indicated that the silk molecules were reorganized by bonding with the absorbed water molecules and formed hydrogel, which has a planar structure. The evaporation of the water molecules in the silk structure was slow, which encouraged the stamped silk to retain a flat structure. The silk films maintained high transparency after being exposed in water and allowed to air dry. This result indicated that the gelation and re-drying of the stamped silks did not change chain conformation of the silk molecule from random coil to β-sheet crystallites. The GT pattern in the stamped silk films was stable after exposing the silk films in water at different period of times. The water-based ink was unable to diffuse out because chain entanglement of the silk random coil inhibited the mobility of the ink molecules. Even though the encapsulation, using the stamping technique,

required two separated free-standing silk films, the high stability of the GT pattern indicated that there was no gap between the free-standing silk films. In addition, the complete fusion of the free-standing silk films from the stamping process shown in Figure 6.3.2 supported this high stability of the GT pattern in the silk films. These results showed the excellent encapsulation stability of this stamping technique.

Inkjet printing and stamping silk for biosensing application

Genetically modified *E-coli* cells were printed on free-standing silk films using inkjet printing. Figure 6.3.6 showed the large printing scale and uniform *E-coli* cell patterns on the silk film. The hydrophobicity of the substrate and printed solutions demonstrated significant role in dot size of printed inks.[253] Higher contact angle substrates limited spreading and dewetting of the ink solution, resulting in smaller dot size. The contact angle silk films were around 70°, which was comparable to poly(4-vinylphenol) (PHS).[254] Therefore, the size of the *E-coli* cell array was around 100 μm that was similar to dot size of aqueous based materials on PHS substrates in previous study.[255]

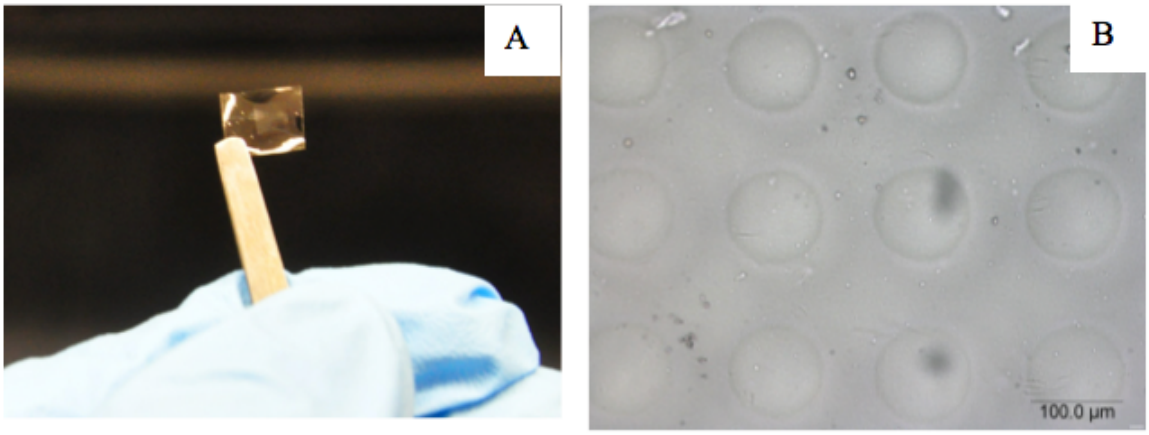

Figure 6.3.6. Photograph (A) Optical image (B) of 20 x 20 array of *E-coli* cells on a free-standing silk film.

The *E-coli* cells were covered by stamping another free-standing silk on top of based free-standing silk as shown in Figure 6.3.7. The *E-coli* array could be examined clearly inside the stamped silk films due to high transparency of the silk films. Figure 6.3.7 B

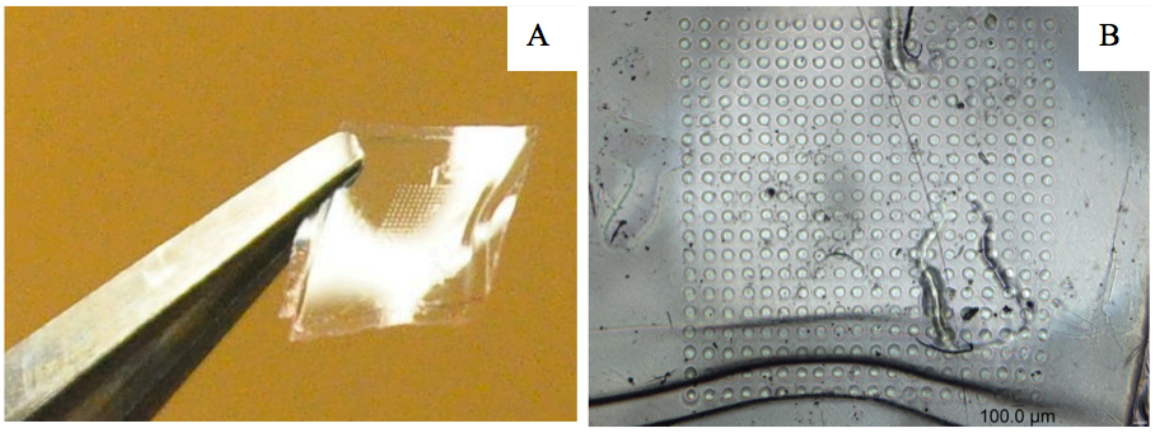

Figure 6.3.7. 20 x 20 array of *E-coli* cells in stamped free-standing silk films. A) Photograph and B) Optical image.

demonstrated some deformation of stamped silk film due to slipping during the manual stamping step. This deformation remained after the encapsulation process was completed. However, the deformation of the film did not affect the overall *E-coli* cell pattern or its biosensing properties. The *E-coli* cells were genetically modified to be sensitive to theophylline. Figure 6.3.8 demonstrated Green Fluorescent Protein (GFP) expression of the *E-coli* cell array in stamped silk films after being exposed to the mixture of theophylline and SMM media. *E-coli* cells in the stamped silk required around 5 hrs for GFP expression, which is longer than that observed in conventional LbL capsules, and is likely due to the thicker protective shells of the stamped silk films (20 µm compared to 2-100 nm in ultra thin LbL shells). The low GFP expression suggests that these stamped silk films may not suitable for biosensing applications that require

high florescence intensity. However, the GFP expression can be increased by increasing number of *E-coli* cells in the printing dots and prolong inoculation times. This GFP expression does indicate that the inkjet printing and stamping technique does not damage *E-coli* cells and therefore could be utilized for other living cell-friendly applications.

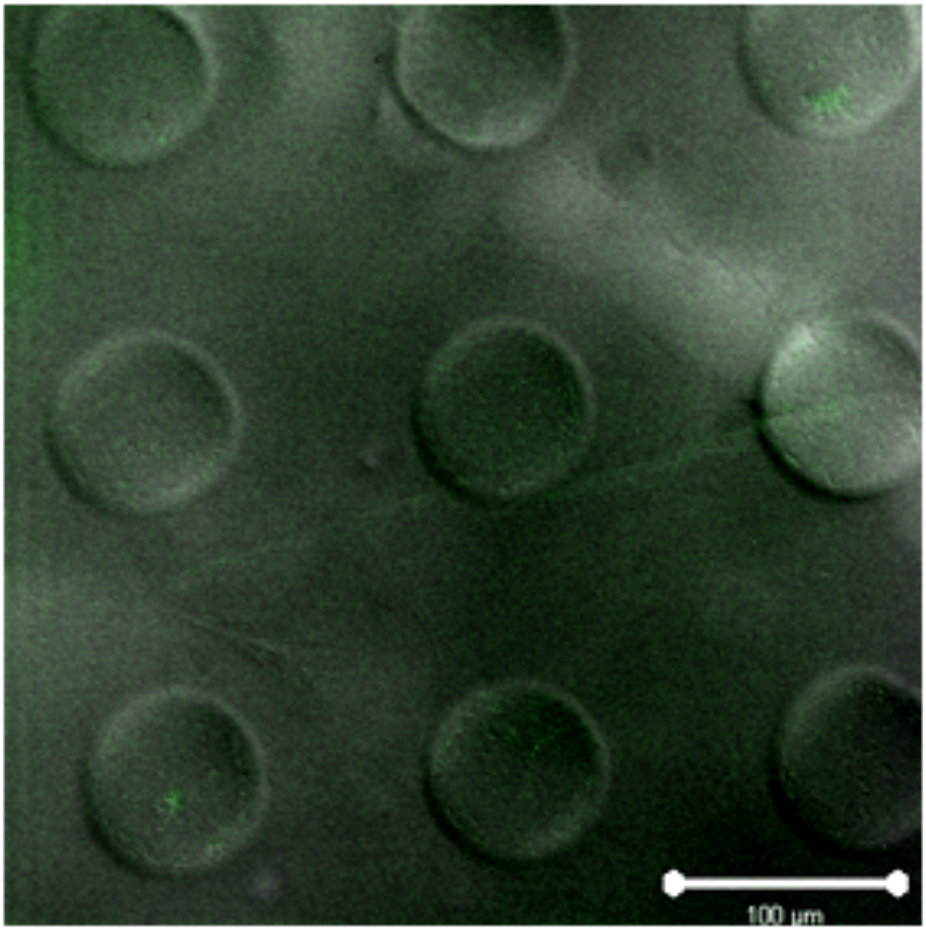

Figure 6.3.8. Confocal image of *E-coli* array in stamped free-standing silk films after exposed in 5 mM theophylline in SMM media for 5 hrs.

CHAPTER 7

GENERAL CONCLUSIONS AND BROADER IMPACT

7.1 General conclusions and discussion

In order to design an effective encapsulation technique for controlled release and bio sensing applications, the fabrication platform needs to be reliable, consistent, and compatible with various loading materials of interest. For these reasons, the formation of discrete LbL encapsulation with controlled shapes and periodic spatial arrangements of components using conventional encapsulation remains a challenge. Furthermore, the encapsulation process should be cost effective and easy to use in the field of applications. Therefore, the proposed encapsulation technique is a promising candidate since it demonstrates low cost for encapsulation, high loading efficiency for a wide range of molecular weights of therapeutic molecules, direct payload delivery to specific positions, low fabrication times, controllable patterning, and is an applicable concept for a variety of responsive shells.

For biosensing research, the encapsulation processes need to utilize fabrication approaches that are friendly to living cells and appropriate for biomolecules detection. The proposed encapsulation concept meets all of the bio-related requirements. In this study, two topics are primarily addressed:

1) Development of LbL encapsulation using inkjet printing for control release and biosensing purposes. Examined how periodic multilayer structures can be fabricated using a drop-on-demand printing technique that does not require intermediate washing

steps. The LbL fabrication processes involve both hydrogen bonding and electrostatic interaction.

2) Improvement of the encapsulation concept by combining inkjet printing and stamping techniques with biocompatible silk materials. Investigate how inkjet printing can be applied for the direct loading of living cells and how the stamping technique can be applied to fabricate stable biocompatible protective shells.

First, the proposed concepts demonstrated that high loading of organic molecules is possible using a simple fabrication process like inkjet printing. *PVPON was printed on a flat substrate followed by printing PMAA on top to assemble LBL films. Rhodamine dye was used as an example for the* therapeutic molecules in this study. One of the significant finding of this study is that *PVPON and PMAA molecular chains form high inter-diffusion hydrogen bonding that causes high structural stability in acidic solutions during inkjet printing because of the absence of intermediate removal of excessive polymer.* The weak bonding polymers were eliminated after exposure in acidic solution and remained as a stable LbL PVPON/PMAA structure. Furthermore, the LbL encapsulation films showed cup-like formations due to the heterogeneous evaporation of the polymer droplets. *The encapsulation efficiency was improved by increasing the number of PVPON/PMAA bilayers because of the higher coffee-ring wall.* Finally, the size of the LbL encapsulation films could be controlled by the hydrophobicity of the substrate.

In the next level of complexity, the inkjet-assisted LbL assembly was applied to electrostatic interaction using ionomeric silk, silk-polylysine and silk-polyglutamic acid. *E-coli* cells were utilized as a bio-detector model for biosensing applications. This work provided specific design guidelines for using inkjet printing to fabricate multilayer biocompatible silk polyelectrolytes on rigid and flexible substrates. *The key discovery in this work was that inkjet printing could be utilized to fabricate living cell-friendly LbL encapsulation with periodicity and patterning abilities.* The *E-coli* cells survived in ionomeric silk protective shells and responded to biochemical sensing. Moreover, *electrostatic LbL assembly using inkjet printing shows a lower structural stability than hydrogen bonding because electrostatic charges require ion pairs for stabilization where as chain entanglement plays critical roles in hydrogen bonding LbL assembly*. Inkjet printing is more likely to induce molecular inter diffusion and chain entanglement rather than ion pair compensation.

Finally, we focused on developing a simpler encapsulation process for future manufacturing fabrication using free-standing silk films. Water-based ink or *E-coli* cells were printed on a free-standing silk film and protected by stamping another silk film on top. From this study, we can conclude that *encapsulation using inkjet printing can be improved by combining it with the stamping technique, providing a faster fabrication process with outstanding structural stability.* Stamping fused free-standing silk films can be used to create protective shells without changing the chain conformation or physical properties of the free-standing silk films. The patterns of water-based ink in silk stamped film retained an identical pattern after long exposure in water. Another significant

finding of this study is that the *E-coli cells can be encapsulated with controllable periodicity using inkjet printing and that the printed E-coli cells can be used for biosensing by expressing green fluorescent after inoculation in an analyte solution.*

7.2 Significance and broader impact

The further development of encapsulation technologies will require fabrication processes that achieve high loading efficiency, responsiveness, compatibility with a variety of loading chemicals, and cost effectiveness. LbL encapsulation is an excellent candidate for achieving most of these requirements. However, conventional LbL encapsulation techniques are fabricated in solutions and require intermediate washing step. This removal of excessive polyelectrolyte is essential in LbL assembly because it prevents the weak structural stability from low inter molecular interactions between each building layer caused by the excessive polyelectrolytes. In addition, encapsulation in solution is limited by loading concentration of the solution and the molecular weight of loading molecules because it utilizes the diffusion mechanism to transfer the loading molecules into the responsive capsules. LbL encapsulation using inkjet printing and stamping can overcome these challenges by fabricating the LbL films and loading the target molecules in the dry state. The work presented here establishes a novel design paradigm for an encapsulation process with complex patterning.

Table 7.2.1 shows a list of issues facing the applications of convention encapsulation and the specific solutions to these challenges that have been described in this dissertation. As is widely accepted, the critical challenges of conventional LbL encapsulation are low loading concentration, restrictions on the molecular weight of the loading chemicals, core template requirement, and the enormous loss of polyelectrolytes from intermediate washing steps. To improve encapsulation, the fabrication process need to be applicable to a wide range of therapeutic molecules, demonstrate the ability to have high loading concentration with a variety of molecular sizes, and be cost effective. In addition, encapsulation with patterning capabilities will broaden the utility of LbL encapsulation in diverse applications, including biosensing and controlled release systems.

Table 7.2.1. The critical issues and possible solutions for improved LbL encapsulation

Grand challenges in LbL Encapsulation	***Progess and novelty in this work***
Materials *Protecting LbL shell with biocompatible, strong and responsive properties.*	• *Use of pH responsive PVPON, PMAA, modified silk fibroin and silk freestanding films for printed encapsulation.*
Fabrication *New robust techniques for encapsulating therapeutic molecules with no limitations on the loading concentration, core template, or molecular size of the loading molecules.*	• *Established a core template-free encapsulation process using inkjet printing with elimination of washing intermediate step.* • *Developed a combined inkjet printing and stamping technique for solid-state encapsulation.*

Table 7.2.1. continued

Grand challenges in LbL Encapsulation	***Progess and novelty in this work***
Fundamental *Understanding phenomena related to the molecular interaction in LbL assembly using a variety of polyelectrolytes.*	• *Molecular orientation of polymers in hydrogen bonded and electrostatic interaction based LbL multilayer films from inkjet printing fabrication without intermediate washing steps.* • *Structural stability of the encapsulated films using the inkjet printing and stamping technique.* • *Effect of the number of bilayers on the release rate of the loading molecules from inkjet-assisted multilayer films.*
Targets *Enhance LbL encapsulation efficiency and applications in new fields*	• *Developed an encapsulation technique with no limitations on the loading materials, and demonstrated patterning and large scale possibilities using the inkjet printing and stamping techniques* • *Developed LbL encapsulation for controlled release and biosensing applications via inkjet printing and stamping processes.*

Types of polymer LbL shell play important roles in their responsive properties. The LbL capsule can be stimulated by external incitements such as temperature, pH, salt concentration, or specific chemicals depending on the responsive properties of the LbL shell. *In this study, inkjet printing was utilized to fabricate LbL films using a variety of polymers that utilized hydrogen bonding and electrostatic interactions.* Conventional LbL encapsulation requires core templates for the deposition of polyelectrolytes, which typically requires strong acid to remove the core, a process that could lead to complications for loading of bio-related chemicals. However, *inkjet-assisted LbL printing is a simple method for fabricating complex array formations that does not require an intermediate washing step, and that does not require a sacrificial solid core template to support the layered formation.* In addition, inkjet-assisted LbL encapsulation only utilizes multi deposition at desired positions, making it a novel fabrication concept that is suitable for the loading of all desired molecules with high loading efficiency.

Another challenge for implementing standard LbL encapsulations is the long times require for fabrication. In addition, conventional LbL encapsulation techniques require dialysis to remove the salt from the polyelectrolyte deposition, which normally lead to assembly process that require several hours to complete. Moreover, loading molecules into LbL capsules is slow because of the long diffusion times of molecules when moving from solution to within the capsules. In this study, we concluded that *LbL encapsulation using inkjet printing demonstrated shorter fabrication times by directly loading materials to the desired position.* There is no limitation due to the slow loading encountered in LbL shell assembly because the inkjet-assisted encapsulation concert does not utilize the

diffusion mechanism to load the molecules. Furthermore, the fabrication time can be reduced from several days to hours after setting printing conditions because the inkjet printing is a direct chemical loading and LbL fabrication on desired positions.

In addition, *the combination of inkjet printing and stamping technique reduced encapsulation preparation time to a few minutes.* The preparation of a protective shell can be shortened by using ready-to-use freestanding silk films. The stamping process can complete the encapsulation procedure within 30 seconds by stamping a protective silk layer on the printed free-standing silk films. Furthermore, *the inkjet printing and stamping technique are friendly for bio cell encapsulation with controllable periodicity at large-scales.* This study demonstrated that *E-coil* cells can be patterned, protected and expressed GFP using both inkjet-assisted ionomeric silk and stamping silk films, which can be utilized for biosensing applications.

We show that the fabrication and characterization of LbL encapsulation using the inkjet printing, and stamping technique discussed in this study will be important for addressing some of the challenges facing the development of high loading efficiency encapsulation with simple, cost effective, living cell friendly and controllable patterning. This approach is not limited to PVPON, PMAA, ionomeric silk, or free-standing silk films, but rather has clear compatibility with a variety of polymer types that exhibit assembly based on hydrogen bonding or electrostatic interactions. Moreover, the encapsulated materials can be varied from small molecules (such as dyes or drug molecules) to large materials (such as living cells or microparticles), making it applicable to a wide-range of applications.

DISSEMINATION OF WORK

This work has been conveyed to the scientific community by the following publications and presentations

Relevant publications

1. Suntivich, R.; Drachuk, I.; Kaplan, D. L.; Tsukruk, V. V., Free standing silk-based encapsulation with inkjet printing and stamping technique, **2014** *(in preparation)*
2. Drachuk, I.; Suntivich, R.; Calabrese, R.; Harbaugh, S.; Kelley-Loughnane, S.; Kaplan, D. L.; Stone, M.; Tsukruk, V. V. Inkjet printing of cell-based biosensor arrays, **2014** *(in preparation)*.
3. Suntivich, R.; Drachuk, I.; Calabrese, R.; Kaplan, D. L.; Tsukruk, V. V., Inkjet Printing of Silk Nest Arrays for Cell Hosting, *Biomacromolecules* **2014,** DOI 10.1021/bm500027c.
4. Suntivich, R.; Shchepelina, O.; Choi, I.; Tsukruk, V. V., Inkjet-Assisted Layer-by-Layer Printing of Encapsulated Arrays *ACS Appl. Mater. Interfaces*, **2012**, *4*, 3102–3110.
5. Suntivich, R.; Choi, I.; Gupta, M. K.; Tsitsilianis, C.; Tsukruk; V. V., Gold nanoparticles grown on star-shaped block copolymer monolayers *Langmuir*, **2011**, *27*, 10730–10738.
6. Choi, I.; Suntivich, R.; Plamper, F. A.; Synatschke, C. V.; Müller, A. H. E.; Tsukruk; V. V., pH-Controlled Exponential and Linear Growing Modes of Layer-by-Layer Assemblies of Star Polyelectrolytes *J. Am. Chem. Soc.*, **2011**, *133*, 9592–9606.

Presentation

1. Suntivich, R.; Drachuk, I.; Calabrese, R.; Kaplan, D. L.; Tsukruk, V. V., Inkjet Printing of Silk Nest Arrays for Cell Hosting **2013 MSE Georgia Institute of Technology poster competition**, Atlanta, GA (*Poster presentation*)
2. Suntivich, R.; Shchepelina, O.; Choi, I.; Tsukruk, V. V., Novel one step encapsulation with hydrogen-bonded layer-by-layer assembly using printing techniques **2011 Material Research Society Fall Meeting,** Boston, MA (*Poster presentation*)
3. Suntivich, R.; Choi, I.; Gupta, M. K.; Tsitsilianis, C.; Tsukruk; V. V., Gold nanoparticles grown on star-shaped block copolymer monolayers **2011 Material Research Society Fall Meeting,** Atlanta, GA (*Poster presentation*)
4. Choi, I.; Suntivich, R.; Plamper, F. A.; Synatschke, C. V. Müller, A.H.E.; Tsukruk. V. V. pH-Controlled Exponential and Linear Growing Modes of Layer-by-Layer Assemblies of Star Polyelectrolytes, **2011 Material Research Society Fall Meeting**, Boston, MA (*Poster presentation*)
5. Choi, I.; Gunawidjaja, R.; Suntivich, R.; Tsitsilianis, C.; Tsukruk. V. V. Surface Behavior of PSn(P2VP-b-PtBA)n Heteroarm Stars, **2011 Material Research Society Fall Meeting**, Boston, MA (*Poster presentation*)
6. Drachuk, I.; Suntivich, R.; Calabrese, R.; Harbaugh, S.; Kelley-Loughnane, N.; Kaplan, D. L.; Stone, M.; Tsukruk, V. V. Inkjet Assisted Encapsulation of Cell-Based Sensors in Silk Hydrogel Matrices, **2014 ACS Spring Meeting**, Dallas, TX *(Poster presentation).*
7. Choi, I.; Gunawidjaja, R.; Suntivich, R.; Tsitsilianis, C.; Tsukruk; V.V., Surface Behavior of $PS_n(P2VP\text{-}b\text{-}PtBA)_n$ Heteroarm Stars *Macromolecules* **2010**, *43*, 6818–6828 *(publication).*

APPENDIX

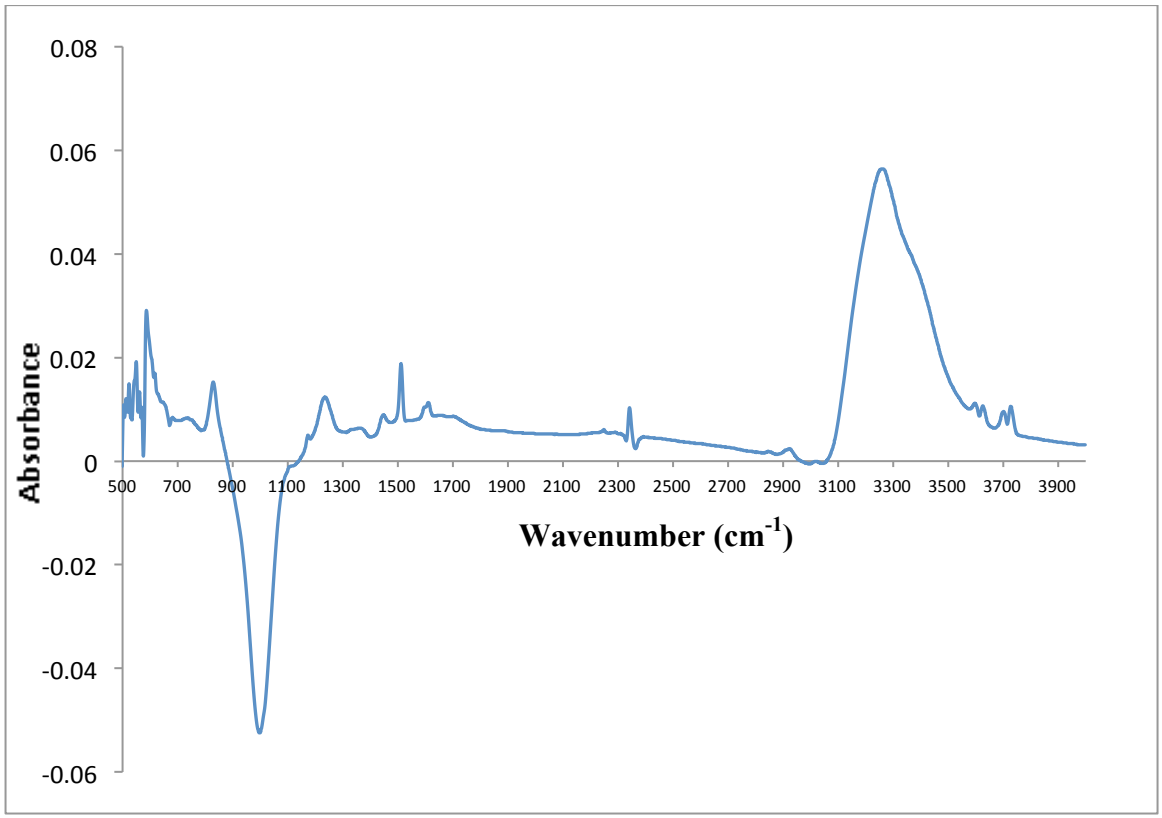

Figure A1: FTIR SPECTRUM OF PVPON/PMAA MULTILAYER FILMS INDICATES THAT THERE IS HYDROGEN BONDING BETWEEN PVPON AND PMAA

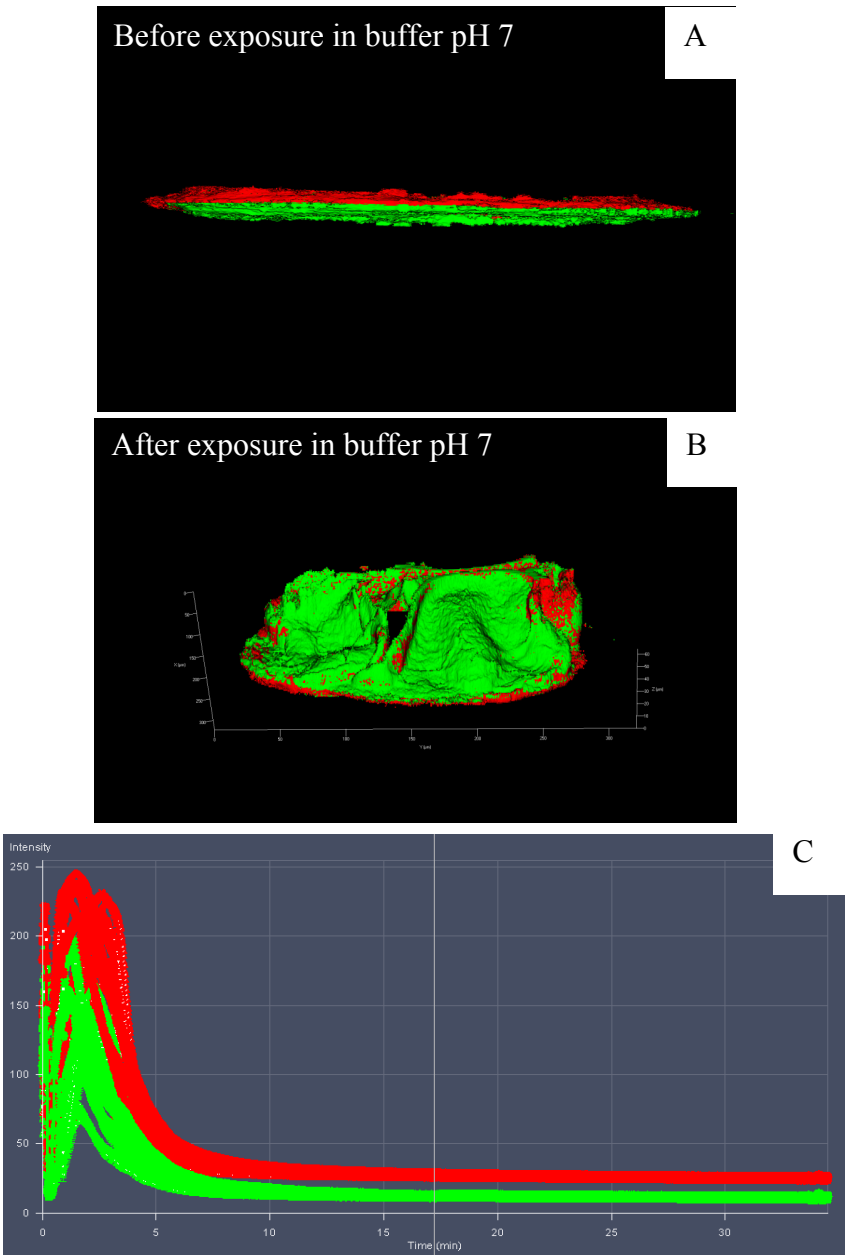

Figure A2: THE DIFFICULTY OF MEASURING THE RELEASE MECHANISM OF PVPON/PMAA MULTILAYER FILMS: A) THE FILM RETAINS A FLAT STRUCTURE BEFORE THE MEASUREMENT, B) THE FILM DEFORMS (BECOMES NON-PLANAR) AFTER BEING EXPOSED TO A BUFFER OF PH 7, AND C) THE DECREASING FLUORESCENT INTENSITY OF THE DYES AFTER EXPOSURE TO A BUFFER OF PH7 RESULTS FROM THE NON-PLANAR DEFORMATION OF THE FILM.

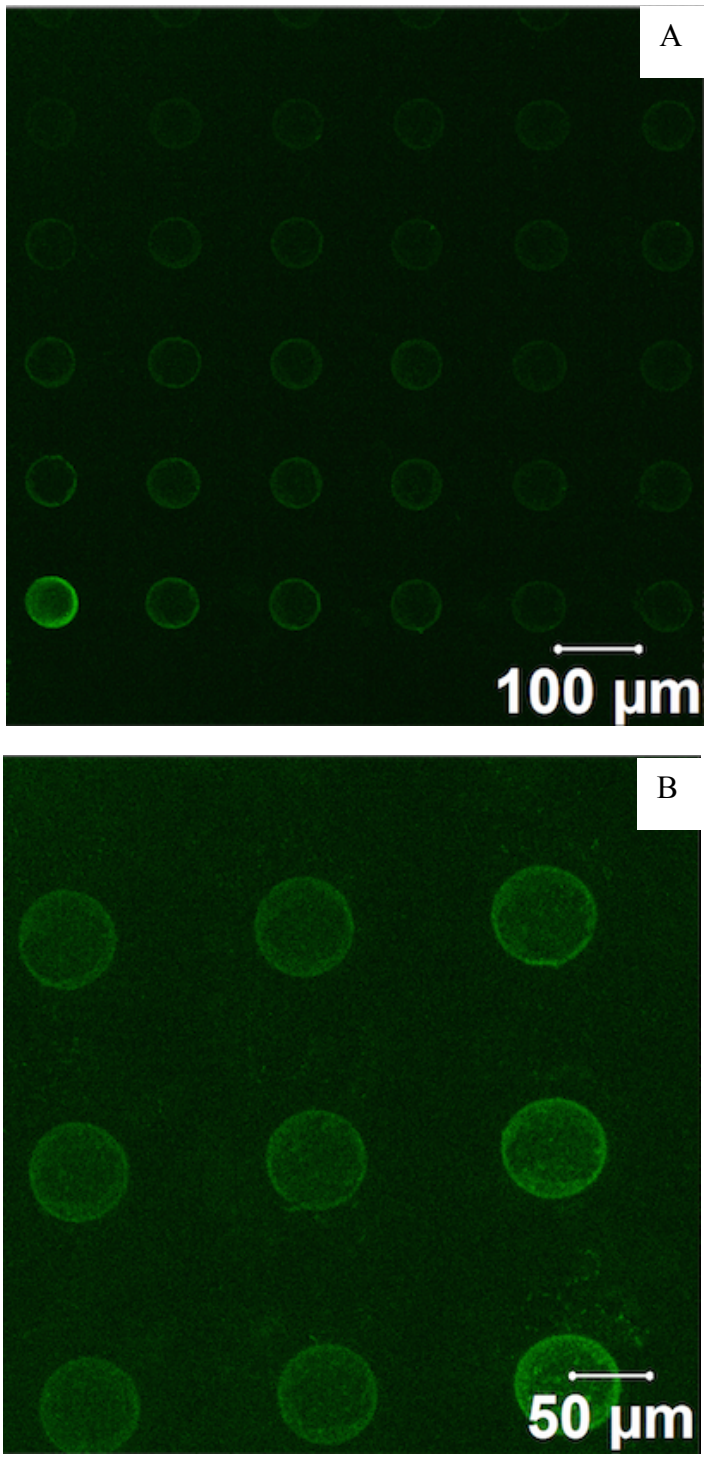

Figure A3: GFP EXPRESSION OF 3BL SILK NESTS IN MEDIA SUPPLEMENTED WITH 5 mM OF THEOPHYLLINE: A) 3 HRS AND B) 5 HRS

REFFERENCES

[1] Tsukruk, V. V. *Prog. Polym. Sci.* **1997,** *22*, 247-311.

[2] Decher, G.; Schlenoff, J. B.; Lehn, J.-M. *Multilayer Thin films:Sequential Assembly of Nanocomposite materials*; WILEY-VCH: Weinheim, 2003, 1-524.

[3] Lvov, Y.; Möhwald, H. *Protein Architecture: Interfacial Molecular Assembly and Immobilization Biotechnology*, Marcel Dekker, New York 2000, 1-394.

[4] Hammond, P. T. *Adv. Mater*. **2004**, *16*, 1271-1293.

[5] Stuart, M. C.; Huck, W.; Genzer, J.; Müller, M.; Ober, C.; Stamm, M.; Sukhorukov, G.; Szleifer, I.; Tsukruk, V. V.; Urban, M.; Winnik, F.; Zauscher, S.; Luzinov, I.; Minko, S. *Nat. Mater.* **2010,** *9,* 101-113.

[6] Ko, H.; Jiang, C.; Tsukruk, V. V. *Chem. Mater.* **2005**, *17*, 5489-5497.

[7] Zhao, W.; Xu, J. –J.; Shi, C. –G.; Chen, H. –Y. *Langmuir* **2005**, *21*, 9630-9634.

[8] Kotov, N. A.; Dékány, I.; Fendler, J. H. *Adv. Mater.* **1996**, *8*, 637-641.

[9] Zheng, H.; Lee, I.; Rubner, M. F.; Hammond, P. T. *Adv. Mater.* **2002**, *14*, 569-572.

[10] Kinnane, C. R.; Such, G. K.; Caruso, F. *Macromolecules*, **2011**, *44*, 1194–1202.

[11] Sukhishvili, S. A. *Curr. Opin. Colloid Interface Sci.* **2005**, *10*, 37-44.

[12] Zhang, H.; Fu, Y.; Wang, D.; Wang, L.; Wang, Z.; Zhang, X. *Langmuir* **2003**, *19*, 8497-8502.

[13] Ariga, K.; Ji, Q.; Hill, J. P. *Adv. Polym. Sci*, **2010**, *229*, 51-87.

[14] Choi, J.; Rubner, M. F. *Macromolecules* **2005**, *38*, 116-124.

[15] Jiang, C.; Tsukruk, V. V. *Adv. Mater.* **2006,** *18*, 829-840.

[16] Caruso, F.; Susha, A. S.; Giersig, M.; Mohwald, H. *Adv. Mater*. **1999**, *11*, 950-953.

[17] deGans, B. J.; Duineveld, P. C.; Schubert, U. S. *Adv. Mater*. **2004**, *16*, 203–213.

[18] Singh, M.; Haverinen, H. M.; Dhagat, P.; Jabbour, G. E. *Adv. Mater*. **2010**, *22*, 673–685.

[19] Gates, B. D.; Xu, Q.; Stewart, M.; Ryan, D.; Willson, C. G.; Whitesides, G. M. *Chem. Rev.* **2005,** *105*, 1171-1196.

[20] Whitesides, G. M.; Ostuni, E.; Takayama, S.; Jiang, X.; Ingber, D. E. *Annu. Rev. Biomed. Eng.* **2001,** *3*, 335–373.

[21] Xia, Y.; Whitesides, G. M. *Angew. Chem. Int. Ed*. **1998**, *37*, 550 -575.

[22] Jiang, X.; Zheng, H.; Gourdin, S.; Hammond, P. T. *Langmuir* **2002**, *18,* 2607-2615.

[23] Quist, A. P.; Pavlovic, E.; Oscarsson, S. *Anal Bioanal Chem* **2005**, *381*, 591–600.

[24] Heckele, M.; Schomburg, W. K. *J. Micromech. Microeng*. **2004**, *14*, R1–R14.

[25] Piner, R. D.; Zhu, J.; Xu, F.; Hong, S.; Mirkin, C. A. *Science* **1999***, 28, 661-663.*

[26] Lavalle, P.; Voegel, J. –C. *Adv. Mater.* **2011**, *23*, 1191–1221.

[27] Schaaf, P.; Voegel, J. –C.; Jierry, L.; Boulmedais, F. *Adv. Mater.* **2012**, *24*, 1001–1016.

[28] Calvert, P. *Chem. Mater.* **2001,** *13,* 3299-3305.

[29] Tekin, E.; Smith, P. J.; Schubert, U. S. *Soft Matter* **2008**, *4*, 703–713.

[30] Deshmukh, P. K.; Ramani, K. P.; Singh S. S.; Tekade, A. R.; Chatap, V. K.; Patil, G. B.; Bari; S. B., *Journal of Controlled Release* **2013**, *166*, 294–306.

[31] Georgieva, R.; Moya, S.; Hin, M.; Mitlöhner, R.; Donath, E.; Kiesewetter, H.; Möhwald, H.; Bäumler, H., *Biomacromolecules* **2002**, *3*, 517-524.

[32] Sukhorukov, G. B.; Antipov, A. A.; Voigt, A.; Donath, E.; Möhwald, H., nanocapsules. *Macromol Rapid Commun* **2001**, *22*, 44-46.

[33] Caruso, F.; Trau, D.; Mo¨hwald, H.; Renneberg, R., *Langmuir* **2000,** *16,* 1485-1488.

[34] Caruso, F.; Yang, W.; Trau, D.; Renneberg, R., *Langmuir* **2000,** *16,* 8932-8936.

[35] Wang, Y.; Yu, A.; Caruso. F.,. *Angew Chem Int Ed* **2005**, *44*, 2888-2892.

[36] Zhu, Y.; Shi, J.; Shen, W.; Dong, X.; Feng, J.; Ruan, M.; Li, Y., *Angew Chem Int Ed* **2005**, *44*, 5083-5087.

[37] Kozlovskaya, V.; Kharlampieva, E.; Drachuk, I.; Cheng, D.; Tsukruk, V. V. *Soft Matter*, **2010**, *6*, 3596–3608.

[38] Ai , H.; Jones , S. A.; de Villiers , M. M.; Lvov, Y. M. *J. Control. Release* **2003***, 86, 59–68.*

[39] Beyer, S.; Mak, W. C.; Trau D., *Langmuir* **2007**, *23*, 8827-8832.

[40] Wang, Y.; Caruso, F., *Chem. Commun.*, **2004**, 1528-1529

[41] Wang, Y.; Caruso, F., *Chem. Mater.* **2005**, *17*, 953-961.

[42] Yu, A.; Wang, Y.; Barlow, E.; Caruso, F. *Adv. Mater.* **2005**,*17*, 1737-1741.

[43] Wang, Y.; Yu, A.; Caruso F., *Angew Chem Int Ed* **2005**, 44, 2888-2892.

[44] Wang, Y.; Bokor, J., *J. Micro/Nanolith. MEMS MOEMS* **2007**, *6*, 043009.

[45] Wijshoff, H., *Physics Reports* **2010**, *491*, 77-177.

[46] Xu, T.; Kincaid, H.; Atala, A.; Yoo, J. J., *J. Manuf. Sci. Eng.* **2008**, *130*, 021017 – 021015.

[47] Poellmann, M. J.; Barton, K. L.; Mishra, S.; Johnson, A. J. W., *Macromol. Biosci.* **2011**, *11*, 1164–1168.

[48] Shah, S. S.; Kim, M.; Cahill-Thompson, K.; Tae, G.; Revzin, A., *Soft Matter*, **2011**, *7*, 3133–3140.

[49] Nakamura, M.; Kobayashi, A.; Takagi, F.; Watanabe, A.; Hiruma, Y.; Ohuchi, K.; Iwasaki, Y.; Horie, M.; Morita, I.; Takatani, S., *Tissue Eng*. **2005**,*11* , 1658-1666.

[50] Derby, B., *J. Mater. Chem.* **2008**, *18*, 5717–5721.

[51] Wong, J. Y.; Leach, J. B.; Brown, X. Q., *Surf. Sci.* **2004**, 570, 119-133.

[52] Veerabadran, N. G.; Goli, P. L.; Stewart-Clark, S. S.; Lvov, Y. M. L.; Mills, D. K., Macromol. Biosci. **2007**, *7*, 877–882.

[53] Yang, S. Y.; Rubner, M. F. *J. Am. Chem. Soc.***2002**, *124*, 2100–2101.

[54] Andres, C, M.; Kotov, N. A. *J. Am. Chem. Soc.***2010**, *132*, 14496-14502.

[55] Johnston, A. P. R.; Cortez, C.; Angelatos, A. S.; Caruso, F., *Curr. Opin. Colloid Interface Sci.* **2006**, *11*, 203-209.

[56] Derby, B. *Annu. Rev. Mater.* Res. **2010**, *40*, 395-414.

[57] Park, J. –U.; Hardy, M.; Kang, S. J.; Barton, K.; Adair, K.; Mukhopadhyay, D. K.; Lee, C. Y.; Strano, M. S.; Alleyne, A. G.; Georgiadis, J. G.; Ferreira, P. M.; Rogers, J. A. Nature Materials **2007**, *6*, 782 – 789.

[58] Zhou, C.-Z.; Confalonieri, F.; Jacquet, M.; Perasso, R.; Li, Z.-G.; Janin,. J.*Proteins* **2001**, *44*, 119-122.

[59] Zhou, C. Z.; Confalonieri, F.; Medina, N.; Zivanovic, Y.; Esnault, C.; Yang, T.; Jacquet, M.; Janin, J.; Duguet, M.; Perasso, R.; Li, Z. G. *Nucleic Acids Res.* **2000**, *28*, 2413-2419.

[60] Altman, G. H.; Diaz, F.; Jakuba, C.; Calabro, T.; Horan, R. L.; Chen, J.; Lu, H.; Richmond, J.; Kaplan, D. L. *Biomaterials* **2003**, *24*, 401-416.

[61] Omenetto, F. G.; Kaplan D. L.; A new route for silk, *Nat. Photon.* **2008**, *2*, 641-643.

[62] Keten, S.; Xu, Z.; Ihle, B.; Buehler, M. J., *Nature Materials* **2010**, *9*, 359–367.

[63] Shulha, H.; Wong, C.; Kaplan, D. L.; Tsukruk, V. V., *Polymer*, **2006**, *47*, 5821-5830.

[64] Jiang, C.; Wang, X.; Gunawidjaja, R.; Lin, Y. –H.; Gupta, M. K.; Kaplan, D. L.; Naik, R. R.; Tsukruk, V. V., *Adv. Funct. Mater.* **2007**, *17*, 2229–2237.

[65] Kim, U.-J.; Park, J. H.; Kim, H. J.; Wada, M.; Kaplan, D. L. *Biomaterials* **2005**, *26*, 2775-2785.

[66] Lawrence, B. D.; Cronin-Golomb, M.; Georgakoudi, I.; Kaplan, D. L.; Omenetto, F. G. *Biomacromolecules* **2008**, *9*, 1214-1220.

[67] Perry, H.; Gopinath, A.; Kaplan, D. L.; Dal Negro, L.; Omenetto, F. G. *Adv. Mater.* **2008**, *20*, 3070-3072.

[68] Omenetto, F. G.;. Kaplan, D. L. *Nat. Photonics* **2008**, *2*, 641-643.

[69] Demura, M. & Asakura, T. *Biotechnology and Bioengineering* **1989**, *33*, 598-603.

[70] Shchepelina, O.; Drachuk, I.; Gupta, M. K.; Lin, J.; Tsukruk, V. V., *Adv. Mater.* **2011**, *23*, 4655–4660.

[71] Phillips, D. M.; Drummy, L. F.; Conrady, D. G.; Fox, D.M.; Naik, R. R.; Stone, M. O.; Trulove, P. C.; Long, H. C. D.; Mantz, R. A., *J. Am. Chem. Soc.*, **2004**, *126*, 14350–14351.

[72] Ye, C.; Shchepelina, O.; Calabrese, R.; Drachuk, I.; Kaplan, D. L.; Tsukruk, V. V., *Biomacromolecules*, **2011**, *12*, 4319–4325.

[73] Szunerits, S.; Boukherroub, R., *Langmuir* **2006**, *22*, 1660-1663.

[74] Sheller, N. B.; Petrash, S.; Foster, M. D.; Tsukruk, V. V.; *Langmuir* **1998**, *14*, 4535-4544.

[75] Tsukruk,V. V.; Bliznyuk, V. N., *Langmuir* **1998,***14,* 446-455.

[76] Harbaugh, S.; Kelley-Loughnane, N.; Davidson, M.; Narayanan, L.; Trott, S.; Chushak, Y. G.; Stone, M. O. *Biomacromolecules* **2009**, *32*, 1610-1614.

[77] Azzam, R. M. A.; Bashara, N. M., *Ellipsometry and Polarized Light*, Elsevier Science Pub Co (**1987**)

[78] Tsukruk, V. V.; Reneker, D. H. *Polymer* **1995**, *36*, 1791-1808.

[79] McConney, M. E.; Singamaneni, S.; Tsukruk, V. V. *Polym. Rev.,* **2010**, *50*, 235-286.

[80] Kharlampieva, E.; Slocik, J. M.; Singamaneni, S.; Poulsen, N.; Kro¨ger, N.; Naik, R. R.; Tsukruk, V. V., *Adv. Funct. Mater.* **2009**, *19*, 2303–2311.

[81] Shchepelina, O.; Drachuk, I.; Gupta, M. K.; Lin, J.; Tsukruk, V. V., *Adv. Mater*. **2011**, *23*, 4655–4660.

[82] Kharlampieva, E.; Zimnitsky, D.; Gupta, M.; Bergman, K. N.; Kaplan, D. L.; Naik, R. R.; Tsukruk, V. V., *Chem. Mater*. **2009**, *21*, 2696-2704.

[83] Decher, G.; Schlenoff, J. B.; Lehn, J.-M. *Multilayer Thin films:Sequential Assembly of Nanocomposite materials*; WILEY-VCH: Weinheim, 2003.

[84] Tsukruk, V. V. *Prog. Polym. Sci.* **1997,** *22*, 247-311.

[85] Lvov, Y.; Möhwald, H. *Protein Architecture: Interfacial Molecular Assembly and Immobilization Biotechnology*, Marcel Dekker, New York 2000.

[86] Hammond, P. T. *Adv. Mater*. **2004**, *16*, 1271-1293.

[87] Stuart, M. C.; Huck, W.; Genzer, J.; Müller, M.; Ober, C.; Stamm, M.; Sukhorukov, G.; Szleifer, I.; Tsukruk, V. V.; Urban, M.; Winnik, F.; Zauscher, S.; Luzinov, I.; Minko, S. *Nat. Mater.* **2010,** *9,* 101-113.

[88] Ko, H.; Jiang, C.; Tsukruk, V. V. *Chem. Mater.* **2005**, *17*, 5489-5497.

[89] Zhao, W.; Xu, J. –J.; Shi, C. –G.; Chen, H. –Y. *Langmuir* **2005**, *21*, 9630-9634.

[90] Kotov, N. A.; Dékány, I.; Fendler, J. H. *Adv. Mater.* **1996**, *8*, 637-641.

[91] Zheng, H.; Lee, I.; Rubner, M. F.; Hammond, P. T. *Adv. Mater.* **2002**, *14*, 569-572.

[92] Kinnane, C. R.; Such, G. K.; Caruso, F. *Macromolecules*, **2011**, *44*, 1194–1202.

[93] Sukhishvili, S. A. *Curr. Opin. Colloid Interface Sci.* **2005**, *10*, 37-44.

[94] Zhang, H.; Fu, Y.; Wang, D.; Wang, L.; Wang, Z.; Zhang, X. *Langmuir* **2003**, *19*, 8497-8502.

[95] Ariga, K.; Ji, Q.; Hill, J. P. *Adv. Polym. Sci*, **2010**, *229*, 51-87.

[96] Choi, J.; Rubner, M. F. *Macromolecules* **2005**, *38*, 116-124.

[97] Jiang, C.; Tsukruk, V. V. *Adv. Mater.* **2006,** *18*, 829-840.

[98] Caruso, F.; Susha, A. S.; Giersig, M.; Mohwald, H. *Adv. Mater*. **1999**, *11*, 950-953.

[99] deGans, B. J.; Duineveld, P. C.; Schubert, U. S. *Adv. Mater*. **2004**, *16*, 203–213.

[100] Singh, M.; Haverinen, H. M.; Dhagat, P.; Jabbour, G. E. *Adv. Mater*. **2010**, *22*, 673–685.

[101] Gates, B. D.; Xu, Q.; Stewart, M.; Ryan, D.; Willson, C. G.; Whitesides, G. M. *Chem. Rev.* **2005,** *105*, 1171-1196.

[102] Whitesides, G. M.; Ostuni, E.; Takayama, S.; Jiang, X.; Ingber, D. E. *Annu. Rev. Biomed. Eng.* **2001,** *3*, 335–373.

[103] Xia, Y.; Whitesides, G. M. *Angew. Chem. Int. Ed*. **1998**, *37*, 550 -575.

[104] Jiang, X.; Zheng, H.; Gourdin, S.; Hammond, P. T. *Langmuir* **2002**, *18,* 2607-2615.

[105] Quist, A. P.; Pavlovic, E.; Oscarsson, S. *Anal Bioanal Chem* **2005**, *381*, 591–600.

[106] Heckele, M.; Schomburg, W. K. *J. Micromech. Microeng*. **2004**, *14*, R1–R14.

[107] Piner, R. D.; Zhu, J.; Xu, F.; Hong, S.; Mirkin, C. A. *Science* **1999***, 28,* 661-663.

[108] Lavalle, P.; Voegel, J. –C. *Adv. Mater.* **2011**, *23*, 1191–1221.

[109] Schaaf, P.; Voegel, J. –C.; Jierry, L.; Boulmedais, F. *Adv. Mater.* **2012**, *24*, 1001–1016.

[110] Calvert, P. *Chem. Mater.* **2001,** *13,* 3299-3305.

[111] Tekin, E.; Smith, P. J.; Schubert, U. S. *Soft Matter* **2008**, *4*, 703–713.

[112] Park, J. –U.; Hardy, M.; Kang, S. J.; Barton, K.; Adair, K.; Mukhopadhyay, D. K.; Lee, C. Y.; Strano, M. S.; Alleyne, A. G.; Georgiadis, J. G.; Ferreira, P. M.; Rogers, J. A. *Nature Materials* **2007**, *6*, 782 – 789.

[113] Yang, S. Y.; Rubner, M. F. *J. Am. Chem. Soc.***2002**, *124*, 2100–2101.

[114] Andres, C, M.; Kotov, N. A. *J. Am. Chem. Soc.***2010**, *132*, 14496-14502.

[115] Derby, B. *Annu. Rev. Mater.* Res. **2010**, *40*, 395-414.

[116] Deegan, R. D.; Bakajin, O.; Dupont, T. F.; Huber, G.; Nagel, S. R.; Witten, T. A. *Nature* **1997**, *389*, 827-829.

[117] Soltman, D.; Subramanian, V. *Langmuir* **2008,** *24,* 2224-2231.

[118] Sharma, V.; Park, K.; Srinivasarao, M. *Mater. Sci. Eng., R* **2009**, *65*, 1-38.

[119] Xu, J.; Xia, J.; Hong, S. W.; Lin, Z.; Qiu, F.; Yang, Y. *Phys. Rev. Lett.* **2006**, *96*, 066104-066108.

[120] Shen, X.; Ho, C. –M.; Wong, T. –S. *J. Phys. Chem. B*, **2010**, 114, 5269–5274.

[121] Weon,B. M.; Je, J. H. *Physical Review E* **2010,** *82*, 015305-4.

[122] Hong, S. W.; Jeong, W.; Ko, H.; Kessler, M. R.; Tsukruk, V. V.; Lin, Z. *Adv. Funct. Mater.* **2008,** *18,* 2114-2122.

[123] Choi, I.; Suntivich, R.; Plamper, F. A.; Synatschke, C. V.; Mueller, A. H. E.; Tsukruk, V. V. *J. Am. Chem. Soc.*, **2011**, *133*, 9592–9606.

[124] Stockton, W. B.; Rubner, M.F. *Macromolecules* **1997**, *30,* 2717-2725.

[125] Kharlampieva, E.; Kozlovskaya, V.; Chan, J.; Ankner, J. F.; Tsukruk, V. V. *Langmuir* **2009***, 25,* 14017-14024.

[126] Kozlovskaya, V.; Kharlampieva, E.; Chang, S.; Muhlbauer, R.; Tsukruk, V. V. *Chem. Mater.* **2009,** *21,* 2158-2167.

[127] Lisunova, M. O.; Drachuk, I.; Shchepelina, O. A.; Anderson, K.; Tsukruk, V. V. *Langmuir,* **2011,** *27,* 11157-11165.

[128] Kozlovskaya, V.; Harbaugh, S.; Drachuk, I.; Shchepelina, O.; Kelley-Loughnane, N.; Stone*,* M.; Tsukruk*,* V. V. *Soft Matter,* **2011,** *7,* 2364-2372.

[129] Kharlampieva, E.; Kozlovskaya, V.; Ankner, J. F.; Sukhishvili, S. A. *Langmuir* **2008,** *24,* 11346-11349.

[130] Kharlampieva, E.; Kozlovskaya, V.; Sukhishvili; S.A. *Adv. Mater*. **2009**, *21*, 3053–3065.

[131] Kozlovskaya, V.; Kharlampieva, E.; Drachuk, I.; Cheng, D.; Tsukruk, V. V. *Soft Matter* **2010**, *6*, 3596–3608.

[132] Zhuk, A.; Pavlukhina, S.; Sukhishvili; S. A. *Langmuir* **2009**, *25*, 14025–14029.

[133] Sukhishvili, S. A.; Granick, S. *Macromolecules* **2002**, *35,* 301-310.

[134] Kozlovskaya, V. A.; Kharlampieva, E. P.; Erel-Unal, I.; Sukhishvili, S. A. *Polym. Sci. Ser A* **2009**, *51*, 719-729.

[135] Sukhishvili, S. A.; Granick, S. *J. Am. Chem. Soc.* **2000**, *122,* 9550-9551.

[136] Seo, J.; Lutkenhaus, J. L.; Kim, J.; Hammond, P. T.; Char, K. *Langmuir* **2008**, *24*, 7995-8000.

[137] Podsiadlo, P.; Michel, M.; Lee, J.; Verploegen, E.; Kam, N. W. S.; Ball, V.; Lee, J.; Qi, Y.; Hart, A. J.; Hammond, P. T.; Koto, N. A. *Nano Lett.*, **2008**, *8*, 1762–1770.

[138] Dubas, S. T.; Schlenof, J. B. *Macromolecules* **1999**, *32*, 8153-8160.

[139] Morgan, H.; Pritchard, D. J.; Cooper. J. M. *Biosensors & Bioelectronics* **1995**, *10,* 841-846.

[140] deGans, B. J.; Duineveld, P. C.; Schubert, U. S. *Adv. Mater*. **2004**, *16*, 203–213.

[141] Singh, M.; Haverinen, H. M.; Dhagat, P.; Jabbour, G. E. *Adv. Mater*. **2010**, *22*, 673–685.

[142] Gates, B. D.; Xu, Q.; Stewart, M.; Ryan, D.; Willson, C. G.; Whitesides, G. M. *Chem. Rev.* **2005,** *105*, 1171-1196.

[143] Whitesides, G. M.; Ostuni, E.; Takayama, S.; Jiang, X.; Ingber, D. E. *Annu. Rev. Biomed. Eng.* **2001,** *3*, 335–373.

[144] Xia, Y.; Whitesides, G. M. *Angew. Chem. Int. Ed*. **1998**, *37*, 550 -575.

[145] Jiang, X.; Zheng, H.; Gourdin, S.; Hammond, P. T. *Langmuir* **2002**, *18,* 2607-2615.

[146] Quist, A. P.; Pavlovic, E.; Oscarsson, S. *Anal Bioanal Chem* **2005**, *381*, 591–600.

[147] Heckele, M.; Schomburg, W. K. *J. Micromech. Microeng*. **2004**, *14*, R1–R14.

[148] Piner, R. D.; Zhu, J.; Xu, F.; Hong, S.; Mirkin, C. A. *Science* **1999***, 28, 661-663.*

[149] Dornelles Mello, L. D.; Kubota, L. T. *Food Chemistry* **2002,** *77,* 237–256.

[150] Jiang, C.; Wang, X.; Gunawidjaja, R.; Lin, Y. –H.; Gupta, M. K.; Kaplan, D. L.; Naik, R. R.; Tsukruk, V. V. *Adv. Funct. Mater*. **2007**, *17*, 2229–2237.

[151] Shao, Z.; Vollrath, F. *Nature* **2002**, *418*, 741

[152] Jin, H. –J.; Kaplan, D. L. *Nature* **2003**, *424*, 1057-1061.

[153] Vollrath, F.; Madsen, B.; Shao, Z. *Proc. R. Soc. Lond. B* **2001**, *268*, 2339-2346.

[154] Chen, X.; Shao, Z.; Vollrath, F. *Soft Matter* **2006**, *2*, *448*–451.

[155] Hu, K.; Gupta, M. K.; Kulkarni, D. D.; Tsukruk, V. V. *Adv. Mater.*, **2013**, *25*, 2301-2307.

[156] Gupta, M. K.; Singamaneni, S.; McConney, M.; Drummy, L. F.; Naik, R. R.; Tsukruk, V. V. *Adv. Mater*., **2010**, *22*, 115-119.

[157] Kharlampieva, E.; Zimnitsky, D.; Gupta, M.; Bergman, K, N.; Kaplan, D. L.; Naik, R. R.; Tsukruk, V. V. *Chem. Mater*. **2009**, *21*, 2696-2704.

[158] Kim, H. –S.; Yoon, S. H.; Kwon, S. –M.; Jin, H. –J. *Biomacromolecules* **2009**, *10*, 82–86.

[159] Wang, S.; Zhang, Y.; Wang, H.; Yin, G.; Dong, Z. *Biomacromolecules* **2009**, *10*, 2240–2244.

[160] Yina, H.; Aia, S.; Shia, W.; Zhu, L. *Sensors and Actuators B* **2009**, *137*, 747–753.

[161] Amsden, J. J.; Domachuk, P.; Gopinath, A.; White, R. D.; Negro, L. D.; Kaplan, D. L.; Omenetto F. G., *Adv. Mater.* **2010**, *22*, 1–4.

[162] Hu, K.; Tolentino, L. S.; Kulkarni, D. D.; Ye, C.; Kumar, S.; Tsukruk, V.V., *Angew. Chem. Int. Ed.* **2013**, *52*, 1–6.

[163] Kharlampieva, E.; Kozlovskaya, V.; Wallet, B.; Shevchenko, V. V.; Naik, R. R.; Vaia, R.; Kaplan, D. L.; Tsukruk, V. V., *ACS Nano*, **2010**, *4*, 7053-7063;

[164] Young, S. L.; Gupta, M.; Hanske, C.; Fery, A.; Scheibel, T.; Tsukruk, V.V. *Biomacromolecules*, **2012**, *13*, 3189-3199.

[165] Krishnaji, S. T.; Huang, W.; Rabotyagova, O.; Kharlampieva, E.; Choi, I.; Tsukruk, V. V.; Naik, R.; Cebe, P.; Kaplan, D. L. *Langmuir*, **2011**, *27*, 1000-1008.

[166] Kharlampieva, E.; Kozlovskaya, V.; Gunawidjaja, R.; Shevchenko, V. V.; Vaia, R.; Naik, R. R.; Kaplan, D. L.; Tsukruk, V. V. *Adv. Funct. Mater.,* **2010**, *20*, 840-846.

[167] Mori, H.; Tsukadar, M. *Reviews in Molecular Biotechnology* **2000,** *74,* 95-103

[168] Zhanga, Y. –Q.; Shena, W. –D.; Gub, R. –A.; Zhuc, J.; Xue, R. -Y. *Analytica Chimica Acta* **1998**, *369*, 123-128.

[169] Drachuk, I., Shchepelina, O.; Harbaugh, S.; Kelley-Loughnane, N.; Stone, M.; Tsukruk, V. V., *Small,* **2013,** *9,* 3128-3137.

[170] Tsukada, M.; Gotoh, Y.; Nagura, M.; Minoura, N.; Kasai, N.; Freddi, G.*; J. Polym. Sci. Part B* **1994**, *32*, 961-968.

[171] Hu, X.; Kaplan, D.; Cebe, P. *Macromolecules*, **2006**, *39*, 6161–6170.

[172] Numata, K.; Subramanian, B.; Currie, H. A.; Kaplan, D. L. *Biomaterials* **2009**, *30*, 5775–5784.

[173] Nagano, A.; Kikuchi, Y.; Sato, H.; Nakazawa, Y.; Asakura, T. *Macromolecules,* **2009**, *42*, 8950–8958.

[174] Lvov, Y.; Möhwald, H. *Protein Architecture: Interfacial Molecular Assembly and Immobilization Biotechnology*, Marcel Dekker, New York 2000, 1-394.

[175] Hammond, P. T. *Adv. Mater*. **2004**, *16*, 1271-1293.

[176] Stuart, M. C.; Huck, W.; Genzer, J.; Müller, M.; Ober, C.; Stamm, M.; Sukhorukov, G.; Szleifer, I.; Tsukruk, V. V.; Urban, M.; Winnik, F.; Zauscher, S.; Luzinov, I.; Minko, S. *Nat. Mater.* **2010,** *9,* 101-113.

[177] Ko, H.; Jiang, C.; Tsukruk, V. V. *Chem. Mater.* **2005**, *17*, 5489-5497.

[178] Zhao, W.; Xu, J. –J.; Shi, C. –G.; Chen, H. –Y. *Langmuir* **2005**, *21*, 9630-9634.

[179] Kotov, N. A.; Dékány, I.; Fendler, J. H. *Adv. Mater.* **1996**, *8*, 637-641.

[180] Zheng, H.; Lee, I.; Rubner, M. F.; Hammond, P. T. *Adv. Mater.* **2002**, *14*, 569-572.

[181] Kinnane, C. R.; Such, G. K.; Caruso, F. *Macromolecules*, **2011**, *44*, 1194–1202.

[182] Sukhishvili, S. A. *Curr. Opin. Colloid Interface Sci.* **2005**, *10*, 37-44.

[183] Zhang, H.; Fu, Y.; Wang, D.; Wang, L.; Wang, Z.; Zhang, X. *Langmuir* **2003**, *19*, 8497-8502.

[184] Ariga, K.; Ji, Q.; Hill, J. P. *Adv. Polym. Sci*, **2010**, *229*, 51-87.

[185] Choi, J.; Rubner, M. F. *Macromolecules* **2005**, *38*, 116-124.

[186] Jiang, C.; Tsukruk, V. V. *Adv. Mater.* **2006,** *18*, 829-840.

[187] Lost, R. M.; Crespilho, F. N. *Biosensors and Bioelectronics* **2012**, *31*, 1–10.

[188] Caruso, F.; Susha, A. S.; Giersig, M.; Mohwald, H. *Adv. Mater*. **1999**, *11*, 950-953.

[189] Ye, C.; Shchepelina, O.; Calabrese, R.; Drachuk, I.; Kaplan, D. L.; Tsukruk, V. V. *Biomacromolecules*, **2011**, *12*, 4319–4325.

[190] Shchepelina, O.; Drachuk, I.; Gupta , M. K.; Lin, J.; Tsukruk, V. V. *Adv. Mater.* **2011**, *23*, 4655–4660.

[191] Ye, C.; Drachuk, I.; Calabrese, R.; Dai, H.; Kaplan, D. L.; Tsukruk, V.V. *Langmuir*, **2012**, *28*, 12235−12244.

[192] B. Wallet, E. Kharlampieva, K. Campbell-Proszowska, V. Kozlovskaya, S. Malak, J. F. Ankner, D. L. Kaplan, V. V. Tsukruk, *Langmuir,* **2012,** *28*, 11481−11489

[193] Wang, X.; Hu, X.; Daley, A.; Rabotyagova, O.; Peggy Cebed, P.; Kaplan, D. L. *J. Control. Release* **2007,** *121***,** 190–199.

[194] Calvert, P. *Chem. Mater.* **2001,** *13,* 3299-3305.

[195] Tekin, E.; Smith, P. J.; Schubert, U. S. *Soft Matter* **2008**, *4*, 703–713.

[196] Yang, S. Y.; Rubner, M. F., *J. Am. Chem. Soc.*, **2002**, *124*, 2100–2101.

[197] Settia, L.; Fraleoni,- M. A.; Ballarinb, B.; Filippinia, A.; Frascaroa, D.; Piana, C. *Biosensors and Bioelectronics* **2005,** *20*, 2019–2026.

[198] L. Setti, L.; Fraleoni-Morgera, A.; Mencarellia, I.; Filippini, A.; Ballarinb, B.; Biase, M. D. *Sensors and Actuators B* **2007**, *126*, 252–257.

[199] Bernacka-Wojcik, I.; Senadeera, R.; Wojcik, P. J.; Silva, L. B.; Doria, G.; Baptista, P.; Aguas, H.; Fortunato, E.; Martins R. *Biosensors and Bioelectronics* **2010,** *25,* 1229–1234.

[200] Ringeisen, B. R.; Pirlo, R. K.; Wu, P. K.; Boland, T.; Huang, Y.; Sun, W.; Hamid, Q.; Chrisey, D. B. *MRS Bull.*, **2013**, *38*, 834-843.

[201] Phillips, D. M.; Drummy, L. F.; Conrady, D. G.; Fox, D.M.; Naik, R. R.; Stone, M. O.; Trulove, P. C.; Long, H. C. D.; Mantz, R. A. *J. Am. Chem. Soc.*, **2004**, *126*, 14350–14351.

[202] Serban, M. A.; Kaplan, D. L. *Biomacromolecules* **2010**, *11*, 3406–3412.

[203] Calabrese, R.; Kaplan, D. L. *Biomaterials* **2012**, *33*, 7375–7385.

[204] Harbaugh, S.; Kelley-Loughnane, N.; Davidson, M.; Narayanan, L.; Trott, S.; Chushak, Y. G.; Stone, M. O. *Biomacromolecules* **2009**, *32*, 1610-1614.

[205] Wang, J. Z., Zheng, Z. H., Li, H. W., Huck W. T. S., Sirringhaus H. *Nature Materials* **2004**, *3*, 171–176.

[206] Suntivich, R., Shchepelina, O., Choi, I., Tsukruk, V. V. *ACS Appl. Mater. Interfaces*, **2012**, *4*, 3102–3110.

[207] Reiter, G., *Langmuir* **1993**, *9*, 1344-1351.

[208] Reiter, G., *Phys. Rev. Lett*. **1992**, *68*, 75–78.

[209] *Shulha*, H.; Wong, C.; Kaplan, D. D.; Tsukruk, V. V. *Polymer*, ***2006***, *47*, 5821-5830.

[210] *Wallet*, B.; Kharlampieva, E.; Campbell-Proszowska, K.; Kozlovskaya, V.; Malak, S.; Ankner, J. F.; Kaplan, D. L.; Tsukruk, V. V. *Langmuir*, ***2012***, *28*, 13345-13353.

[211] Shen, X.; Ho, C. –M.; Wong, T. –S. *J. Phys. Chem. B*, **2010**, 114, 5269–5274.

[212] Weon,B. M.; Je, J. H. *Physical Review E* **2010,** *82*, 015305-4.

[213] Hong, S. W.; Jeong, W.; Ko, H.; Kessler, M. R.; Tsukruk, V. V.; Lin, Z. *Adv. Funct. Mater.* **2008,** *18,* 2114-2122.

[214] Sharma, V.; Park, K.; Srinivasarao, M. *Mater. Sci. Eng., R* **2009**, *65*, 1-38.

[215] Deegan, R. D.; Bakajin, O.; Dupont, T. F.; Huber, G.; Nagel, S. R.; Witten, T. A. *Nature* **1997**, *389*, 827-829.

[216] Xu, J.; Xia, J.; Hong, S. W.; Lin, Z.; Qiu, F.; Yang, Y. *Phys. Rev. Lett.* **2006**, *96*, 066104-066108.

[217] Soltman, D.; Subramanian, V. *Langmuir* **2008,** *24,* 2224-2231.

[218] Choi, I., Suntivich, R., Plamper, F. A., Synatschke, C. V., Müller, A. H. E., Tsukruk, V. V. *J. Am. Chem. Soc.*, **2011**, *133*, 9592–9606.

[219] Zhuk, A.; Pavlukhina, S.; Sukhishvili; S. A. *Langmuir* **2009**, *25*, 14025–14029.

[220] Kozlovskaya, V. A.; Kharlampieva, E. P.; Erel-Unal, I.; Sukhishvili, S. A. *Polym. Sci. Ser A* **2009**, *51*, 719-729.

[221] Ye, C.; Shchepelina, O.; Calabrese, R.; Drachuk, I.; Kaplan, D. L.; Tsukruk, V. V., *Biomacromolecules* **2011**, *12*, 4319–4325.

[222] Gibbs, B. F.; Kermasha, S.; Alli, I.; Mulligan, C. N., *Int J Food Sci Nutr* **1999**, 50, 213-224.

[223] Discher, B. M.; Won, Y. Y.; Ege, D. S.; Lee, J. C. M.; Bates, F. S.; Discher, D. E.; Hammer, D. A., *Science* **1999**, *284*, 1143−1146.

[224] Jang, J.; Ha, H., *Langmuir* **2002**, *18*, 5613−5618.

[225] Huang, H. Y.; Remsen, E. E.; Kowalewski, T.; Wooley, K. L., *J. Am. Chem. Soc.* **1999**, *121*, 3805−3806.

[226] Chunhong Ye, C.; Shchepelina, O.; Calabrese, R.; Drachuk, I.; Kaplan, D. L.; Tsukruk, V. V., *Biomacromolecules* **2011**, *12*, 4319−4325.

[227] Hakim, L. F.; Blackson, J.; George, S. M.; Weimer, A. W., *Chem. Vap. Deposition* **2005**, *11*, 420-425.

[228] Lau, K. K. S.; Gleason, K. K., *Adv. Mater.* **2006**, *18*, 1972–1977.

[229] Zheng, H.; Berg, M. C.; Rubner, M. F.; Hammond, P. T., *Langmuir* **2004**, *20*, 7215-7222.

[230] Quist, A. P.; Pavlovic, E.; Oscarsson, S., *Anal Bioanal Chem* **2005**, *381*, 591–600.

[231] Karbasian, H.; Tekkaya, A. E., *J. Mater. Process. Technol*. **2010**, *210*, 2103–2118.

[232] Jiang, X.; Zheng, H.; Gourdin, S.; Hammond, P. T., *Langmuir* **2002**, *18*, 2607-2615.

[233] Meitl, M. A.; Zhu, Z. –T.; Kumar, V.; Lee, K. J.; Feng, X.; Huang, Y. Y.; Adesida, I.; Nuzzo, R. G.; Rogers, J. A., *Nat. Mater.* **2006***, 5*, 33 – 38.

[234] Omenetto, F. G.; Kaplan, D. L. *Nat. Photonics* **2008**, *2*, 641−643.

[235] Hofmann, S.; Foo, C. T.; Rossetti, F.; Textor, M.; Vunjak-Novakovis, G.; Kaplan, D. L., *J. Controlled release* **2006**, *111*, 219-227.

[236] Altman, G. H.; Diaz, F.; Jakuba, C.; Calabro, T.; Horan, R. L.; Chen, J.; Lu, H.; Richmond, J.; Kaplan, D. L., *Biomaterials* **2003**, *24*, 401–416.

[237] Hermanson, K. D.; Huemmerich, D.; Scheibel, T.; Bausch, A. R., *Adv. Mater.* **2007**, *19*, 1810–1815.

[238] Shchepelina, O.; Drachuk , I.; Gupta, M. K.; Lin , J.; Tsukruk, V. V., *Adv. Mater.* **2011**, *23*, 4655–4660.

[239] Ye, C.; Drachuk, I.; Calabrese, R.; Dai, H.; Kaplan, D. L.; Tsukruk, V. V., *Langmuir* **2012**, *28*, 12235−12244.

[240] Phillips, D. M.; Drummy, L. F.; Conrady, D. G.; Fox, D.M.; Naik, R. R.; Stone, M. O.; Trulove, P. C.; Long, H. C. D.; Mantz, R. A. *J. Am. Chem. Soc.*, **2004**, *126*, 14350–14351.

[241] Harbaugh, S.; Kelley-Loughnane, N.; Davidson, M.; Narayanan, L.; Trott, S.; Chushak, Y. G.; Stone, M. O. *Biomacromolecules* **2009**, *32*, 1610-1614.

[242] Jiang, C.; Wang, X.; Gunawidjaja, R.; Lin, Y. –H.; Gupta, M. K.; Kaplan, D. L.; Naik, R. R.; Tsukruk, V. V., *Adv. Funct. Mater.* **2007**, *17*, 2229–2237.

[243] Kaplan, D.L.; Fossey, S.; Mello, C.M. *MRS Bull* **1992**, *17*, 41-47.

[244] Zhou, C. –Z.; Confalonieri, F.; Medina, N.; Zivanovic, Y.; Esnault, C.; Yang, T.; Jacquet, M.; Janin, J.; Duguet, M.; Perasso, R.; Li, Z. –G., *Nucleic Acids Res*. **2000**, *28*, 2413-2419.

[245] Canetti, M.; Seves, A.; Secundo, F.; Vecchio, G., *Biopolymers.* **1989**, *28*, 1613-1624.

[246] Chen, X.; Knight, D. P.; Shao, Z.; Vollrath, F., *Polymer* **2001**, *42*, 9969-9974.

[247] Tao, H.; Brenckle, M. A.; Yang, M.; Zhang, J.; Liu, M.; Siebert, S. M.; Averitt, R. D.; Mannoor, M. S.; McAlpine, M. C.; Rogers, J. A.; Kaplan, D. L.; Omenetto, F. O., *Adv. Mater.* **2012**, *24*, 1067-1072.

[248] Jin, H. J.; Kaplan, D. L. *Nature* **2003**, *424*, 1057-1061.

[249] Kim, U. –J.; Park, J.; Li, C.; Jin, H. –J.; Valluzzi, R.; Kaplan, D. L., *Biomacromolecules* **2004**, *5*, 786-792.

[250] Johnston, A. P. R.; Cortez, C.; Angelatos, A. S.; Caruso, F., *Curr. Opin. Colloid Interface Sci.* **2006**, *11*, 203-209.

[251] Khopade, A. J.; Caruso, F., *Biomacromolecules*, **2002**, *3*, 1154–1162.

[252] Becker, A. L.; Johnston, A. P. R.; Caruso, F., *small* **2010**, *6*, 1836–1852.

[253] de Gans, B. –J.; Schubert, U. S., *Langmuir* **2004**, *20*, 7789-7793.

[254] Dutta, S.; Talukdar, B.; Bharali, R.; Rajkhowa, R.; Devi, D., Biopolymers **2013**, *99*, 326–333.

[255] Suntivich, R.; Shchepelina, O.; Choi, I., Tsukruk, V. V., *ACS Appl. Mater. Interfaces* **2012**, *4*, 3102–3110.

VITA

Rattanon Suntivich

Rattanon Suntivich was born in Suphanburi province, Thailand on February 13, 1984 to Sukannika and Boondarik Suntivich. . He attended Samsen wittayalai high school and earned his Bachelor of Science degree in Chemistry from Mahidol University in 2006. He pursued a Ph.D. in Materials Science and Engineering at Georgia Institute of Technology with Professor Vladimir V. Tsukruk. After graduating, Rattanon will begin his career as a researcher at the Siam Cement Public Company Limited, Thailand.